UNIVERSITÀ
DI PAVIA

SCUOLA DI ALTA FORMAZIONE DOTTORALE
MACRO-AREA SCIENZE E TECNOLOGIE
Dottorato di Ricerca in Scienze della Terra e dell’Ambiente

Anna Barbaro

Shock origin of carbon phases in ureilites

Anno Accademico 2020/2021
Ciclo XXXIV

Coordinator
Prof. Roberto Sacchi

Tutors
Prof. Maria Chiara Domeneghetti
Prof. Fabrizio Nestola

TABLE OF CONTENTS

PREFACE

This PhD thesis aims to shed light on the origin of carbon phases in ureilites meteorites using a multimethodological approach by Scanning Electron Microscopy (SEM), Micro-Raman Spectroscopy, Micro-X-ray diffraction (XRD) and Transmission Electron Microscopy (TEM). I investigated the carbon phases (graphite and diamond) of various ureilites focusing on their characterization, determination of their crystallite size and temperature recorded by graphite. One of the most crucial goals of this PhD project is to understand the diamond formation process in ureilites. In particular, during these years I was involved as a team member in the project "Carbon minerals in Frontier Mountain ureilites of the Museo Nazionale dell'Antartide (COMMANDER)", Programma Nazionale di Ricerche in Antartide (PNRA) 2018 grant PNRA18 00247–A to F. Nestola (University of Padova). The manuscript about the results on five Frontier Mountain ureilitic samples whit different shock level is in preparation and will be submitted in a peer-reviewed journal in the next months.

One of the main problems in studying diamonds in ureilites (and in general in meteorites) is the conflicting hypotheses about diamond formation. In details, such hypotheses were the following: i) formation by chemical vapour deposition, ii) formation within a deep interior of a differentiated planetary body and iii) formation by shock event on prior graphite in a parent body. I am confident that the results obtained during my PhD research contributed to understand the best formation process candidate among the above hypotheses. In addition, I was able to investigate a) the role of Fe-Ni phases in diamond growth in ureilites and b) the temperature recorded by graphite on all studied meteorites (by Micro-Raman Spectroscopy) to understand if such temperature is related to the shock levels.

During these three years, I also collaborated with Prof. Brenker (University of Frankfurt, Germany), who introduced me to the Transmission Electron Microscopy, a very efficient technique to investigate the presence of stacking faults defect in ureilitic diamonds, which are usually identified as shock markers.

During my PhD period, before the restriction due to Covid 19, I spent a month in Wien where, under the supervision of Dr Lidia Pittarello (curator of the Natural History Museum Wien), I improved my knowledge about meteorite classification. My supervisors, Prof. M. C. Domeneghetti and Prof. F. Nestola, and I, with the help of Dr Lidia Pittarello, have also submitted to Meteoritical Bulletin a proposal for a new meteorite which was found in Lombardy (Italy) in June 2020.

In the meantime, I was involved in one side project named “Olivine-bearing ungrouped achondrites and their parent bodies (OL-BODIES)” by C. Carli. In this project, I selected the samples and performed the data reduction and the structural refinements of X-ray diffraction data collected on clino- and orthopyroxenes of some ungrouped achondrites in order to apply an intracrystalline geothermometer and provide information about the thermal history of the samples.

This PhD Thesis is organized into six chapters and two appendices:

Chapter 1 is the PhD thesis introduction which concerns a brief discussion of all the main aspects of state of the art on ureilites and carbon phases. Firstly, I reported the petrogenesis for these meteorites, paying attention to the shock evidence in ureilitic silicates. In addition, we reported the knowledge about carbon phases in ureilites before our works.

Chapter 2 is the paper entitled “Impact shock origin of diamond in ureilites” by Fabrizio Nestola, Cyrena A. Goodrich, Marta Morana, Anna Barbaro, Ryan S. Jakubek, Oliver Christ, Frank E. Brenker, M. Chiara Domeneghetti, M. Chiara Dalconi, Matteo Alvaro, Anna M. Fioretti, Konstantin D. Litasov, Marc D. Fries, Matteo Leoni, Nicola P. M. Casati, Peter

Jenniskensl, and Muawia H. Shaddad. It is the first paper from our research group on which we investigated three diamond-bearing ureilites (from Almahata Sitta ureilite and NWA 7983) by a multimethodological approach using scanning electron microscopy, micro-X-ray diffraction, transmission electron microscopy, and micro-Raman spectroscopy, with the purpose to investigate the origin of the diamonds. Our results show that the formation of both micro diamonds and nanodiamonds in ureilites can be explained by impact shock events on a small planetesimal and does not require long growth times at high static pressures within a Mercury- or Mars-sized body. This paper was submitted to Proceeding of the National Academy of Sciences journal on October 31st, 2019, accepted on August 12th, 2020 and published on September 28th, 2020. My contribution to this work was the acquisition of the XRD and TEM data, the data treatment of powder diffraction patterns and the determination of the crystallite sizes of graphite and diamond. I was also involved in writing the first draft of this manuscript and the supplementary information.

Chapter 3 is the paper entitled "Graphite based Gothermometry on Almahata Sitta Ureilitic Meteorites", by Anna Barbaro, M. Chiara Domeneghetti, Cyrena A. Goodrich, Moreno Meneghetti, Lucio Litti, Anna Maria Fioretti, Peter Jenniskens, Muawia H. Shaddad and Fabrizio Nestola. In this study, which is my first paper as first and corresponding author, in order to elucidate the nature of graphite in different ureilitic fragments of Almahata Sitta (AhS) ureilites, we performed micro Raman spectroscopy to apply a graphite-based geothermometer (recently applied to chondrites by Cody et al. 2008, and to other AhS ureilites by Ross et al. 2011) on graphite of three ureilitic AhS fragments (AhS 209b, AhS 72 and AhS A135A two of which were studied by XRD by Nestola et al. 2020). This paper was submitted to Minerals journal on October 13st, 2020, accepted on November 10th, 2020 and published on November 12th, 2020.

Chapter 4 is the paper entitled "Characterization of carbon phases in Yamato 74123 ureilite to constrain the meteorite shock history" by Anna Barbaro, Fabrizio Nestola, Lidia Pittarello, Ludovic Ferrière, Mara Murri, Konstantin D. Litasov, Oliver Christ, Matteo Alvaro and M. Chiara Domeneghetti. In this work, we present the results of a multi-methodological study on diamond and graphite aggregates observed in Yamato 74123, to add further hints on the shock formation of carbon phases in ureilites. In addition, a comparison with similar carbon phases in other ureilitic meteorites reported in literature, is also reported. This paper was submitted to the American Mineralogist journal on November 21st, 2021, accepted on March 3rd, 2021and published on March 1st , 2022.

Chapter 5 is the paper entitled "Origin of micrometer-sized impact diamonds in ureilites by catalytic growth involving Fe-Ni-silicide: The example of Kenna meteorite" by Anna Barbaro, M. Chiara Domeneghetti, Konstantin D. Litasov, Ludovic Ferrière, Lidia Pittarello, Oliver Christ, Sofia Lorenzon, Matteo Alvaro, Fabrizio Nestola. In this paper, we analyzed the carbon-bearing aggregates (diamond, graphite and other minor phases) of Kenna ureilite in order to understand their origin, following the same experimental approaches adopted by Nestola et al. (2020) and Barbaro et al. (2021). During our investigations, we found, for the first time in a ureilite (and the second occurrence in a natural sample), a recently discovered Ni_3Si phase called carletonmooreite. We submitted this paper to Geochimica et Cosmochimica Acta on March 5th, 2021, accepted on June 16th, 2021 and published on September 15th, 2021.

The conclusions of this PhD thesis, future perspectives and projects related to the current PhD topics are discussed in **Chapter 6**.

APPENDIX I reports the supplementary information related to the "Impact shock Origin of diamond in ureilite" paper, which are cited in it.

APPENDIX II lists the other activities that I carried out during the three years of my PhD.

CHAPTER 1

1 INTRODUCTION

The origin of carbon phases in meteorites is still a debated issue among the scientific community as it has a significant implication for the carbon cycle in our Solar System. Carbon phases occur in various meteorites, spanning from undifferentiated, like carbonaceous and enstatite chondrites, to differentiated meteorites, like achondritic ureilites and iron meteorites. The main expected outcome of this thesis is to provide further insights on the origin, formation, and relationships among carbon phases in ureilitic differentiated meteorites and focusing on the origin of diamond in these achondrites and on the diamond formation process.

1.1 Ureilites

1.1.1 Petrogenesis of ureilites

Ureilites represent the second largest group of achondrites (635 samples at the time of writing) after howardites-eucrites-diogenites (HED group). Ureilites are mainly composed of olivine and pigeonite with a significant presence of carbon (<10 wt%), Fe-Ni metal (<5 wt%), and traces of sulfide located along silicate grain boundaries (Goodrich et al. 1992; Collinet et al. 2020). In a few samples, orthopyroxene and augite are also found instead of or in addition to pigeonite (e.g., Takeda 1989; Goodrich et al. 2001). As reported in the literature, if we do not consider the brecciated ureilites (i.e., polymict ureilites) and a single monomict ureilite (Collinet et al. 2020), these achondrites are entirely devoid of plagioclase. The analysis on mafic silicates of ureilites suggested that the Ureilitic Parent Body (UPB) must have a diameter close to 180 km (Warren 2012). Also, the investigation of small asteroidal bodies, as the possible link to ureilitic daughter bodies (formed after the catastrophic disruption of the UPB), by Jennisken et al. (2010) assessed that probably the original dimension of the UPB diameter was <200 km. Goodrich (1992) reported that ureilites silicates (olivine and pigeonite) core compositions are very homogeneous in terms of Mg ratio and minor elements. In particular, as reported by Goodrich et al. (l987), intragrain variation in major or minor element concentrations was not found beyond analytical uncertainty among various ureilitic samples (see Table 1 of Goodrich et al. 1992). Narrow reduction rims on olivine grains, of about 10-100 ~µm, are usually present in contact with the carbonaceous matrix material, and this is recognized as a characteristic feature of ureilites (Berkley et al. 1980; Goodrich 1992). As evidenced in Fig. 1c of Goodrich (1992), these reduction rims usually consist of olivine and/or enstatite almost entirely depleted in FeO, but in these zones Fe-Ni metal inclusions usually occur. The boundaries between the reduction rims and the cores are slightly sharp, indeed as reported by Miyamoto et al. (1985) in their work on Antarctic ureilites, the zonation can be detected only over 30-40 µm. In addition, Goodrich (1992) reported that also ureilitic pigeonite grains can present reduction rims, consisting of enstatite with metal. The reduction rims in pigeonite crystals are usually narrower than the olivine reduction rims or may be absent. The reduction rims appear as consequences of the reaction between olivine or pigeonite grains and carbon which is present as interstitial material (Goodrich 1992).

It is common among the scientific community to affiliate all ureilitic fragments to the same parent body, the UPB. The UPB was catastrophically disrupted (Goodrich et al. 2004) by violent impact(s) event(s) while its internal temperature was estimated to be still high (about 1150 °C–1300 °C as reported in the literature by Takeda 1989; Sinha et al. 1997; Goodrich et al. 2004; Herrin et al. 2010). The abundance of graphite and oxygen isotopes found in ureilites point to a connection with carbonaceous chondrites as precursor material of the UPB (Clayton and Mayeda 1988; Goodrich et al. 2015). Instead, the nucleosynthetic anomalies in Cr, Ti, and Ni are more akin to ordinary chondrites and characteristic of the "non-carbonaceous group" (Warren 2011).

Another feature of ureilites is that their bulk composition is slightly depleted in incompatible lithophile elements and chalcophile elements compared to all chondrites. For this reason, as reported by Collinet et al. (2020), ureilites are described as ultramafic igneous cumulates (Berkley et al. 1980; Goodrich et al. 1987), and most of them are also usually recognized as residues of partial melting representing the mantle of a planetesimal that lost abundant Fe-Ni-sulfide eutectic melts (e.g., Warren et al. 2006; Goodrich et al. 2013) and silicate melts (Warren and Kallemeyn 1992; Scott et al. 1993; Barrat et al. 2016).

1.1.2 Shock evidences in ureilites

The optical evaluation of possible shock features in ureilitic silicates is crucial for interpreting the processes that involved the UPB. For example, some ureilites show mosaicized olivine and deformed pigeonite, suggesting a possible exposition of these minerals to shock event(s) at moderate-high temperature, possibly related to the breakup of the UPB or to its reassembly.

The optical determination of the shock level in silicates was firstly proposed by Stöffler et al. (1999) and then revised by Stöffler et al. (2018). These authors proposed six stages of shock, based on shock effects in olivine, pyroxene and plagioclase (if any). However, as Nakamuta et al. (2016) reported in their study, the shock features observed in ureilitic silicates need to be correlated with the carbon phases present in the samples. Fig. 1.1 shows the optical microscopy images of different shock level on ureilitic fragments reported by Nakamuta et al. (2016). The characteristic shock features usually observed in ureilites by optical microscopy for S1 level are: sharp optical extinction of olivine (unshocked); for S2 level: undulatory extinction of olivine (low shock degree); for S3 level: planar features in olivine (medium shock degree); for S4 level: mosaicism in olivine (moderate shock degree); for S5 level: isotropization of plagioclase (if any) and planar deformation features in olivine (high shock degree); and for S6 level: recrystallization of olivine (very high shock degree).

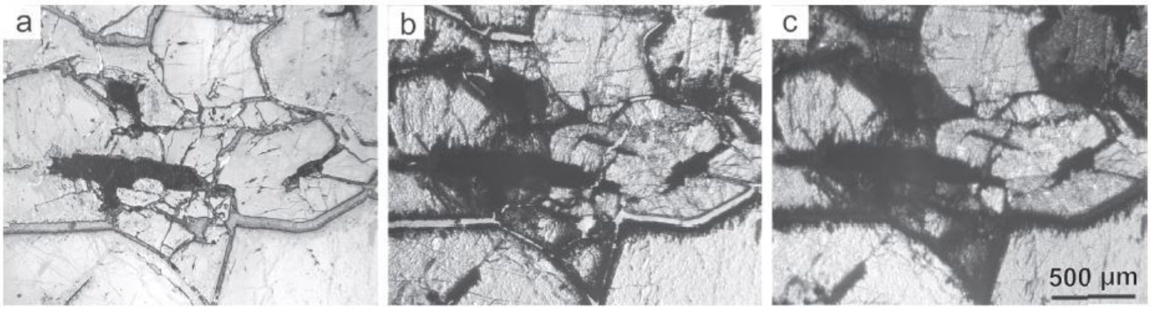

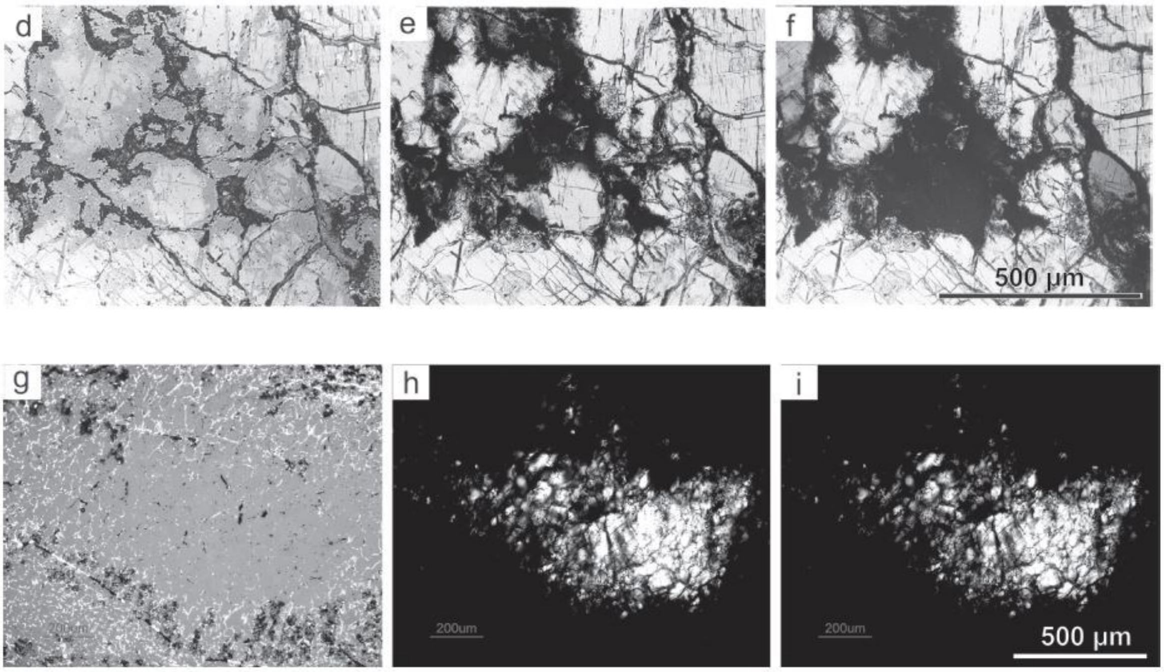

Fig.1.1 Optical microscope images of ureilites with low-shock (a, b, c), moderate-shock (d, e, f) and high-shock features (g, h, i), from Nakamuta et al. (2016).

The evaluation of the shock event(s) that affected a meteorite may be interpreted not only considering what is observed by optical microscopy but also considering the effects of shock impedance contrast between component minerals distributed through the meteorite (Ogilvie et al., 2011). In particular, shock impedance means the heterogeneity of the shock waves propagations attributed to the contrast between contiguous phases and, as Ogilvie et al. (2011) reported, this heterogeneous shock effect distribution is a signature of disequilibrium at low scale. The expression of shock amplification appears where shock impedance contrast is greatest, while shock suppression appears where shock impedance contrast is least (Ogilvie et al., 2011). Another method that could improve the estimation of the shock level was given by Vinet et al. (2011), who proposed for evaluating the shock level of some terrestrial olivine crystals (natural deformed samples) an approach based on Single Crystal X-Ray Diffraction technique (SCXRD) equipped with an area detector. SCXRD appeared to be easy to use, fast, low-cost, non-destructive and less ambiguous than optical microscopy. Since there are significant correlations between deformation intensity (strain-related mosaicity) and olivine composition and crystal size, it is possible by SCXRD to evaluate more in detail the shock level of a crystal. In particular, as reported by Flemming (2007), the two-dimensional images acquired with a General Area Detector Diffraction System (GADDS) yield information in both the 2θ and chi (χ) dimensions. Indeed, in the X-ray diffraction images, polycrystalline samples show powder rings, or Debye rings, indicative of small crystallites and/or crystals strained all orientated simultaneously. In contrast, unstrained single crystals are represented by sharp spots as indicator of a single orientation. Instead, for homogeneously strained crystals the strain-related mosaicity is reported in diffraction images as elongation or streaking along the Debye ring; it is possible to measure this elongation of the spots by χ angle. In Fig. 1.2 the model by Vinet et al. (2011) which simplifies in 2D the three different results observed by SCXRD at different shock levels is shown. In particular, as previously explained, the olivine crystal that optically exhibits low deformation (step 1) corresponds in XRD images to sharply defined spots; instead, olivine crystal which optically shows an increase of deformation with sub-grains formation (medium-high mosaicism), corresponds to the presence of stretched spots in XRD images (step 2); on the other hands, high level of deformation in olivine crystal occurs with asterism (step 3) in XRD images. As reported by Vinet et al. (2011), the asterism represents the migration of defects or dislocations to form line dislocations or sub-grain boundaries as the result of resolving strain within the crystal lattice.

This protocol by SCXRD was adopted also for some enstatite and ordinary chondrites (Izawa et al. 2011; Rupert et al. 2020), and also for ureilitic olivine crystals by Li et al. (2021). In particular, Li et al. (2021) in their study performed in situ micro-X-ray diffraction analysis with the aim to examine the strain-related deformation in ureilitic olivine. Fig. 1.2 shows that also in silicate of these meteorites the undeformed crystals exhibit single spots on the X-ray diffraction images (Fig.1.2, step 1 corresponds to the diffraction image of EET 96042 ureilites studied by Li et al. 2021), while crystals with an increase mosaic spread of orientations show streaked peaks along the Debye rings on the 2-D X-ray diffraction images (Fig.1.2, step 2 corresponds to the diffraction image of NWA 2221 ureilites studied by Li et al. 2021); moreover, olivine crystals which present high mosaicism show asterism in X-ray diffraction images (Fig.1.2, step 3 corresponds to the diffraction image of LAR 04315 ureilites studied by Li et al. 2021). In their paper, the authors claimed that the asterism can be used to reconstruct the mosaic spread of the original grain and thus its original strain condition prior to sub-grain formation.

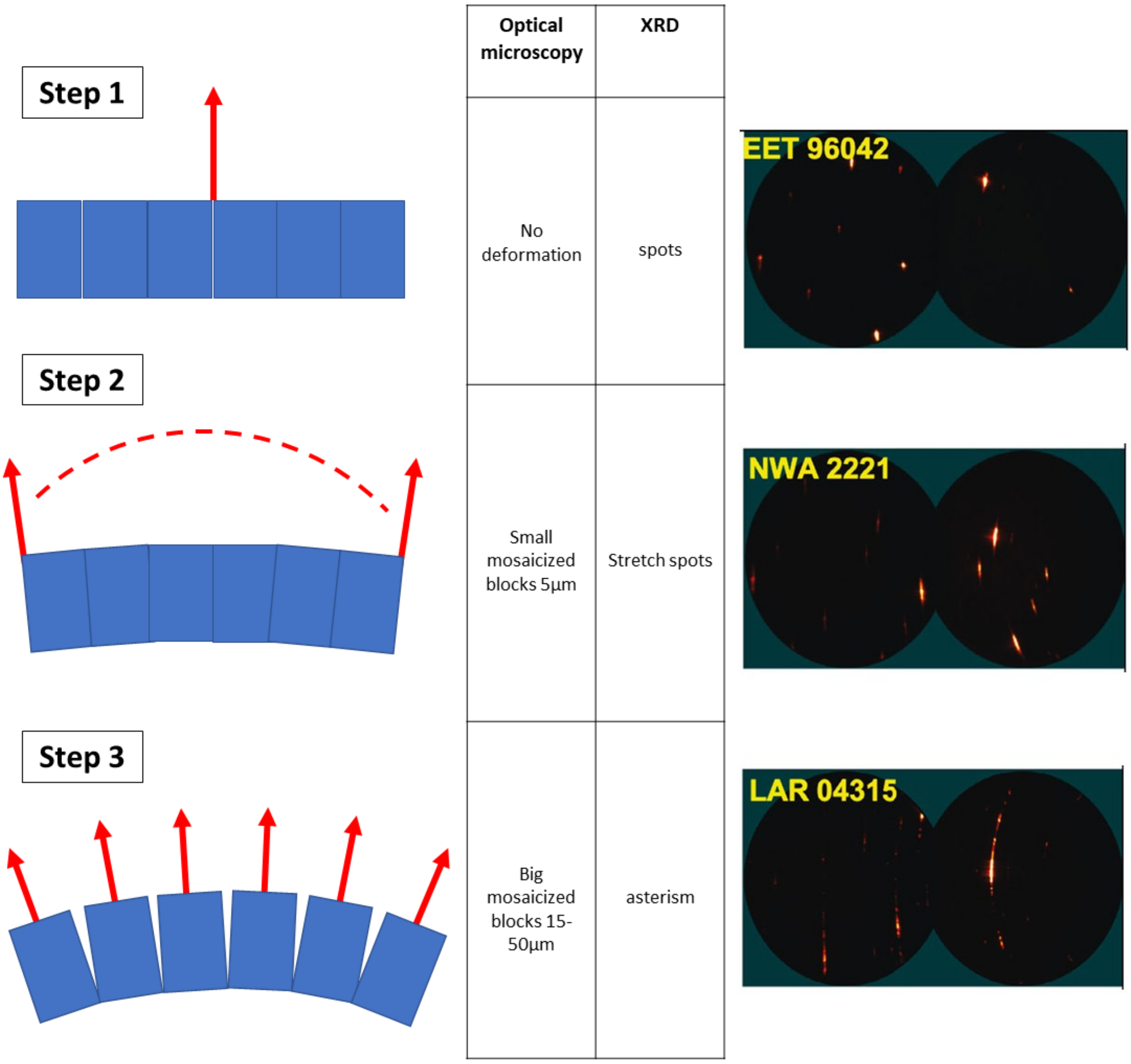

Optical microscopy	XRD
No deformation	spots
Small mosaicized blocks 5µm	Stretch spots
Big mosaicized blocks 15-50µm	asterism

Fig. 1.2 Gaphical representation of the three XRD different results observed at different shock levels by Vinet et al. (2011) on olivine crystal (on the left of the figure). On the right the diffraction images referred to EET 96042, NWA 2221 and LAR 04315 samples by Li et al. 2021 are reported. Modified image after Vinet et al. (2011) and Li et al. (2021).

1.2 Carbon phases in ureilites

As Lodders (2003) reported, carbon is one of the most abundant elements in the Solar System, but its abundance in ureilitic meteorites is less than 10%vol. The electron configuration of C allows this element to form a vast variety of chemical compounds such as organic species, carbonates, carbides, and allotropes (Storz et al., 2021).

In meteorites like ureilites, graphite and diamond are the primary carbon-bearing phases (Grady and Wright, 2003; Goodrich et al., 2015), usually located in the interstitial part of silicate phases and always mixed with Fe-Ni alloys. However, in addition to graphite and diamond, organic carbon compounds (e.g. the hydrocarbons in Almahata Sitta fragments reported by Sabbah et al. 2010) are also reported in some ureilitic fragments.

1.2.1 Graphite in ureilites

Graphite is the prevalent carbon phase in ureilitic meteorites. As reported in Fig. 1.3, hexagonal graphite has a crystal structure built of flat layers in which the carbon atoms occupy the lattice sites of a two-dimensional honeycomb network (Tuinstra and Koenig 1970) corresponding to the space group $P6_3/mmc$.

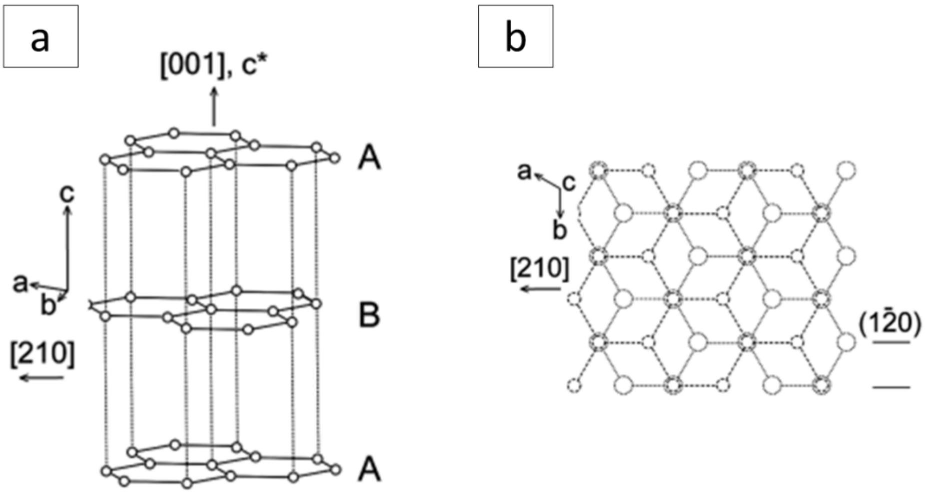

Fig.1.3 Crystal structure of hexagonal graphite, Fig.7a from Nakamuta et al. (2013).

Graphite consists of hexagonal networks of carbon atoms (Fig. 1.3) with covalent sp^2 bonding between C within a plane and weak Van der Waals interaction between planes (see Fig. 1.3a). The graphite unit cell parameters are a = 2.4560 and c =6.6960, α = 90° and γ = 120°, with a unit cell volume of 34.98 Å. In X-ray diffraction, the most intense peaks of graphite are: 3.34 Å (I = 100 %), 2.02 Å (I = 17 %) and 1.15 Å (I = 10 %). In addition to hexagonal graphite, Nakamuta and Aoki (2000) reported in their X-ray diffraction study of ureilites, also the presence of "compressed graphite". These authors observed the "compressed graphite" on the basis of a slightly smaller *d*-spacing of the highest peak compared to that of "normal" hexagonal graphite (*d*-spacing close to 3.2 Å compared to 3.34 Å) [see Table I of Nakamuta and Aoki (2000)]. Nakamuta and Aoki (2000) ascribed the presence of "compressed graphite" to the initial stage of the direct transformation from graphite to diamond and claimed that "the presence of the compressed graphite in ureilites, therefore, provides clear evidence that the diamond formed by high-pressure direct conversion of graphite".

1.2.2 Micro-Raman Spectroscopy of graphite

One of the best techniques to investigate carbon phases is the Micro-Raman Spectroscopy, as each carbon phase presents different features in Raman spectrum. In particular, Raman spectroscopy technique was very important in the past in the structural characterization of graphitic materials (Dresselhaus et al. 1988; Dresselhaus et al. 2005) such as pyrolytic graphite, carbon fibers (Dresselhaus et al. 1988) glassy carbon, nano-graphite ribbons (Cancado et al. 2004) fullerenes and carbon nanotubes (Saito et al. 1998). Indeed, the features that strongly affect the Raman spectra of graphite are based on the structural properties, such as in-plane crystallite size, and out-of-plane stacking order (Pimenta et al. 2007 and references therein). The vibrational modes of graphite are referred to $2E_{2g}$, $2B_{2g}$, E_{lg}, and A_{1g} (Tuinstra and Koenig 1970, Ferrari and Robertson 2000; 2004), but only the two E_{2g} modes are

Raman active and have been identified with the Raman band close to 1580 cm^{-1}, called G band. In a highly ordered pyrolytic graphite sample, we should observe a spectrum which presents only the 1580 cm^{-1} band in the fundamental first Raman order region between 1100 and 1800 cm^{-1}, and in addition features on the second Raman order region between 2400 and 3300 cm^{-1} (Nemanich and Solin, 1979; Beyssac et al. 2002). In particular, Nemanich and Solin (1979) indicate the strong feature on the second Raman order close to ~ 2720 cm^{-1} and weaker peaks close to ~2450 and 3248 cm^{-1}. In graphite presenting some disorder level a band close to 1350 cm^{-1} Raman shifts is present; in this case, the band at 1350 cm^{-1} appears, due to the new vibrational modes of the lattice that may then become active. In particular the A_{1g} mode became active, as proposed by Tuinstra and Koenig (1970). Raman spectra of ureilitic graphite usually show first order Raman bands at ~1580 cm^{-1} and ~1352 cm^{-1} and sometimes at ~1620 cm^{-1}. As reported above, these bands are the so-called G-band, D-band and D'-band of graphite, respectively (Ferrari and Robertson, 2000). Tuinstra and Koenig (1970) reported in their work that the spectrum of graphite changes significantly for finite-sized microcrystallites ($L_a < 1000$ Å), but the origin of the changes is not clear. The most obvious effect is the appearance of a band close to 1350 cm^{-1} which increases its intensity with decreasing of the microcrystallite size. These relations were reported by Tuinstra and Koenig (1970), who noted an important relationship between the ratio of the intensity of D-band and G-band (I(D)/I(G)) and the average of the crystalline size of graphite (L_a) [$I(D)/I(G) = C(\lambda L)/L_a$]. In the equation proposed by these authors, the presence of the parameter C ($\lambda L = 514$ nm) is related to the wavelength of the laser used during the data acquisition and, in their work, it corresponds to ~ 44 Å (the wavelength-dependent prefactor). The wavelength dependency of C was considered by Matthews et al. (1999), who reported the following relation: $C(\lambda L) \approx C0 + \lambda LC1$, where $C0 = -12.6$ nm and $C1 = 0.033$, valid for wavelength (λL) between 400 nm and 700 nm.

1.2.3 Graphite-based geothermometry

Graphite was deeply investigated in order to retrieve the temperatures of graphite-bearing terrestrial rocks. The most cited graphite-based geothermometer was published by Beyssac et al. (2002) and is based on the broadening of graphite peaks by micro-Raman spectroscopy. This geothermometer was developed for carbonaceous material contained in metasedimentary rocks and can be applied to rocks which underwent temperatures between about 330 and 650± 50 °C. However, Cody et al. (2008) reported that carbonaceous material and graphite present in terrestrial rocks were never subjected to the high temperatures, which can be typical of meteorites rocks (e.g. the graphite present in the veins of graphitic marble records metamorphic fluid temperature close to 600 to 700 °C). These authors developed a new Raman based graphite geothermometer to be used for higher temperatures with respect to the Beyssac et al. (2002) geothermometer. Cody et al. (2008) identified a unique spectroscopic feature using carbon X-ray Absorption Near-Edge Structure (XANES) spectroscopy investigating twenty-five different samples of meteoritic insoluble organic matter (IOM) spanning multiple chemical classes, groups, and petrologic types of chondrites. Cody et al. (2008) in their manuscript showed a relationship between the petrological type and $T_{\underline{max}}$: the higher the petrological type, the higher the experienced T_{max}. The intensity of 1s−σ∗ exciton appeared to provide a precise measure of parent body thermal metamorphism for chondrites. Moreover, Cody et al. (2008) observed a good correlation between the intensity of the 1s−σ∗ exciton and previously published micro-Raman spectral data (Busemann et al. 2007). Cody et al. (2007) correlated the data obtained on a large set of samples (many of them analyzed by Busemann et al., 2007) using the line width of the so-called Raman G-band with the aim to estimate the parent body maximum temperature through a Raman based thermometric expression. This geothermometer (Eq. 1) can be used and applied to graphite Raman spectra of ureilites, by estimating the Full Width at Half Maximum (FWHM) of the G-band of graphite, which is indicated in Eq.1 with Γ.

(1) $$T_{max}(°C) = 1594.4 - 20.4\Gamma_{G} - 5.8 \times 10^{-2}\Gamma_{G}^{2}$$

In particular, the Eq. 1 given by Cody et al. (2008) was used for the first time on ureilites by Ross et al. (2011), who in their study on sample AhS#7 calculated a temperature recorded by graphite close to 900± 120 °C (2σ). In particular, the temperature measured by Ross et al. (2011) for AhS#7 sample slightly overlap with those reported for equilibration temperatures measured adopted other mineral-based geothermometer (e.g. Herrin et al. 2010). The error of ± 120 °C, was assumed by Cody et al. (2008) as the uncertainty in the T_{max} represented by the distribution of points off curves of their Eq. 5 (Cody et al. 2008). However, Ross et al. (2011) in order to adopt the same equation by Cody et al. (2008) (Eq. 1) had to use a standard calibration material to determine the instrumental broadening (e.g., each micro-Raman spectrometer shows its typical peak broadening) and used for this purpose a high-quality octahedral gemstone lithospheric diamond, which was collected using the same instrument used by Cody et al. (2008). Ross et al. (2011) in their work reported that also graphite of their studied ureilitic fragments presents the G-band at around 1580 cm^{-1} (which is inherent to ordered graphite), the D-band at around 1350 cm^{-1} (which is defect-induced) and a third band, named D′-band that may also be observed at around 1620 cm^{-1} as a shoulder on the G-band.

1.2.4 Diamonds in ureilites: the three hypotheses on their origin

Diamond was commonly found in ureilitic meteorites (Urey 1956; Lipshutz 1964; Fukunaga et al. 1987). It has a cubic crystal structure built of carbon atoms with sp^3 covalent bond that occupy layers stacked in a repeating ABCABC structure; the schematic representation of this structure is shown in Fig. 1.5.

Diamond has a cubic unit cell with the cell edge *a* = 3.5668 Å and unit cell volume of 45.38 Å^3. In X-ray diffraction, the highest peaks of diamond are: 2.06 Å (I = 100%), 1.26 Å (I = 39%) and 1.07 Å (I = 10 %).

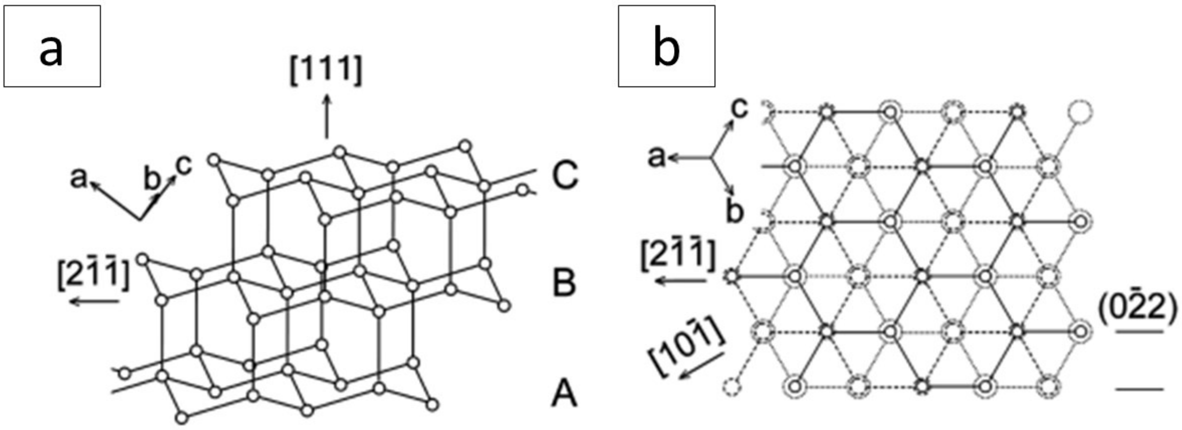

Fig. 1.5 Crystal structure of cubic diamond, Fig.7c from Nakamuta et al. (2013).

The presence of diamond in ureilites was reported for the first time in Novo Urei meteorite by Jerofejeff and Satschinoff (1888), and since then, the scientific community has been questioning the origin formation process of this high-pressure carbon phase. The most accepted hypotheses about the origin of diamond in ureilites are: i) formation under high static pressure in the deep interior of a planetary body, similar to Earth's mantle diamonds (Urey 1956), ii) shock formation from a prior carbon (probably graphite) present on the UPB (Lipschutz, 1964) and iii) formation by chemical vapour deposition (CVD) prior to the accretion of UPB (Fukunaga et al., 1987). These hypotheses are well resumed and explained in Goodrich et al. (2021).

The first of these hypotheses was proposed by Urey (1956), who suggested that diamond formed under static high pressures in a large, at least Moon-sized, parent body. On this hypothesis, some criticisms have been raised (see Goodrich et al. 2021 and references therein), based not only on diamond properties but also on the hypothetical size of the asteroidal parent body of ureilites, which was supposed to be too small to ensure the formation condition for diamonds (a few hundred kilometres in diameter, e.g. Warren 2012). However, the same hypothesis formulated by Urei (1956) was recently supported by Miyahara et al. (2015) and Nabiei et al. (2018). These authors studied diamonds in MS-170 Almahata Sitta (AhS) polymict ureilite. They found that in the carbon areas, diamonds are particularly abundant and that they often occur as tens of micrometer-sized clusters of isolated grains; in their study (in which no X-ray diffraction was performed to test the size of the diamond grains), the authors assessed that these diamond clusters presented similar crystallographic orientations and interpreted them as remnants of up to 100 µms in size single diamond crystal. The study of MS-170 AhS fragment have led Nabiei et al. (2018) to conclude that the parent body of ureilites must have been at least Mars-sized. In addition, a recent work by Desch et al. (2019) proposed that diamond formed in the interior of Mars and then ejected during an impact; in this scenario, the fragments generated from this impact became intermixed with ureilitic material (Desch et al. 2019).

A second hypothesis about the diamond formation process was proposed by Lipschutz (1964), who argued that the nanometer-size of diamonds and the observation of their preferred orientation are indicators of direct transformation from graphite by shock during an impact event. Lipschutz (1964) relied his assumption on the X-ray pattern of diamonds found in Goalpara, Zachariasen, Dyalpur and Novo Urei [the same meteorite studied by Urey (1956)], and in his work, he stated that his results were similar to those of diamonds synthesized at dynamic shock pressure of 30 GPa. Lipschutz (1964) also reported a measure of the crystallite size providing an estimation of the average crystallite size for Goalpara and Zachariasen meteorites close to 10 nm and above 30 nm for Dyalpur and Novo Urei ureilites, respectively. Since 1964 the methods to estimate the crystallite sizes from XRD powder diffraction patterns have been improved thanks to the line profile analysis fitting using different software (e.g.

HighScore Plus, Topas, DiffaX). This allowed to obtain the Integral Breadth values (see Fig. 1.6) of the diffraction peaks, through which it is possible to determine the crystallite size using the Scherrer equation (Eq.2):

(1)
$$\beta(2\theta) = \frac{K_\beta \times \lambda}{<D>_V \cos\theta_{hkl}}$$

Eq. 2 gives a correlation between peak broadening (β) of the peak at the 2θ (°) position (where θ is the Bragg angle), the dimension of the diffracted domain and the crystallite size (D_V). K is a constant value between 0.5 and 1, and describes the contribution of crystallites shape. K is a parameter that depends on the scattering vector's relative orientation to the crystallite's external shape. In detail, as reported in the graphical representation of Fig. 1.6, with an increase of the integral breadth value, the crystallite size decreases, while a decrease of the integral breadth value corresponds to an increase of the crystallite size.

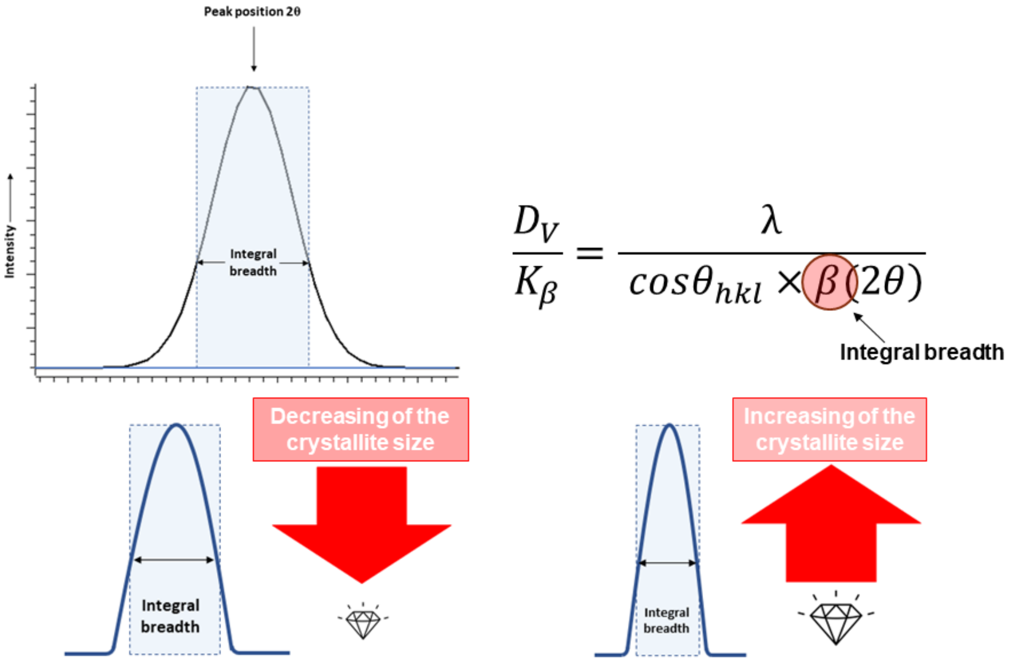

Fig. 1.6 Graphical representation of the Integral Breadth and of the crystallite size variation related to the Integral Breadth.

Lipschutz (1964) showed the simultaneous presence of graphite, diamond, and kamacite in their ureilitic fragments, suggesting that these carbon-bearing grains were not equilibrium assemblages. However, even if he claimed the shock event as the origin of these phases in ureilites, the question of whether these assemblages represented an arrested stage in the conversion of graphite to diamond (or vice versa) and the process through which they formed during the impact event, remained unsolved. The shock formation origin was also supported by Nakamuta et al. (2016), who observed the same simultaneous presence of graphite, nano- and micro- diamonds. In particular, one of the points supporting the formation of ureilitic diamond by shock event(s) is also the presence of lonsdaleite (Nakmuta et al. 2013; Nakamuta et al. 2016). Lonsdaleite is a carbon phase (IMA 1966-044) consisting of hexagonal carbon planes stacked with the AB′-sequence, which buckle to form boat-type connections with adjacent planes (Nakamuta et al., 2013 and references therein), which is considered as shock indicator (Németh et al. 2014). More recently, lonsdaleite recently was proposed to be a nano-twinning diamond with stacking-disordered sequences (Murri et al. 2019; Nèmeth et al. 2020).

Some years later, Fukunaga et al. (1987) proposed a third hypothesis about the formation process for ureilitic diamonds based on the chemical vapour deposition (CVD) in the solar nebula. In the CVD synthesis of diamonds, the substrate [for example in the experiment by Fukunaga et al. (1987) they used scratched silicon wafer substrates, but it is possible to use alumina or carbides as used by (Knight and White (1989)] is exposed to C gaseous precursors, which react and/or decompose on the substrate surface to produce the desired diamond and graphite deposit. As reported by Grossman and Larimer (1974), the major element of the solar nebula was hydrogen, and even if Fukunaga et al. (1987) assumed that CO is the dominant carbon-bearing compound at high temperature, so this phase progressively transformed to CH_4 on cooling. In their work, Fukunaga et al. (1987) synthesized diamonds by CVD from a gaseous mixture of H_2 and CH_4, including Argon (Ar), using experimental apparatus. These authors included Ar in the gaseous mixture because they want to try to explain the process through which a large number of noble gases concentrated in carbon veins of ureilites. For this reason, they used a mass spectrometry instrument to measure the Ar entrapped in the CVD synthesized diamonds. Nagashima et al. (2012) also supported the CVD diamond formation assessing that the shifts of the diamond Raman peak position to higher-wave number(of + 2-4 cm^{-1}) is a strong indicator of this formation process and that the shock model cannot explain the elemental and isotopic features of noble gases and nitrogen for graphite and diamond.

1.2.5 The role of Fe-Ni in diamond growth

Carbon phases are always present in ureilitic samples mixed with Fe-Ni compounds, posing the question of whether there is any correlation between the diamond growth and the presence of these phases.

Since the first reproducible experiment of diamond synthesis carried out in 1950 (Bundy et al. 1955) by General Electric Co. (at P=5GPa and T=1400-1600°C) using a high-pressure and high-temperature method, the growth of diamonds has attracted considerable interest due to their industrial use (e.g. machine tools, optical coatings, high-temperature electronics, etc.). Industrial synthesis of diamond was successful in both low-pressure and high-temperature [chemical vapor deposition (CVD) method], and high-pressure and high-temperature conditions. Diamond at high PT conditions was synthesized with metal–solvent catalysts (Bundy et al., 1955; Bovenkerk et al., 1959), from a COH supercritical fluid (e.g. Akaishi and Yamaoka, 2000), and directly from graphite without any catalysts (Irifune et al., 2003). Fig. 1.7 shows the phase diagram of carbon for fast direct reaction (image Fig. 2 by Dobrzhinetskaya 2011), in which the stability pressure-temperature regions for diamond and graphite (Fig. 1.7), together with the condition of diamond synthesis are shown.

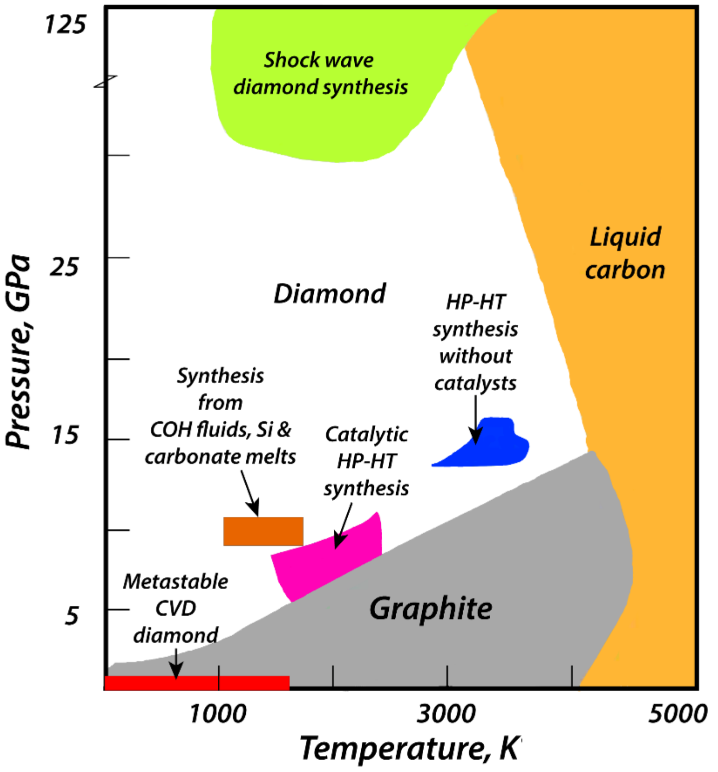

Fig. 1.7 Figure 2 from Dobrzhinetskaya (2011). The image shows the phase diagram of elemental carbon (Bundy, 1980) with additional fields of diamond syntheses from C–O–H fluids and Si and carbonate melts (data adopted from Akaishi et al., 1990; Hong et al., 1999; Pal'yanov et al., 1999; Akaishi and Yamaoka, 2000; Arima et al., 2002; Pal'yanov et al., 2000; Sokol et al., 2000; Kumar et al., 2001; Sokol et al., 2001; Pal'yanov et al., 2002; Dobrzhinetskaya et al., 2004; Dobrzhinetskaya and Green, 2007b).

The conversion of graphite into diamond is characterized by a small, positive value of $\Delta G°$ ($C_{graphite} \leftrightarrow C_{diamond}$ $\Delta G° = + 2895$ J g-atom^{-1} at 25 °C and 1 atm;), and this indicates that thermodynamically diamond is more unstable than graphite at those conditions and that the reaction proceeds from diamond to graphite (Ferro 2002).

Among different methods adopted to synthesize diamond, the most widely used are the CVD and the shock methods (De Carli 1995, 2002; Sung 2000; Ferro 2002). Direct transformation of the graphite to diamond without any metal-solvent catalysts, or a COH fluid, would have occurred at P>12 GPa and T=2000 °C according to experiments. (Bundy et al. 1980). However, usually in both methods, the synthesis of diamond has been accompanied by metal catalysts, such as Fe, Co, and Ni (Achard et al. 2020; Chen et al. 2020), to improve the nucleation and growth of diamond crystals. Indeed, as clearly evidenced in Fig. 1.7, the synthesis of diamond with the presence of catalysts occurred at lower P-T conditions compared to diamond formed by non-catalytic synthesis.

In most diamond synthesis processes, diamond formation usually occurs in very thin film of molten metal in contact with graphite (Strong et al. 1967, Bundy et al. 1996). As reported by Strong et al. (1967), in diamond synthesis process the growth rates ranging from 0.2 to 0.4 μm/s at 5.4 GPa and 1127 °C to 30 to 60 μm/s at 4.5 GPa and 1100 to 1200 °C (Bezrukov et al. 1975). However, as demonstrated by Varfolomeeva (1968), diamond can be formed also using a technique of pulsed heating of a graphite-metal experimental charge in a static high-pressure apparatus at 8 to 14 GPa. This author reported the formation of diamonds up to 10 μm in size near the catalyst and nanodiamonds in other parts of the experimental charge (Fig. 1.8). Varfolomeva (1968) and Vereschagin et al. (1977) reported in their works (see Fig. 1.8) an example of sample configuration of ballas-type (a-b) and carbonado-type (c-d) synthesis of polycrystalline diamonds (in toroid-type apparatus) from graphite with the help of metal catalysts. This apparatus (Fig. 1.8) simulates natural impact processes with respect to the duration of peak pressures and temperatures. For example, in Fig.1.8, microphotographs of diamond crystallites near and away from metal catalyst synthesized at 8 GPa and 2000°C for 1-2 s run duration are shown (Varfolomeva 1968). At the beginning of their experiments, the graphite sample was compressed to the target at pressure of about 6 GPa and then single-time pulse-heated was applied. In calibrated experiments, the electric power used for these experiments corresponds to about 2000 °C. According to static experiments, the pressure applied simultaneously on the sample was 7-9 GPa, where the pressure increase rate during heating is 0.7-1 MPa/°C (Varfolomeva 1968; Vereschagin et al., 1977). These authors observed that, in less than 1-2 seconds, they had the total transformation of a 6-7 mm graphite source to nanocrystalline diamonds with grain size from 10 nm to 1 µm in the bulk sample and up to 5-10 µm crystals in the area close to the metal catalyst.

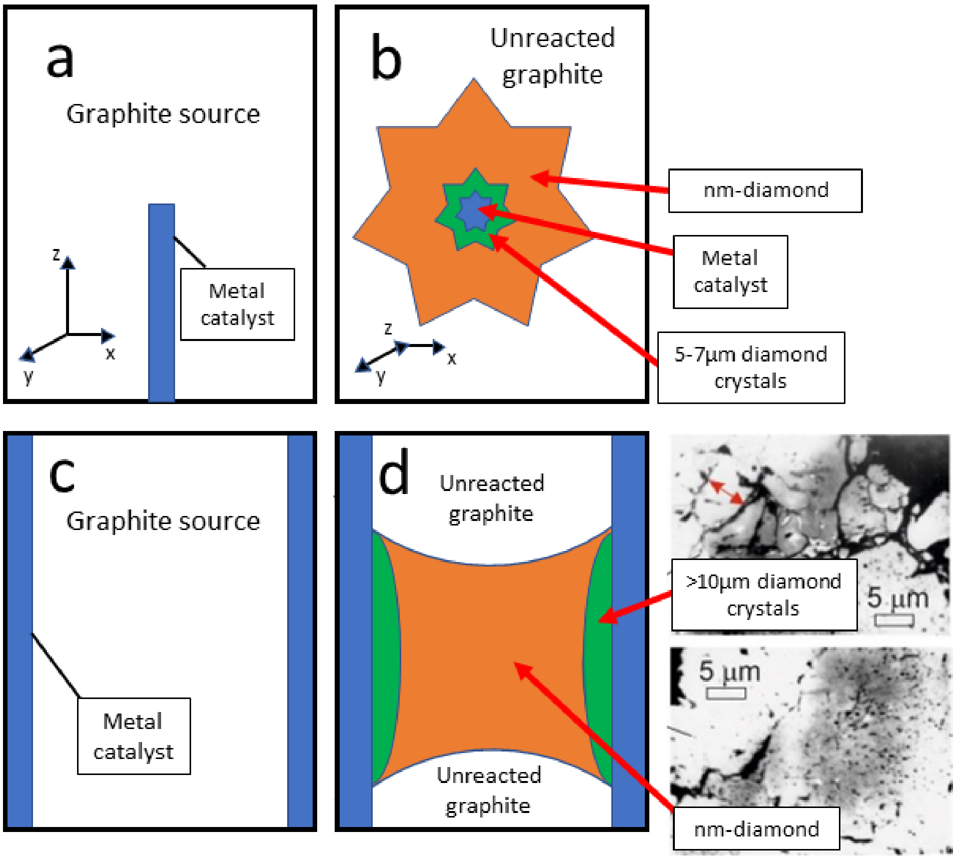

Fig. 1.8 An example of sample configuration for the synthesis of polycrystalline diamonds of ballas-type (a-b) and carbonado-type (c-d) in toroid-type apparatus. Modified after Varfolomeva (1968).

The toroid-type device is considered a traditional static HP device, not a shock device, but the pulsed heating in this experiment simulates shock. Therefore, we can consider this experiment, carried out by Varfolomeva (1968) and Vereschagin et al. (1977), as a close analogue of the long duration shock event in the natural impact process.

1.3 References

Achard, J., Jacques, V., and Tallaire, A. "Chemical vapour deposition diamond single crystals with nitrogen-vacancy centres: a review of material synthesis and technology for quantum sensing applications." Journal of Physics D: Applied Physics 53.31 (2020): 313001.

Akaishi, M., and Yamaoka, S. “Crystallization of diamond from C–O–H fluids under high-pressure and high-temperature conditions.” Journal of Crystal Growth, 209, no. 4, (2000): 999-1003.

Barrat, J.-A., Jambon, A., Yamaguchi, A., Bischoff, A., Rouget, M.-L., and Liorzou, C. "Partial melting of a C-rich asteroid: Lithophile trace elements in ureilites." Geochimica et Cosmochimica Acta 194 (2016): 163-178.

Berkley, J. L., Taylor, G. J., Keil, K., Harlow, G. E., and Prinz, M. "The nature and origin of ureilites." Geochimica et Cosmochimica Acta 44, no. 10 (1980): 1579-1597.

Beyssac, O., Goffé, B., Chopin, C., and Rouzaud, J. N. "Raman spectra of carbonaceous material in metasediments: a new geothermometer." Journal of metamorphic Geology 20, no. 9 (2002): 859-871.

Bezrukov, G. N., Butuzov, V. P., Vorzheikin, K. F., Korolev, D. F., and Laptev, V. A. “Kinetic features of diamond crystallization.” In РОСТ КРИСТАЛЛОВ/Rost Kristallov/Growth of Crystals (pp. 74-77). Springer, Boston, MA, 1975.

Bovenkerk, H. P., Bundy, F. P., Hall, H. T., Strong, H. M., and Wentorf, R. H. “Preparation of diamond.” Nature, 184, no. 4693, (1959): 1094-1098.

Bundy, F. P., Hall, H. T., Strong, H. M., and Wentorfjun, R. H. "Man-made diamonds." Nature 176, no. 4471 (1955): 51-55.

Bundy, F. P., Bassett, W. A., Weathers, M. S., Hemley, R. J., Mao, H. U., and Goncharov, A. F. "The pressure-temperature phase and transformation diagram for carbon; updated through 1994." Carbon 34, no. 2 (1996): 141-153.

Bundy, F. P. “The P, T phase and reaction diagram for elemental carbon, 1979.” Journal of Geophysical Research: Solid Earth, 85, no. B12, (1980): 6930-6936.

Busemann, H., Alexander, M. O. D., & Nittler, L. R. “Characterization of insoluble organic matter in primitive meteorites by microRaman spectroscopy.” Meteoritics & Planetary Science, no. 42, (2007): 1387-1416.

Cancado, L. G., Pimenta, M. A., Neves, B. R. A., Dantas, M. S. S., & Jorio, A. “Influence of the atomic structure on the Raman spectra of graphite edges.” Physical review letters, no. 93, (2004): 247401.

Chen, N., Zhang, G., Li, R., Xu, G., Wang, F., Ma, H., and Jia, X. "Defect and stress reduction in high-pressure and high-temperature synthetic diamonds using gradient cooling technology." Crystal Growth & Design 20, no. 5 (2020): 3358-3364.

Clayton, R. N., and Mayeda, T. K. "Formation of ureilites by nebular processes." Geochimica et Cosmochimica Acta 52, no. 5 (1988): 1313-1318.

Cody, G. D., Yabuta, H., Kilcoyne, A. L. D., Araki, T., Ade, H., Dera, P., Fogel, M., Militzer, B., and Mysen, B. O. "Organic thermometry for chondritic parent bodies." Earth and Planetary Science Letters 272, no. 1-2 (2008): 446-455.

Collinet, M., and Grove, L. T. "Incremental melting in the ureilite parent body: Initial composition, melting temperatures, and melt compositions." Meteoritics & Planetary Science 55, no. 4 (2020): 832-856.

De Carli, P. S. "Shock wave synthesis of diamond and other phases." MRS Online Proceedings Library (OPL) 383 (1995).

De Carli, P. S., Bowden, E., Jones, A., and Price, G. “Laboratory impact experiments versus natural impact events” in Catastrophic Events and Mass Extinctions: Impacts and Beyond, C. Koeberl, K. G. MacLeod, Eds. (GSA Special Paper, Geological Society of America, Boulder, CO, no. 356, (2002): 595–605.

Desch, S. J., O'Rourke, J. G., Schaefer, L. K., Sharp, T. G., and Schrader, D. L. "Diamonds in ureilites from Mars." In Lunar and Planetary Science Conference, no. 2132, (2019): 1646.

Dobrzhinetskaya, L. F. “Microdiamonds—frontier of ultrahigh-pressure metamorphism: a review.” Gondwana Research, 21, no. 1, (2012): 207-223.

Dresselhaus, M. S., Dresselhaus, G., Sugihara, K., Spain, I. L., & Goldberg, H. A. “Synthesis of graphite fibers and filaments.” Graphite fibers and filaments, (1988): 12-34.

Dresselhaus, M. S., Dresselhaus, G., Saito, R., & Jorio, A. “Raman spectroscopy of carbon nanotubes.” Physics reports. 409, no. 2 (2005): 47-99.

Ferrari, A. C., and Robertson, J. “Interpretation of Raman spectra of disordered and amorphous carbon.” Physical review B, 61, no. 20, (2000): 14095.

Ferrari, A. C., and Robertson, J. “Raman spectroscopy of amorphous, nanostructured, diamond–like carbon, and nanodiamond.” Philosophical Transactions of the Royal Society of London. Series A: Mathematical, Physical and Engineering Sciences, 362, no. 1824, (2004): 2477-2512.

Ferro, S. “Synthesis of diamond.” Journal of Materials Chemistry, 12, no. 10, (2002): 2843-2855.

Flemming, R. L. “Micro X-ray diffraction (μXRD): a versatile technique for characterization of Earth and planetary materials.” Canadian Journal of Earth Sciences, 44, no. 9, (2007): 1333-1346.

Fukunaga, K., Matsuda, J. I., Nagao, K., Miyamoto, M., and Ito, K. “Noble-gas enrichment in vapour-growth diamonds and the origin of diamonds in ureilites.” Nature, 328, no. 6126, (1987): 141-143.

Goodrich, C. A., Jones, J. H., & Berkley, J. L. Origin and evolution of the ureilite parent magmas: Multi-stage igneous activity on a large parent body. Geochimica et Cosmochimica Acta, (1987): 51(9), 2255-2273.

Goodrich, C. A. "Ureilites: A critical review." Meteoritics 27, no. 4 (1992): 327-352.

Goodrich, C. A. "Magmatic inclusions in Frontier Mountain 90054 and Elephant Moraine 96328: complex petrogenesis of the olivine-(augite)-orthopyroxene ureilites." In Lunar and Planetary Science Conference, (2001): 1300.

Goodrich, C. A., Scott, E. RD, and Fioretti, A. M. "Ureilitic breccias: clues to the petrologic structure and impact disruption of the ureilite parent asteroid." Geochemistry 64, no. 4 (2004): 283-327.

Goodrich, C. A., Ash, R. D., Van Orman J. A., Domanik K., and McDonough W. F. "Metallic phases and siderophile elements in main group ureilites: Implications for ureilite petrogenesis." Geochimica et Cosmochimica Acta 112 (2013): 340-373.

Goodrich, C. A., Hartmann W. K., O'Brien D. P., Weidenschilling S. J., Wilson L., Michel, P., and Jutzi, M. "Origin and history of ureilitic material in the solar system: The view from asteroid 2008 TC3 and the Almahata Sitta meteorite." Meteoritics & planetary science 50, no. 4 (2015): 782-809.

Goodrich, C. A., Nestola, F., and Jakubek, R. S. "Diamonds in Ureilites: the Never-Ending Story." Elements: An International Magazine of Mineralogy, Geochemistry, and Petrology 17.4 (2021): 292-293.

Grady, M. M., and Wright I. P. "Elemental and isotopic abundances of carbon and nitrogen in meteorites." Space Science Reviews 106, no. 1 (2003): 231-248.

Grossman, L., and Larimer, J. W. “Early chemical history of the solar system.” Reviews of Geophysics, 12, no. 1, (1974): 71-101.

Herrin, J.S., Zolensky, M.E., Ito, M., Le, L., Mittlefehldt, D.W., Jenniskens, P., Ross, A.J. and Shaddad, M.H. “Thermal and fragmentation history of ureilitic asteroids: Insights from the Almahata Sitta fall.” Meteoritics & Planetary Science, n.o. 45(10-11), (2010): 1789-1803.

Irifune, T., Kurio, A., Sakamoto, S., Inoue, T., and Sumiya, H. “Correction: ultrahard polycrystalline diamond from graphite.” Nature, 421(6925), (2003): 806-806.

Izawa, M. R., Flemming, R. L., Banerjee, N. R., & McCausland, P. J. “Micro-X-ray diffraction assessment of shock stage in enstatite chondrites.” Meteoritics & Planetary Science, no. 46(5), (2011): 638-651.

Jerofejeff, M., and Satschinoff, I., (1888). Sot: Russe Miner. 24, 263.

Knight, D. S., and White W. B. "Characterization of diamond films by Raman spectroscopy." Journal of Materials Research 4, 2 (1989): 385-393.

Lipschutz, M. E. "Origin of diamonds in the ureilites." Science 143, no. 3613 (1964): 1431-1434.

Li, Y., McCausland, P. JA, and Flemming, R. L. "Quantitative shock measurement of olivine in ureilite meteorites." Meteoritics and Planetary Science (2021): 1422-1439.

Lodders, K. "Solar system abundances and condensation temperatures of the elements." The Astrophysical Journal 591, no. 2 (2003): 1220.

Matthews, M. J., Pimenta, M. A., Dresselhaus, G., Dresselhaus, M. S., and Endo, M. “Origin of dispersive effects of the Raman D band in carbon materials.” Physical Review B, 59, no.10, (1999): 6585.

Miyamoto, M., Takeda, H., and Toyoda, H. "Cooling history of some Antarctic ureilites." Journal of Geophysical Research: Solid Earth 90, no. S01 (1985): 116-122.

Miyahara, M., Ohtani E., El Goresy, A., Lin Y., Feng, L., Zhang, J. C., Gillet, P., Nagase, T., Muto, J., and Nishijima, M. "Unique large diamonds in a ureilite from Almahata Sitta 2008 TC3 asteroid." Geochimica et Cosmochimica Acta 163 (2015): 14-26.

Murri, M., Smith, R. L., McColl, K., Hart, M., Alvaro, M., Jones, A. P., Németh, P., Salzmann, C. G., Corà, F., Domeneghetti, M. C., Nestola, F., Sobolev, N. V., Vishnevsky, S. V., Logvinova, A.M. and McMillan, P. F. “Quantifying hexagonal stacking in diamond.” Scientific reports, 9, no.1, (2019): 1-8.

Nabiei, F., Badro, J., Dennenwaldt, T., Oveisi, E., Cantoni, M., Hébert, C., El Goresy, A., Barrat, J.-A., and Gillet, P. "A large planetary body inferred from diamond inclusions in a ureilite meteorite." Nature communications 9, no. 1 (2018): 1-6.

Nagashima, K., Nara, M., and Matsuda, J. "Raman spectroscopic study of diamond and graphite in ureilites and the origin of diamonds." Meteoritics & Planetary Science, 47.11 (2012): 1728-1737.

Nakamuta, Y., and Aoki, Y. "Mineralogical evidence for the origin of diamond in ureilites." Meteoritics & Planetary Science 35, no. 3 (2000): 487-493.

Nakamuta, Y., and Toh, S. Transformation of graphite to lonsdaleite and diamond in the Goalpara ureilite directly observed by TEM. American Mineralogist, 98, no. 4 (2013): 574-581.

Nakamuta, Y., Kitajima, F., and Shimada, K. "In situ observation, X–ray diffraction and Raman analyses of carbon minerals in ureilites: Origin and formation mechanisms of diamond in ureilites." Journal of Mineralogical and Petrological Sciences (2016): 150906.

Németh, P., Garvie, L. A., Aoki, T., Dubrovinskaia, N., Dubrovinsky, L., and Buseck, P. R. “Lonsdaleite is faulted and twinned cubic diamond and does not exist as a discrete material.” Nature communications, 5, no.1, (2014) 1-5.

Németh, P., McColl, K., Garvie, L. A., Salzmann, C. G., Murri, M., and McMillan, P. F. “Complex nanostructures in diamond.” Nature materials, 19, no. 11, (2020): 1126-1131.

Nemanich, R. J., and Solin, S. A. “First-and second-order Raman scattering from finite-size crystals of graphite.” Physical Review B, 20, no. 2, (1979): 392.

Ogilvie, P., Gibson, R. L., Reimold, W. U., Deutsch, A., and Hornemann, U. "Experimental investigation of shock metamorphic effects in a metapelitic granulite: The importance of shock impedance contrast between components." Meteoritics & Planetary Science 46, no. 10 (2011): 1565-1586.

Pimenta, M. A., Dresselhaus, G., Dresselhaus, M. S., Cancado, L. G., Jorio, A., & Saito, R. (2007). Studying disorder in graphite-based systems by Raman spectroscopy. Physical chemistry chemical physics, 9(11), 1276-1290.

Ross, A. J., Steele, A., Fries, M. D., Kater, L., Downes, H., Jones, A. P., Smith, C. L., Jenniskens, P M., Zolensky, M. E., and Shaddad, M. H. "MicroRaman spectroscopy of diamond and graphite in Almahata Sitta and comparison with other ureilites." Meteoritics & Planetary Science 46, no. 3 (2011): 364-378.

Rupert, A. N., McCausland, P. J., and Flemming, R. L. “Ordinary chondrite shock stage quantification using in situ 2-DX-ray diffraction of olivine.” Meteoritics & Planetary Science, 55, no. 10, (2020): 2224-2240.

Sabbah, H., Morrow, A. L., Jenniskens, P., Shaddad, M. H. and Zare, R. N. "Polycyclic aromatic hydrocarbons in asteroid 2008 TC3: Dispersion of organic compounds inside asteroids." Meteoritics & Planetary Science 45, no. 10-11 (2010): 1710-1717.

Saito, R., Takeya, T., Kimura, T., Dresselhaus, G., and Dresselhaus, M. S. “Raman intensity of single-wall carbon nanotubes.” Physical Review B, 57, no. 7, (1998): 4145.

Sinha, S. K., Sack, R. O., and Lipschutz, M. E. "Ureilite meteorites: Equilibration temperatures and smelting reactions." Geochimica et Cosmochimica Acta 61, no. 19 (1997): 4235-4242.

Scott, E. R.D, Taylor, G. J., and Keil, K. "Origin of ureilite meteorites and implications for planetary accretion." Geophysical Research Letters 20, no. 6 (1993): 415-418.

Stöffler, D., Keil, K., and Edward, R. D. S. “Shock metamorphism of ordinary chondrites”. Geochimica et Cosmochimica Acta, 55, (1991): 3845–3867.

Stöffler, D., Hamann, C., and Metzler, K. "Shock metamorphism of planetary silicate rocks and sediments: Proposal for an updated classification system." Meteoritics & Planetary Science 53, no. 1 (2018): 5-49.

Storz, J., Ludwig, T., Bischoff, A., Schwarz, W. H., and Trieloff, M. "Graphite in ureilites, enstatite chondrites, and unique clasts in ordinary chondrites–Insights from the carbon-isotope composition." Geochimica et Cosmochimica Acta, 307 (2021): 86-104.

Strong, H-M, and Hanneman, R. E. "Crystallization of diamond and graphite." The Journal of Chemical Physics 46, no. 9 (1967): 3668-3676.

Sung, J. “Graphite→ diamond transition under high pressure: A kinetics approach.” Journal of Materials Science, 35, no. 23, (2000): 6041-6054.

Tuinstra, F., and Koenig, J. L. "Raman spectrum of graphite." The Journal of chemical physics 53, no. 3 (1970): 1126-1130.

Takeda, H. "Mineralogy of coexisting pyroxenes in magnesian ureilites and their formation conditions." Earth and Planetary Science Letters 93, no. 2 (1989): 181-194.

Warren, P. H., and Kallemeyn, G. W. "Ureilites: The graphite f (O2) buffer, explosive volcanism, and the gross dissipation of basalt from the parent asteroid(s)." In Lunar and Planetary Science Conference, vol. 23. (1992).

Warren, P. H., Ulff-Møller, F., Huber, H., and Kallemeyn, G. W. “Siderophile geochemistry of ureilites: A record of early stages of planetesimal core formation.” Geochimica et Cosmochimica Acta, 70, no. 8, (2006): 2104-2126.

Warren, P.H. "Stable isotopes and the noncarbonaceous derivation of ureilites, in common with nearly all differentiated planetary materials." Geochimica et Cosmochimica Acta 75, no. 22 (2011): 6912-6926.

Urey, H. C. “Diamond, meteorites, and the origin of the solar system.” American Astronomical Society, (1956): 623–637.

Varfolomeeva, T. D. “Synthesis and investigation of polycrystalline diamond” PhD thesis, Institute for High Pressure Physics, USSR Academy of Sciences (1968), p. 154.

Vereshchagin, L. F., & Fateeva, N. S. (1977). Melting temperatures of refractory metals at high pressures. High Temperatures-High Pressures, 9, no. 6, 619-628.

Vinet, N., Flemming, R. L., and Higgins, M. D. "Crystal structure, mosaicity, and strain analysis of Hawaiian olivines using in situ X-ray diffraction." American Mineralogist 96, no. 4 (2011): 486-497.

CHAPTER 2

IMPACT SHOCK ORIGIN OF DIAMONDS IN UREILITE METEORITES

Fabrizio Nestola[a,b], Cyrena A. Goodrich[c], Marta Morana[d], Anna Barbaro[d], Ryan S. Jakubek[e], Oliver Christ[a], Frank E. Brenker[b], M. Chiara Domeneghetti[d], M. Chiara Dalconi[a], Matteo Alvaro[d], Anna M. Fioretti[f], Konstantin D. Litasov[g], Marc D. Fries[h], Matteo Leoni[i,j], Nicola P. M. Casati[k], Peter Jenniskens[l], and Muawia H. Shadda[d]

[a]Department of Geosciences, University of Padova, I-35131 Padova, Italy; [b]Geoscience Institute, Goethe University Frankfurt, 60323 Frankfurt, Germany; [c]Lunar and Planetary Institute, Universities Space Research Association, Houston, TX 77058; [d]Department of Earth and Environmental Sciences, University of Pavia, I-27100 Pavia, Italy; [e]Astromaterials Research and Exploration Science Division, Jacobs Johnson Space Center Engineering, Technology and Science, NASA, Houston, TX 77058; [f]Institute of Geosciences and Earth Resources, National Research Council, I-35131 Padova, Italy; [g]Vereshchagin Institute for High Pressure Physics RAS, Troitsk, 108840 Moscow, Russia; [h]NASA Astromaterials Acquisition and Curation Office, Johnson Space Center, NASA, Houston, TX 77058; [i]Department of Civil, Environmental and Mechanical Engineering, University of Trento, I-38123 Trento, Italy; jSaudi Aramco R&D Center, 31311 Dhahran, Saudi Arabia; [k]Swiss Light Source, Paul Scherrer Institut, 5232 Villigen, Switzerland; [l]Carl Sagan Center, SETI Institute, Mountain View, CA 94043; and [m]Department of Physics and Astronomy, University of Khartoum, 11111 Khartoum, Sudan

Published version in Proceedings of the National Academy of Sciences of the United States of America 117(41), pp 22310-25318 Open Access.

Received for review October 31, 2019, edited by Mark Thiemens, University of California San Diego, La Jolla, CA, approved on August 12, 2020 and published on October 13, 2020.

ABSTRACT

The origin of diamonds in ureilite meteorites is a timely topic in planetary geology as recent studies have proposed their formation at static pressures >20 GPa in a large planetary body, like diamonds formed deep within Earth's mantle. We investigated fragments of three diamond-bearing ureilites (two from the Almahata Sitta polymict ureilite and one from the NWA 7983 main group ureilite). In NWA 7983 we found an intimate association of large monocrystalline diamonds (up to at least 100 μm), nanodiamonds, nanographite, and nanometric grains of metallic iron, cohenite, troilite, and likely schreibersite. The diamonds show a striking texture pseudomorphing inferred original graphite laths. The silicates in NWA 7983 record a high degree of shock metamorphism. The coexistence of large monocrystalline diamonds and nanodiamonds in a highly shocked ureilite can be explained by catalyzed transformation from graphite during an impact shock event characterized by peak pressures possibly as low as 15 GPa for relatively long duration (on the order of 4 to 5 s). The formation of "large" (as opposed to nano) diamond crystals could have been enhanced by the catalytic effect of metallic Fe-Ni-C liquid coexisting with graphite during this shock event. We found no evidence that formation of micrometer(s)-sized diamonds or associated Fe-S-P phases in ureilites require high static pressures and long growth times, which makes it unlikely that any of the diamonds in ureilites formed in bodies as large as Mars or Mercury.

INTRODUCTION

The origin of diamonds in ureilite meteorites is a highly controversial topic among planetary geologists with three main hypotheses being debated: 1) formation by impact shock conversion from graphite (1–7), 2) formation at low pressure in the solar nebula by chemical vapor deposition (8–10), and 3) formation at high static pressures in a planetary-sized body (11–13). The ureilites form the second largest group of achondrites. They are ultramafic rocks mainly composed of olivine and pyroxene, with interstitial carbon, metal, and sulfide phases (14–19). They represent the mantle of a partially differentiated parent body (the ureilite parent body, or UPB) that experienced igneous processing at temperatures up to 1,200 to 1,300 °C (18). The UPB was catastrophically disrupted by a major impact before it had completely cooled, with ureilites being derived from daughter bodies that reassembled in the aftermath of the disruption (17, 19–21). Carbon abundances are notably high in ureilites, ranging up to 8.5 wt% (19, 22), with the carbon occurring principally as graphite (18). In ureilites of very low shock level (based on shock indicators in the silicates), the graphite occurs as millimeter-sized euhedral (blade-shaped or tabular) crystals showing prominent (0001) cleavage, closely associated with Fe, Ni metal, and sulfides (23, 24) (SI Appendix, Fig. S1). Diamonds have not been reported in the lowest-shock samples (2, 25). Most ureilites, however, are shocked to various degrees and in these samples the graphite areas, though still having external blade-shaped morphologies, are internally polycrystalline (18). Diamonds and lonsdaleite [diamond with stacking faults and twinning defects (26)] occur embedded in these areas, constituting a volumetrically minor (thus disproportionately illustrious) component of ureilites. Although the presence of diamonds in these meteorites was reported more than a century ago, the process by which the diamonds formed has been hotly debated and is still controversial. The first hypothesis on the origin of diamond in ureilites dates back to 1956, when Urey (11) proposed that diamonds may form under static high-pressure conditions in the interior of large meteorite parent bodies. A few years later, in his seminal work on diamonds from the Goalpara and Novo Urei ureilites, Lipschutz (1) proposed that diamonds in ureilites were formed by shock conversion of graphite, a hypothesis that has been supported by many subsequent studies (2–7). A third hypothesis that has been discussed is that diamonds in ureilites formed at low pressure in the solar nebula by chemical vapor deposition (8–10).

Recent work on the Almahata Sitta (AhS) polymict ureilite (12, 13) reported the presence of large diamonds (with inclusions of chromite and Fe-S-P phases) in a ureilitic clast and suggested that such diamonds could only be formed at static pressures higher than 20 GPa. This would imply either that the UPB was similar in size to Mercury or Mars (13), or that diamonds in ureilites are exogenous to the UPB (27). In order to provide insight into the origin of diamonds in ureilites, we investigated carbon phases in two ureilitic stones from AhS, samples AhS 209b and AhS 72, and also the NWA 7983 main group ureilite (28), by single-crystal micro X-ray diffraction (XRD) both in-house at the University of Padova (all three samples) and using synchrotron radiation at Paul Scherrer Institute, Villigen, Switzerland (AhS samples only). In addition, micro-Raman spectroscopy was performed on several carbon

areas in NWA 7983 at ARES (Astromaterials Research and Exploration Science), Johnson Space Center, NASA, Houston, TX. Our results cast reasonable doubt on purported evidence for formation of ureilitic diamonds under high static pressures and provide strong evidence for their formation by impact shock at pressure peaks possibly as low as 15 GPa.

METHODS

Petrological and mineralogical features of silicate and carbon phases in ureilites AhS 209b, AhS 72, and NWA 7983 were studied in polished sections by optical microscopy and electron microscopy (SEM) at the Lunar and Planetary Institute (Universities Space Research Association, Houston, TX), the ARES division at NASA, JSC, and the University of Padova. Carbon phases were additionally studied by XRD at the University of Padova, synchrotron radiation X-ray microdiffraction at the Paul Scherrer Institute, TEM at Goethe University in Frankfurt, and micro-Raman spectroscopy at JSC. Contamination of the samples by diamond from the cutting and polishing was avoided by polishing the samples with silicon carbide paper. Further details of the techniques used in this work are provided in SI Appendix.

RESULTS

Samples

AhS 209b and 72 are two stones from the AhS meteorite, which fell in the Nubian desert in 2008 (19, 29–31). They are fine-grained, porous ureilites showing various degrees of “impact smelting” and shock metamorphism as previously described for fine-grained AhS ureilites and a few main group ureilites (32, 33). Olivine areas in AhS 209b are completely mosaicized (SI Appendix, Fig. S2). They consist of aggregates of ∼5- to 20-µm-sized equigranular tiles (adopting the terminology of ref. 32) with tiny amounts of interstitial pyroxene and Si+Alrich glass, which are inferred to represent recrystallized versions of originally ~0.5- to 1-mm-sized primary grains (e.g., refs. 32 and 33). The olivine largely preserves a typical ureilite olivine core composition of Fo ~79, except in reduction rims near inferred original grain boundaries and/or carbon areas. Reduction rim compositions range up to Fo ~93. Pigeonitic pyroxene areas in AhS 209b also show complete mosaicism with extensive in situ reduction and porosity. They consist of aggregates of ~5- to 10-µm-sized subhedral to anhedral grains, with varying amounts of interstitial Ca-enriched pyroxenes and Si-Al-enriched glass. Pores and small grains of metal and sulfide among the pyroxene grains are common. The pyroxene tiles show reverse zoning. Cores are reduced (core Mg# up to ~93) relative to inferred primary compositions (~Mg# 81, such as would have been in equilibrium with Fo ~79 olivine in a typical lower-shock ureilite) with varying Wo contents (~2 to 8). Pyroxene textures such as these were described by Warren and Rubin (32) in several main group and AhS ureilites and attributed

to “impact smelting” (concomitant melting and chemical reduction by carbon) of originally larger primary pigeonite grains. Elongated masses of carbon phases and metal grains are dispersed throughout the sample, commonly occurring along inferred primary silicate grain boundaries (Fig. 1 A and B and SI Appendix, Fig. S3).

The fragment of AhS 72 that we examined is dominated by olivine and shows a higher degree of shock metamorphism than 209b. Olivine is completely recrystallized to ~1- to 20-µm-sized equigranular (anhedral to subhedral) grains in a groundmass (of varying proportions relative to the amount of olivine) of pyroxene. The olivine grains are highly reduced (Fo ~99) and nearly free of inclusions, suggesting recrystallization from a melt (or at least at very high temperatures) under highly reducing conditions. Interstitial pyroxene compositions range from Wo 0.8 to Wo 34 and are also reduced (Mg# 88 to 99). Pores, masses of carbon phases (~20 to hundreds of micrometers), and grains of metal are abundant throughout the section.

The NWA 7983 meteorite was found in 2013 in Morocco. The stone has a total mass of 424.3 g and was classified as a main group ureilite (28). The original description noted that the meteorite was extremely resistant to cutting and polishing and suggested that diamond was abundant (28), and our work confirms this. We studied four polished sections of NWA 7983. A polished thick section with an area of about 2 cm^2 was used for scanning electron microscopy (SEM) observations (not carboncoated; see SI Appendix, sections 1.1 and 1.2) followed by micro XRD. Three polished thin sections were used for optical microscopy and additional SEM observations (both carbon-coated and not carbon-coated). NWA 7983 consists mainly of olivine, minor pyroxene, and ∼6 vol % masses of carbon phases. Metal, Fe-oxides/hydroxides (presumed terrestrial replacements of metal), troilite, and Cr-rich sulfides occur cross-cutting silicates and as blebs. The olivine shows a high degree of shock metamorphism, with textures similar to those in AhS 72 (SI Appendix, Fig. S4). All olivine areas are either mosaicized with ∼2- to 12-μm-sized euhedral tiles and very minor interstitial feldspathic material, or recrystallized to ∼1- to 20-μm-sized equigranular (anhedral to subhedral) grains in a groundmass of minor pyroxene. The degree of reduction of the olivine varies greatly. Some areas (inferred original grains) are dominantly Fo 82 to 83, which may be close to the primary composition, while others are strongly reduced with Fo ∼90 to 98. The interstitial pyroxenes vary in Wo from ∼2 to 33 and Mg# ∼84 to 92. Elongated masses of carbon phases, as well as metal ± sulfide grains (wholly or partly altered to terrestrial Fe-hydroxides), are dispersed throughout the sample. Similar to AhS 72, the degree of recrystallization of the silicates is so high that the outlines of primary silicate grain boundaries are difficult to discern.

The carbon masses typically occur as elongated (blade shaped), internally layered structures of up to 1 mm in length and 300 μm in width (Fig. 1 C–E and SI Appendix, Figs. S5 and S6). In one of the sections that we studied, such blades form a nearly continuous vein ∼1 cm long. In reflected light, the carbon masses contain elongated, highly reflective, high-relief stripes that are parallel to the external morphology of the carbon mass in the long dimension and are inferred to be diamond, based on their optical properties and fluorescence under an electron beam (Fig. 1D and SI Appendix, Figs. S5 A-C and S6A). Some of these contain structures that resemble {111} crystal faces of octahedral diamonds. In back-scattered electron images (BEI), the carbon masses also show a striped appearance (parallel to the external morphology of the carbon mass), which is defined by light and dark areas (Fig. 1C and SI Appendix, Figs. S5 D and E and S6B). The lighter areas contain numerous tiny, bright grains of what appears to be metallic Fe and Fe-sulfides, based on energy dispersive X-ray spectroscopy (EDS) spectra showing peaks for C, Fe, and S. The darker areas appear to be largely free of inclusions and have EDS spectra showing only C. Based on fluorescence under the electron beam, diamonds are abundant in both the light and the dark areas. In general, the high reflectance, high-relief areas observed in reflected light correspond closely to the darker areas in BEI (Fig. 1C and D and SI Appendix, Fig. S6 A and B).

None of the samples studied in this work shows any high-pressure polymorphs of olivine such as wadsleyite and ringwoodite, even in veins or fractures where we specifically searched for them by micro-Raman spectroscopy.

Micro-XRD

Using reflected light and/or back-scattered electron images of thick sections that were not carbon-coated we located carbon areas for micro XRD in the three samples. We gently removed portions of such carbon areas (SI Appendix, section 1.3) and analyzed them by micro XRD.

AhS 72 and AhS 209b

The sections of carbon materials removed from the AhS 209b and AhS 72 samples were two irregularly shaped grains of 320 μm and 380 μm, respectively, along their longest dimension

(SI Appendix, Fig. S7). Synchrotron radiation micro XRD showed that these two fragments are both composed mainly of diamonds, graphite and metallic iron (minor troilite was also detected; see SI Appendix, section 1.4). Fig. 2A show the X-ray diffractogram and the diffraction image of the AhS 209b fragment. As demonstrated by the diffraction rings (rather than individual diffraction spots), the sample is polycrystalline. A similar observation was made for the AhS 72 sample (the diffractogram and diffraction images for AhS 72 are shown in SI Appendix, Fig. S8). Diffraction line profile analysis (34) using the High Score Plus software package (Panalytical) was applied to estimate the crystallite size of the carbon phases (SI Appendix, section 1.4). The results of this analysis are given in SI Appendix, Table S1 and show that diamonds in both AhS 209b and AhS 72 are nanometric with crystal size of 17 to 19 nm for AhS 209b and 18 to 25 nm for AhS 72. However, both of the AhS samples show a typical feature of diamond stacking faults (see the shoulder of the 2.06 Å peak of diamond in Fig. 2A, more evident in the magnification in SI Appendix, Fig. S9) and in order to take into account any defects in diamond and eventually graphite (which shows a significant peak asymmetry and broadening) not considered in the previous profile analysis, we performed a further profile analysis by using DIFFaX+ software (35) (SI Appendix, sections 1.4 and 1.5 and Fig. S10) which provides more reliable results for defect-bearing powder materials. This revealed that the samples are characterized by two diamond domain sizes: smaller domains are on average 3 to 12 nm, whereas the larger ones are larger than 50 nm; for sizes >100 nm, diffraction is no longer reliable for the determination of size and defects in materials. The average graphite crystal size was estimated to be 20 nm. These analyses indicate that in the AhS ureilite fragments studied here diamonds are nanometric with an average size of about 25 nm.

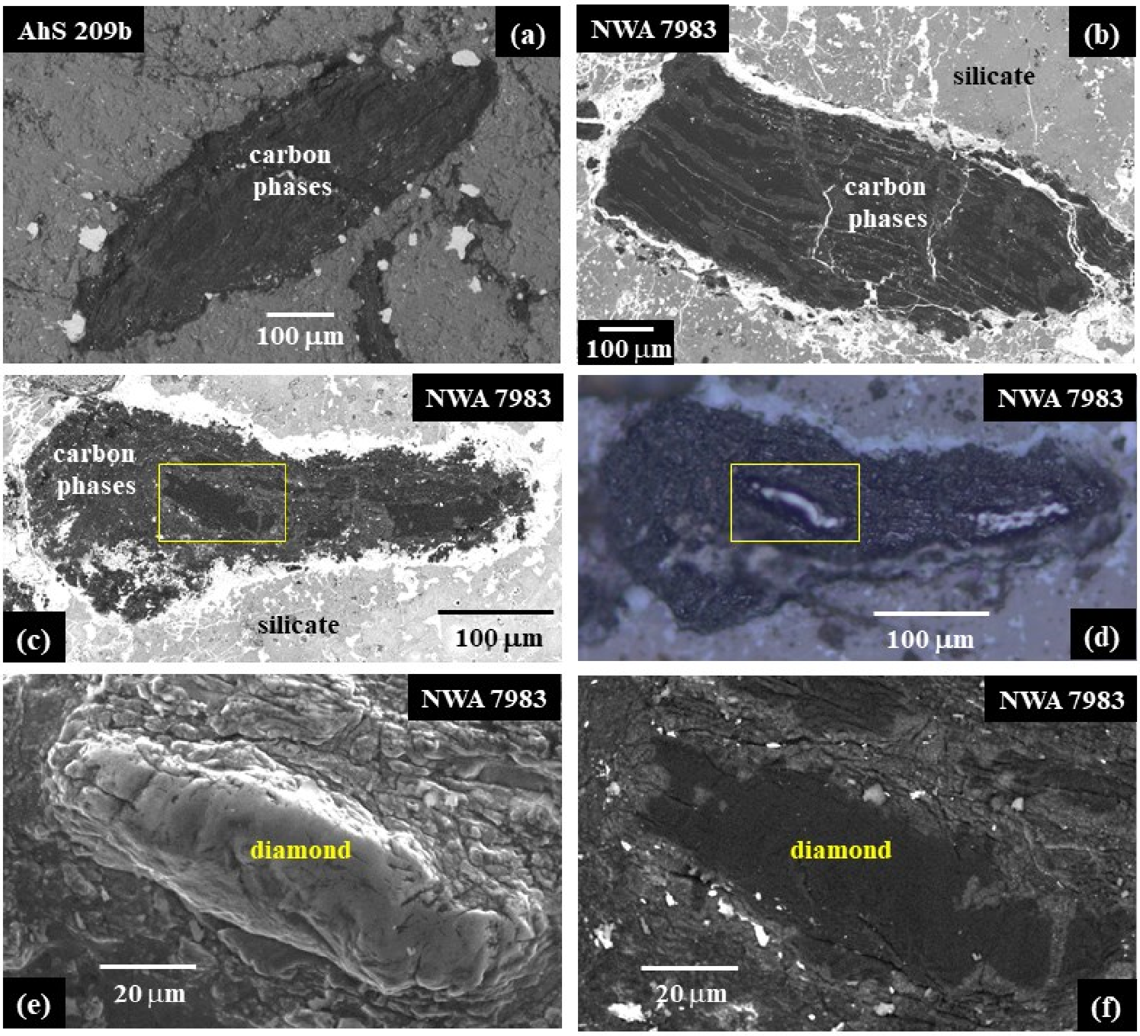

Fig. 1. Carbon masses in polished sections of AhS 209b and NWA 7983. (A) BEI of AhS 209b, showing elongated masses of carbon phases located along inferred primary silicate grain boundaries (see also SI Appendix, Fig. S3 for a lower-magnification view). (B) BEI of non-carbon-coated section of AhS 209b in low-vacuum mode (hence low contrast). BEI of other carbon areas in AhS 209b are shown in SI Appendix, Fig. S3. (C) BEI of carbon-coated section of NWA 7983 in high-vacuum mode. Carbon masses in this sample tend to have elongated, blade-like morphology and internally show a structure of dark and light stripes parallel to the long edges of the carbon mass (see also SI Appendix, Fig. S4). Dark areas show only C, whereas lighter areas show C, Fe, and S peaks in EDS spectra. (D) Reflected light image of same area as in C. Highly reflective, high-relief stripes correlate with dark areas in BEI and are inferred to be diamond from their optical properties, as well as fluorescence under the electron beam. (E) Raman phase map of area in C and D. The intensity of the red color corresponds to the intensity of the diamond ~1,332 cm^{-1} band. The intensity of the blue color corresponds to the intensity of the graphite G band (~1,575 cm^{-1}). In nanodiamonds, the ~1,332 cm^{-1} band is broad, has low intensity, and is downshifted, making it difficult to detect. Thus, the Raman image is predominantly sensitive to large diamonds (red) while most nanodiamonds likely go undetected (38, 39). In this Raman image, nanodiamonds were detected only in a few areas, although XRD results indicate that they are present throughout the carbon mass. (F) Raman spectra of large diamonds (red) and nanodiamonds (black) from E.

NWA 7983

The BEI observations described above revealed that the carbon masses in NWA 7983 show distinct internal stripes of dark and light areas (Fig. 1 C and D and SI Appendix, Figs. S5 and S6), correlating with stripes of high reflectance and high relief and low reflectance and low relief (respectively) in reflected light. We removed fragments from both dark and light areas within five different carbon masses and investigated them by micro XRD in-house (SI Appendix, section 1.5 and S11). The XRD images of dark areas in several of the carbon masses (e.g., Fig. 2) showed no evidence of diffraction rings but only diffraction spots typical of monocrystals. Based on the sizes of the removed fragments, the monocrystals that we investigated ranged from ~20 to at least 100 μm in size (longest dimensions). The diffraction image for the largest monocrystal that we observed is shown in Fig. 2B (BEI and reflected light images of this carbon mass, indicating the area removed and analyzed, are given in SI Appendix, Fig. S12). The unit-cell edge length that we determined for this crystal is a = 3.569 Å (SI Appendix, Table S1), typical of cubic diamond. The absence of evidence for any other phases in the diffractogram of this crystal (or similar ones that we analyzed) is consistent with the observations from EDS analyses in the SEM that only C was detected in dark areas of the carbon masses in this sample. In other fragments removed from dark areas, the diffractograms showed the simultaneous presence of diffraction spots (indicating single crystal diamonds) and diffraction rings (e.g., SI Appendix, Fig. S13), indicating that in some of the darker areas large diamond monocrystals are intimately intermixed with nanodiamonds on a scale below that detectable in reflected light or BEI imaging.

The diffraction results for fragments removed from the lighter carbon areas (as seen in BEI) in NWA 7983 yielded results very similar to those obtained on the AhS ureilite fragments. Fig. 2C shows that such areas are polycrystalline and mainly composed of diamond, graphite, cohenite (ideally Fe3C), troilite, and minor metallic iron, consistent with EDS spectra showing the presence of Fe and S in addition to C in such areas. The small shoulder at higher d-spacing (e.g., 2.18 Å) with respect to the main peak of diamond at 2.06 Å is characteristic of lonsdaleite as already observed for the AhS 209b and AhS 72 samples. The profile analysis for polycrystalline diamonds in both the light areas and the dark areas indicates that the polycrystalline diamond is nanometric and even smaller than diamonds in the AhS fragments with a size of 9 nm (SI Appendix, Table S1). Although it was not possible to model the diffraction peaks of graphite, based on the peak broadening of its most intense peak it is likely that the graphite is also nanometric.

In this study an intimate association of micro- and nanodiamonds has been reported in natural samples, either terrestrial or extraterrestrial. Unfortunately, it was not possible to distinguish microdiamonds from nanodiamonds in either reflected light or BEI, and so our principal method of locating microdiamonds was a “hit-or-miss” approach of removing fragments from sections and X-raying them. This approach was time-consuming, thus limiting the number of areas that could be studied, and resulted in loss of textural context of the diamonds. In order to get an idea of the distribution, shapes, and relative abundance of microdiamonds in situ, we used micro-Raman imaging on several areas using 488 nm excitation (Fig. 1 E and F and SI Appendix, Fig. S6 C–E). Raman mapping of these areas easily identifies larger diamond grains [>∼45 nm (36)] from the narrow, high intensity band at ∼1,332 cm^{-1} (37), although it does not allow definitive determination of their sizes (38). These Raman maps show clearly that in a number of places the large diamond grains are elongated along the direction of the stripes seen in BEI and reflected light (parallel to external morphology of the carbon mass) and (as shown particularly in SI Appendix, Fig. S6) are concentrated along the stripes, that is, forming stripes of their own. We note that nanodiamonds are not easily identified in Raman spectra (38, 39) and so the Raman images (Fig. 1 E and F) are less useful for showing their distribution.

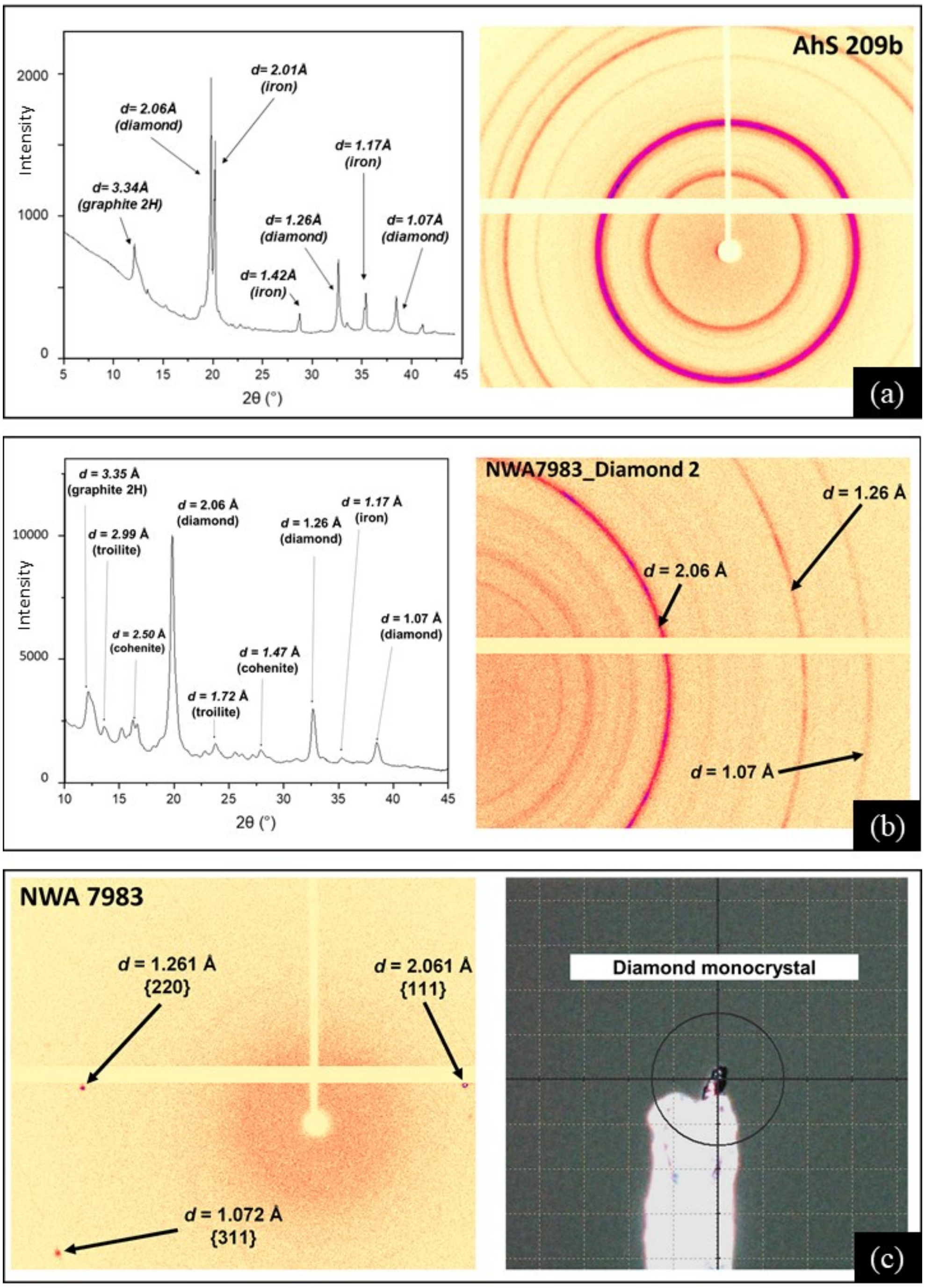

Fig. 2. (A) The diffractogram (Left) and the diffraction image (Right) of the AhS 209b sample, analyzed by micro X-ray powder diffraction at the Paul Scherrer Institute, Villigen, Switzerland. In the diffractogram the most abundant phases found in the carbon-bearing aggregate, polycrystalline diamond, graphite, and iron metal are shown. (B) Diffraction image (Left) for a fragment of a carbon area in NWA 7983 (from an area that was dark in BEI), showing only diffraction spots typical of a monocrystalline diamond. This monocrystal must be at least 100 µm (the size of the whole fragment removed along its longest dimension). We determined its unit-cell edge length, a = 3.569 Å, typical of diamond. (C) Diffractogram (Left) and the diffraction image (Right) of another fragment of NWA 7983, this one from an area that was lighter in BEI. This sample was analyzed by the Rigaku-Oxford Diffraction Supernova kappa-geometry goniometer at the Department of Geoscience, University of Padova. In this fragment polycrystalline diamond, graphite, iron, cohenite, and a minor abundance of troilite are detected.

Nevertheless, the XRD analyses showed clearly that nanodiamonds are present in both light and dark areas of the carbon masses.

Transmission Electron Microscopy

The same fragments of AhS 209b and AhS 72 investigated by XRD were analyzed by transmission electron microscopy (TEM) with the main goal being to verify the crystallite size compared with the results from synchrotron micro XRD. The presence of diamond stacking faults (lonsdaleite), as predicted by micro XRD showing the typical shoulders at higher d-spacing with respect to the 2.06 Å peak of diamond (SI Appendix, Fig. S9), was confirmed by TEM.

Sections of AhS 72 and AhS 209b suitable for TEM analyses were prepared by focused ion beam and investigated by a Philips 200 CM transmission electron microscope (SI Appendix, section 1.6). A typical bright-field image of the AhS 72 sample (Fig. 3, Left) shows diamond domains with size between about 20 and 150 nm. At the same time, electron diffraction images (Fig. 3, Right) indicate that nanodiamonds are associated with graphite (see the ring at about 3.35 Å) and lonsdaleite (see ring at about 2.18 Å), confirming the XRD results. In addition to these main phases, TEM analyses of the AhS 72 sample also revealed the presence of nanometric metallic iron (evident by XRD) and other phases including cohenite Fe3C, iron sulphide, and Fe-Ni-P compounds. By XRD we determined the iron sulphide to be troilite, but unfortunately due to the extremely small crystal size between 50 and 100 nm we were unable to determine the identity or stoichiometry of the Fe-Ni-P compounds, which could for example be schreibersite (Fe,Ni)P3. Due to the nanometric size of the diamonds in this sample, we cannot state definitively whether these other phases are inclusions in diamonds or just coexist with diamonds in the carbon masses.

DISCUSSION

AhS 72 and AhS 209b.

The results from synchrotron diffraction and TEM analyses of the AhS ureilites studied in this work show nanodiamonds associated with nanographite. In addition, they show metallic iron, troilite, cohenite, and nanometric grains of Fe-Ni-P (likely schreibersite) associated with the diamond phases. The diamond–metal–sulfide–carbide–phosphide association in these AhS stones is the same phase assemblage as that reported in AhS stone MS-170 (13), which argues that the diamond had a common origin in all three stones. However, AhS 72 and AhS 209b are highly shocked ureilites, based on shock features in their silicates (complete mosaicism of olivine). This strongly suggests that the diamonds formed as a result of the same shock event that affected the silicates.

The association of metal, sulfide, carbide, and phosphide phases with diamonds in AhS 72 and AhS 209b is especially significant because Nabiei et al. (13) argued that these phases were definitive evidence of diamond formation at $\geq$21 GPa static pressure within a parent body with size comparable to Mercury or Mars. Nabiei et al. (13) base this interpretation on the measured molar (Fe+Ni)/(S+P) ratios of the bulk composition of multiphase (metal–sulfide–phosphide) inclusions in diamond, which were close to 3:1. They argue that this implies that the inclusions were trapped as crystals of the phase $(Fe,Ni)_3(S,P)$, which (for $P/[P+S] < 0.2$) is only stable at pressures above 21 GPa. However, this argument is flawed, because at temperatures above 1,275 °C (or lower if S is present) the $(Fe,Ni)_3(S,P)$ phase melts (40, 41). This temperature is almost certainly much lower than temperatures in a Mars-sized body 4.55 Ga ago at depths equivalent to 21 GPa (42). This means either that the interpretation that the inclusions were trapped as $(Fe,Ni)_3(S,P)$ solids is incorrect and their apparent stoichiometry is only a coincidence, or that the proposed formation in a Mars-sized body is incorrect, or both. In fact, the $(Fe,Ni)_3(P,S)$ phase can be formed simultaneously with diamonds by shock compression and quenching, as in shock melt veins in IIE iron meteorite Elga (43). Therefore, the presence of these inclusions does not in any way require a static pressure (large parent body) origin.

With respect to AhS 209b and AhS 72, based on the highly shocked nature of the silicates, and the association of nanodiamond, lonsdaleite, and nanographite, we argue that diamonds in these two ureilites most likely formed by a shock event (44-46) with a peak pressure possibly as low as 15 GPa, based on mosaicism of olivine (47). The presence of the same phase assemblage (diamond–metal–sulfide–carbide–phosphide) in AhS stone MS-170 (13) as in the highly shocked AhS stones studied here strongly suggests that diamond had a common origin in all three samples. However, based on these samples alone, it cannot be ruled out that preexisting, large, defect-poor diamonds [formed, e.g., at high static pressures (12,13)] were reduced in grain size and acquired stacking faults during the shock event that affected the silicates, and that in MS-170 some of these preexisting diamonds happened to survive. Nevertheless, additional evidence provided by NWA 7983 (discussed below) leads to the conclusion that this possibility would be extremely unlikely.

NWA 7983.

NWA 7983 is a crucial sample for understanding the origin of diamonds in ureilites because its silicates record a high degree of shock (again, complete mosaicism of olivine) and yet it contains large diamonds (i.e., single crystal diamonds up to at least 100 µm in size) in addition to the nanodiamonds that are accepted to be a common product of shock (44–46). This discovery suggests the possibility that the large diamonds in this ureilite were also formed by the shock process, rather than simply having fortuitously survived it.

A first-order argument supporting this interpretation is the predominantly blade-shaped morphology of the carbon masses in which the diamonds are embedded along with graphite

(Fig. 1 and SI Appendix, Fig. S5). This external morphology of the carbon areas is the same as that of millimeter-sized euhedral laminate (or tabular) graphite crystals that occur in very-low-shock-level ureilites (SI Appendix, Fig. S1) and have been argued to represent the primary form of carbon in all ureilites (23, 24). If the diamonds in NWA 7983 were only remnants of larger diamonds that had formed at high static pressures during long residence times in a planetary mantle, the external shapes of the carbon areas would not be those of graphite crystals (even if graphite laths had been the precursor material) but would be those of typical diamonds formed deep within the Earth's mantle (48). Instead, their shapes, and the prominent striped texture (Fig. 1 and SI Appendix, Figs. S5 and S6) of both the nanodiamond aggregates and the larger diamonds within these blade-shaped regions, parallel to the long dimension of the laths which likely represents the trace of (0001) in original graphite (23, 24), strongly suggests that the diamonds are pseudomorphing original graphite crystals and formed in a rapid process that did not allow time for external graphite morphology to be replaced by diamond morphology. In fact, diamonds pseudomorphing original graphite forms is what is observed for diamonds formed in the Popigai impact crater (49, 50) in which aggregates of submicron-sized diamonds show external tabular shapes preserving the crystal habit of precursor graphite flakes (though we note that the primary graphite morphologies inferred for ureilites differ from those at Popigai).

As emphasized above, our observations of NWA 7983 represent an astonishing intimate association of micro- and nanodiamonds reported in a natural sample. The nanodiamond aggregates in NWA 7983 are especially abundant and render this ureilite even more resistant to cutting and polishing than most ureilites, similar to industrially produced ultrahard nanodiamonds (51, 52). As discussed by refs. 44–46, nanodiamonds of this type are the typical product of shock compression of disordered graphite, and nanodiamonds in ureilites and other meteorites are widely interpreted to be the product of impact shock (1, 4, 53, 54).

However, the formation mechanism of the large diamonds observed in NWA 7983, and the question of whether they formed at the same time as the nanodiamonds, are the critical issues in this investigation, as refs. 12 and 13 argue that such large sizes require long growth times under static high-pressure conditions. Hezel et al. (3) reported diamonds up to 5 μm in size (identified by in situ XRD) in a ureilite, and based on their close association with compressed graphite and secondary, polycrystalline graphite argued for formation of the diamonds by shock. The diamonds observed in this work are even larger and may require additional evidence to support formation in a shock event, the principal objections being the extremely short duration of peak pressure conditions during a shock event (45, 51, 55) and the kinetic/energetic limitations associated with direct transformation from graphite (45). We address both of these issues.

First, although the effective duration of a typical laboratory shock experiment is on the order of a microsecond, and so does not allow time for the growth of diamonds beyond very small (less than micrometer) sizes (46), large natural impacts have a significantly longer duration of high-pressure conditions (45). The largest craters on asteroid 4 Vesta, with a diameter of 400 to 500 km, could have formed from a 25- to 30-km impactor, with peak shock pressure during the compression stage lasting for 4 to 5 s (56). During the major impact event of UPB disruption, which is the most likely event in the history of ureilites to explain the majority of their shock features (17, 21, 32), the duration of the compression stage could have been comparably long, based on the impact parameters of ref. 57 for catastrophic disruption of the UPB and equations of ref. 56.

Second, although the direct transformation of graphite to diamond may require higher pressures and/or longer duration of pressure than those of many shock events (44, 45, 58) the catalyzed formation of diamonds in metallic (Fe,Ni,Co)-C melts proceeds at notably lower pressures and higher reaction rates and has long been used in industrial production of diamonds

(59–64). Catalysis by metallic melts (referred to as the solvent method or solvent-catalysis in some literature) is likely to have been a significant factor in formation of diamonds in ureilites. As shown in SI Appendix, Fig. S1, the millimeter-sized euhedral graphite crystals in ureilites of very low shock level are intimately associated with Fe,Ni metal. Such metal is a common interstitial component associated with carbon in most ureilites (18, 65). Goodrich et al. (65) argued that the metal in ureilites represents Fe-Ni-C melt that was present at $T \geq 1{,}150$ °C and remained after extraction of lower-temperature Fe,S-enriched melt during the igneous stage of ureilite formation. The presence in ureilite silicates of ∼5- to 150-µm-diameter metallic spherules, consisting of cohenite (Fe_3C), metal, schreibersite (Fe_3P), and sulfide, constitute direct evidence for the presence of such melts at magmatic temperatures (65, 66). The impact disruption of the UPB occurred while the silicates were still hot, ∼1,050 ± 50 °C (18, 21). The temperature increase associated with this impact shock event, assuming a 5 $km \cdot s^{-1}$ relative velocity, would have been on the order of 200 to 300 °C (67). Thus, grain boundary metal would have been remelted to create Fe-Ni-C liquids, and it seems inescapable that they would have had a large effect on the growth rate of diamonds forming during the shock event. The importance of such metallic liquids in catalyzing the formation of diamonds from graphite in ureilites was previously suggested by ref. 6 though not discussed for diamonds of such large sizes as those observed here.

There is, in fact, a vast literature on the formation of diamonds via the catalytic method, because of the industrial importance of diamond. In general, the catalyzed formation of diamonds from graphite occurs in a very thin film of molten metal in contact with graphite (62, 64, 68), with reported diamond growth rates ranging from 0.2 to 0.4 µm/s at 5.4 GPa and 1,127 °C (62) to 30 to 60 µm/s (in the first 20 s) at 4.5 GPa and 1,100 to 1,200 °C (59).

The latter rates would easily permit formation of a 100-µm-sized diamond, as observed in NWA 7983, in the ∼4 to 5 s estimate made above for the duration of peak pressure during the catastrophic disruption of the UPB. This evidence is sufficient to show that formation of large diamonds in ureilites during shock events is plausible and to cast reasonable doubt on the necessity for much longer growth times under static high-pressure conditions (12, 13).

Catalyzed formation of diamonds during a shock event can also account for simultaneous formation of micro- and nanodiamonds in ureilites. For example, using a technique of pulsed heating of a graphite-metal experimental charge in a static high-pressure apparatus at 8 to 14 GPa, which simulates natural impact processes (45, 55) with respect to duration of peak pressures and temperatures, Varfolomeeva (60) reported formation of up to 10-µm-sized diamonds near the catalyst and nanodiamonds in other parts of the experimental charge (SI Appendix, Fig. S14).

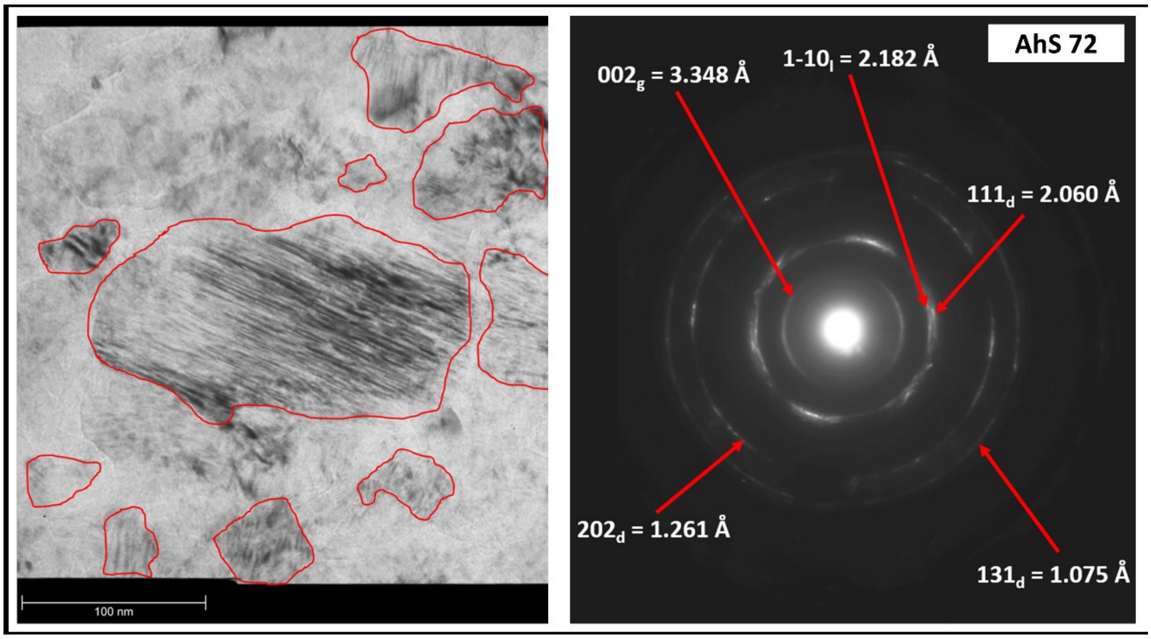

Fig. 3. (Left) A typical bright-field image of the AhS 72 sample, which shows diamond domains with size ranging from 20 to 150 nm. The corresponding electron diffraction image (Right) indicates that nanodiamonds are associated with graphite (see the ring at about 3.35 Å) and diamond with stacking faults, that is, lonsdaleite (see ring at about 2.18 Å), confirming the XRD results. The diffraction line indicators are represented by the (hkl) planes of diamond (indicated with the subscript "d") and graphite (indicated with the subscript "g") and give the spacing in angstroms. These images were obtained with a Philips CM200 transmission electron microscope.

Catalysis of diamond formation from graphite via metallic melts may also explain other features of the diamonds in NWA 7983. For example, we hypothesize that the striped internal textures of the carbon areas, defined by stripes of concentrated (higher abundance of larger) diamonds and C-dominated (Fe, S absent) chemistry (darker in BEI) alternating with stripes of dominantly nanodiamonds and C+Fe+S chemistry, could have formed if the metallic melts were injected between (0001) graphite platelets [assuming the long dimensions of the carbon masses to represent the trace of (0001) in original large graphite crystals]. Growth of larger diamonds then proceeded to form the largely Fe-free dark stripes adjacent to the metallic liquids, while the lighter stripes retain concentrations of residual Fe intermixed with nanodiamonds. In addition, ref. 59 suggested that the growth of diamonds from metallic liquids proceeded through the intermediate step of carbide formation, which could explain the association of cohenite (Fe_3C) with diamonds observed in this work (Fig. 2C). Another type of inclusion, chromite, reported by ref. 13 in ureilite diamonds, could also support catalytic formation of diamonds during a shock event. Nabiei et al. (13) noted that the nearly pure (Al-Ti-Mg-free) compositions of the chromite required crystallization from metallic melts (references 22 and 23 in ref. 13). We agree with this interpretation, which is strongly supported by the presence of similarly pure chromite in the metallic metal–cohenite–sulfide–phosphide spherules in ureilite silicates mentioned above (65, 66). However, in contrast to Nabiei et al. (13), who argued that the presence of such melts was inconsistent with the low-pressure igneous setting of ureilite formation, we note that the metallic spherules provide direct evidence that such melts were present in the primary ureilite silicate assemblage (65, 66) and so could have been remobilized to catalyze the formation of diamonds in an impact shock event.

Additional Evaluation of Proposed Evidence for High Static Pressure.

The 100-µm-sized single diamond crystal that we observed in NWA 7983 constitutes the first definite report of diamonds of this size in a ureilite. Nabiei et al. (13) did not determine the sizes of the diamonds they studied in MS-170 (e.g., no micro XRD was performed showing diffraction spots) but rather relied on the previous report by Miyahara et al. (12) of large diamonds in this sample. In fact, the “large” diamonds reported by Miyahara et al. (12) in MS-170 were not actually large single crystals but rather aggregates of many individual (unconnected) segments having almost the same crystallographic orientation. These aggregates were interpreted (12, 13) to have originally been large single crystals. However, this is not the only possible interpretation. In fact, an aggregate of similarly oriented small crystals is what is expected for diamonds formed by shock compression of oriented graphite (50, 69, 70), as noted also by ref. 6. Miyahara et al. (12) stated that they did not observe the predicted crystallographic relationship between diamond and graphite, and used this as an argument against a shock origin. However, if originally large single graphite crystals had been internally recrystallized in a shock event to nanometric, randomly oriented grains (like those observed in the samples studied here), which is likely (71), their current orientations relative to the diamond are irrelevant. Instead, the orientation of the diamonds would have to be compared with the original orientation of the graphite precursors.

By contrast, the presence of a truly single-crystal 100-μm-sized diamond in a highly shocked ureilite (NWA 7983) makes it more likely that such diamonds actually formed as a result of the shock process, rather than just having survived it. The shock state of silicates in MS-170 was not investigated by refs. 12 and 13 but was classified as S3 by ref. 31, which implies shock pressures of 5 to 10 GPa (47), sufficient to produce diamonds (see ref. 6). Critically, the external morphologies of the carbon masses in MS-170 are no different from those in NWA 7983 or other ureilites - that is, they are elongated masses along silicate grain boundaries, suggesting that they were originally large, single crystals of graphite, as discussed above for all ureilites. This can be observed from inspection of figure 1 of ref. 13 compared with SI Appendix, Fig. S1 and was confirmed by recent studies of our own on MS-170. This makes it extremely unlikely that the diamonds formed during long residence times at high pressures, because if they had then external diamond morphologies would have formed. In other words, there is no evidence that MS-170 is an unusual ureilite preserving diamonds formed in a planetary mantle.

Finally, Miyahara et al. (12) also reported the observation of sector zoning of nitrogen in diamond assemblages in MS-170 and argued that this required “sluggish growth” as in a static high-pressure setting. However, the evidence they present for sector zoning (e.g., figure 5 of ref. 12) is at best ambiguous. Heterogeneous nitrogen distribution is clearly shown, but its relationship to diamond crystal morphology is unclear, given that the diamond consists of several unconnected segments separated by areas of graphite (as discussed above) and no crystal orientation information is given. Furthermore, even if sector zoning of nitrogen is present in large ureilite diamonds, this would not require long, slow growth. For example, diamonds grown by the DeBeers Diamond Research Laboratory using an Fe-Ni metal catalyst for diamond growth developed strong sector zonation of nitrogen in 15 to 20 s (SI Appendix, Fig. S15), which is hardly “sluggish.” The distribution of nitrogen in large ureilite diamonds, and what it implies for their formation, warrants further investigation, but at this time there is no evidence that it supports a high static pressure.

CONCLUSIONS

In conclusion, the results from combined micro XRD, TEM, SEM, EMPA, and micro-Raman spectroscopy of three highly shocked ureilites suggest that the most likely process by which both microdiamonds and nanodiamonds in ureilites formed is in a shock event characterized by a peak pressure possibly as low as 15 GPa, the shock level recorded by the silicates. Micrometersized diamonds can form from crystalline graphite in shock events when catalyzed by metallic Fe-Ni-C liquid, which was demonstrably present during the major shock events that occurred on the UPB, and do not require high static pressures and long growth times.

None of the minor Fe-S-P phases associated with the diamonds in ureilites require high static pressures either, nor does sector zonation of nitrogen in diamonds. We find no compelling evidence that diamonds in ureilites formed in large planetary bodies or planetary embryos (13).

Aknowledgments

We thank Marco van Gemeren for sample preparation and Kent Ross for assistance with SEM/EMPA. We are grateful to James Van Orman, Allan Treiman, and Maurizio Bellotto for helpful discussions. This work was supported by Programma Nazionale di Ricerche in Antartide (PNRA) 2018 grant PNRA18 00247–A to F. N. and NASA grants 80NSSC17K0165, NNX17AH09GS03, and 80NSSC19K0507 to C.A.G. M.M., A.B., M.C. Domeneghetti, and M.A. were funded by the IMPACt project (R164WEJAHH); M.C. Domeneghetti was funded by the PNRA 2016 to L. Folco. This is Lunar and Planetary Institute (LPI) contribution 2393. LPI is operated by USRA under a cooperative agreement with the Science Mission Directorate of NASA.

References

1. M. E. Lipschutz, Origin of diamonds in the ureilites. Science 143, 1431–1434 (1964).

2. Y. Nakamuta, Y. Aoiko, Mineralogical evidence for the origin of diamond in ureilites.

Meteorit. Planet. Sci. 35, 487–493 (2000).

3. D. C. Hezel et al., In situ micro-Raman and X-ray diffraction study of diamonds and petrology of the new ureilite UAE 001 from the United Arab Emirates. Meteorit. Planet. Sci. 43, 1127–1136 (2008).

4. C. Le Guillou, J. N. Rouzaud, L. Remusat, A. Jambon, M. Bourot-Denise, Structures, origin and evolution of various carbon phases in the ureilite Northwest Africa 4742 compared with laboratory-shocked graphite. Geochim. Cosmochim. Acta 74, 4167–4185 (2010).

5. A. J. Ross et al., MicroRaman spectroscopy of diamond and graphite in Almahata Sitta and comparison with other ureilites. Meteorit. Planet. Sci. 46, 364–378 (2011).

6. Y. Nakamuta, F. Kitajima, K. Shimada, In situ observation, X–ray diffraction and Raman analyses of carbon minerals in ureilites: Origin and formation mechanisms of diamond in ureilites. J. Mineral. Petrol. Sci. 111, 252–269 (2016).

7. C. A. Lorenz, A. A. Shiryaev, I. I. Vlasov, S. E. Borisovsky, Metamorphism of four desert ureilites and luminescence spectroscopy of defects in ureilitic diamonds. Meteorit. Planet. Sci. 54, 1197–1214 (2019).

8. K. Fukunaga, J. Matsuda, K. Nagao, M. Miyamoto, K. Ito, Noble-gas enrichment in vapour-growth diamonds and the origin of diamond in ureilites. Nature 328, 141–143 (1987).

9. J. I. Matsuda, K. Fukunaga, K. Ito, Noble gas studies in vapor-growth diamonds: Comparison with shock produced diamonds and the origin of diamonds in ureilites. Geochim. Cosmochim. Acta 55, 2011–2023 (1991).

10. J. I. Matsuda, A. Kusumi, H. Yajima, Y. Syono, Noble gas studies in diamonds synthesized by shock loading in the laboratory and their implications on the origin of diamonds in ureilites. Geochim. Cosmochim. Acta 59, 4939–4949 (1995).

11. H. C. Urey, Diamonds, meteorites, and the origin of the solar system. Astrophys. J. 124, 623–637 (1956).

12. M. Miyahara et al., Unique large diamonds in a ureilite from Almahata Sitta 2008 TC3 asteroid. Geochim. Cosmochim. Acta 163, 14–26 (2015).

13. F. Nabiei et al., A large planetary body inferred from diamond inclusions in a ureilite meteorite. Nat. Commun. 9, 1327 (2018).

14. G. Vdovykin, Ureilites. Space Sci. Rev. 10, 483–510 (1970).

15. J. L. Berkley, G. J. Taylor, K. Keil, G. E. Harlow, M. Prinz, The nature and origin of ureilites. Geochim. Cosmochim. Acta 44, 1579–1597 (1980).

16. C. A. Goodrich, Invited review. Ureilites: A critical review. Meteorit. Planet. Sci. 352, 327–352 (1992).

17. C. A. Goodrich, E. R. D. Scott, A. M. Fioretti, Ureilitic breccias: Clues to the petrologic structure and impact disruption of the ureilite parent body. Chem. Erde 64, 283–327 (2004).

18. D. W. Mittlefehldt, T. J. McCoy, C. A. Goodrich, A. Kracher, Non-chondritic meteorites

from asteroidal bodies. Rev. Mineral. Geochem. 36, 4.1-4.195 (1998).

19. C. A. Goodrich et al., Origin and history of ureilitic material in the solar system: The view from asteroid 2008 TC3 and the Almahata Sitta meteorite. Meteorit. Planet. Sci. 50, 782–809 (2015).

20. H. Downes, D. W. Mittlefehldt, N. T. Kita, J. W. Valley, Evidence from polymict ureilites for a disrupted and re-accreted single ureilite parent asteroid gardened by several distinct impactors. Geochim. Cosmochim. Acta 72, 4825–4844 (2008).

21. J. S. Herrin et al., Thermal and fragmentation history of ureilitic asteroids: Insights from the Almahata Sitta fall. Meteorit. Planet. Sci. 45, 1789–1803 (2010).

22. E. A. Cloutis et al., Spectral reflectance properties of ureilites. Meteorit. Planet. Sci. 45, 10–11 (2010).

23. J. L. Berkley, J. H. Jones, Primary igneous carbon in ureilites: Petrological implications. J. Geophys. Res. 87, A353–A364 (1982).

24. A. H. Treiman, J. L. Berkley, Igneous petrology of the new ureilites Nova 001 and Nullarbor 010. Meteoritics 29, 843–848 (1994).

25. J. F. Wacker, Noble gases in the diamond-free ureilite ALHA78019: The roles of shock and nebular processes. Geochim. Cosmochim. Acta 50, 633–642 (1986).

26. M. Murri et al., Quantifying hexagonal stacking in diamond. Sci. Rep. 9, 10334 (2019).

27. S. J. Desch, J. G. O'Rourke, L. K. Schaefer, T. G. Sharp, D. L. Schrader, Diamonds in ureilites from Mars. Lunar Planet. Sci. Conf. Abstr 50, 1646 (2019).

28. A. Ruzicka, J. Grossman, A. Bouvier, D. K. Herd, B. Agee, The Meteoritical Bulletin, No. 102. Meteorit. Planet. Sci. 50, 1662 (2015).

29. P. Jenniskens et al., The impact and recovery of asteroid 2008 TC_3. Nature 458, 485–488 (2009).

30. M. H. Shaddad et al., The recovery of asteroid 2008 TC3. Meteorit. Planet. Sci. 45, 1557–1589 (2010).

31. M. Horstmann, A. Bischoff, The Almahata Sitta polymict breccia and the late accretion of asteroid 2008 TC3. Chem. Erde 74, 149–183 (2014).

32. P. H. Warren, A. E. Rubin, Pyroxene-selective impact smelting in ureilites. Geochim. Cosmochim. Acta 74, 5109–5133 (2010).

33. J. L. Berkley, Four Antarctic ureilites: Petrology and observations on ureilite petrogenesis. Meteoritics 21, 169–189 (1981).

34. R. Delhez, E. J. Mittemeijer, Determination of crystallite size and lattice distortions through X-ray diffraction line profile analysis. Anal. Chem. 312, 1–16 (1982).

35. M. Leoni, F. Gualtieri, N. Roveri, Simultaneous refinement of structure and microstructure of layered materials. J. Appl. Cristallogr. 37, 166–173 (2004).

36. V. I. Korepanov, H. Witek, H. Okajima, E. Osawa, H. O. Hamaguchi, Communication: Three-dimensional model for phonon confinement in small particles: Quantitative bandshape analysis of size-dependent Raman spectra of nanodiamonds. J. Chem. Phys. 140, 041107 (2014).

37. S. A. Solin, A. K. Ramdas, Raman spectrum of diamond. Phys. Rev. B 1, 1687–1698 (1970).

38. S. Osswald, V. N. Mochalin, M. Havel, G. Yushin, Y. Gogotsi, Phonon confinement effects in the Raman spectrum of nanodiamond. Phys. Rev. B 80, 75419 (2009).

39. A. C. Ferrari, J. Robertson, Raman spectroscopy of amorphous, nanostructured, diamond-like carbon, and nanodiamond. Philos. Trans. A Math. Phys. Eng. Sci. 362, 2477–2512 (2004).

40. D. A. Minin, A. Shatskiy, K. D. Litasov, H. Ohfuji, The Fe–Fe2P phase diagram at 6 GPa. High Pressure Res. 39, 50–68 (2019).

41. A. J. Stewart, M. W. Schmidt, Sulfur and phosphorus in the Earth's core: The Fe-P-S system at 23 GPa. Geophys. Res. Lett. 34, 5–9 (2007).

42. K. Righter, N. L. Chabot, Moderately and slightly siderophile element constraints on the depth and extent of melting in early Mars. Meteorit. Planet. Sci. 176, 157–176 (2011).

43. K. D. Litasov, S. N. Teplyakova, A. Shatskiy, K. E. Kuper, Fe-Ni-P-S melt pockets in Elga IIE iron meteorite: Evidence for the origin at high-pressures up to 20 GPa. Minerals 9, 616 (2019).

44. P. S. De Carli, Shock wave synthesis of diamond and other phases. MRS Proc. 383, 21–31 (1995).

45. P. S. De Carli et al., "Laboratory impact experiments versus natural impact events" in Catastrophic Events and Mass Extinctions: Impacts and Beyond, C. Koeberl, K. G. MacLeod, Eds. (GSA Special Paper, Geological Society of America, Boulder, CO, 2002), Vol. 356, pp. 595–605.

46. P. S. Decarli, J. C. Jamieson, Formation of diamond by explosive shock. Science 133, 1821–1822 (1961).

47. D. Stöffler, C. Hamann, K. Metzler, Invited Review, Shock metamorphism of planetary silicate rocks and sediments: Proposal for an updated classification system. Meteorit. Planet. Sci. 49, 5–49 (2018).

48. F. Nestola et al., CaSiO3 perovskite in diamond indicates the recycling of oceanic crust into the lower mantle. Nature 555, 237–241 (2018).

49. C. Koeberl et al., Diamonds from the Popigai impact structure, Russia. Geology 25, 967–970 (1997).

50. H. Ohfuji et al., Natural occurrence of pure nano-polycrystalline diamond from impact crater. Sci. Rep. 5, 14702 (2015).

51. T. Irifune, A. Kurio, S. Sakamoto, T. Inoue, H. Sumiya, Materials: Ultrahard polycrystalline diamond from graphite. Nature 421, 599–600 (2003). Correction in: Nature 421, 806 (2003).

52. F. Isobe, H. Ohfuji, H. Sumiya, T. Irifune, Nanolayered diamond sintered compact obtained by direct conversion from highly oriented graphite under high pressure and high temperature. J. Nanomater. 2013, 380165 (2013).

53. L. A. J. Garvie, P. Németh, P. R. Buseck, Transformation of graphite to diamond via a topotactic mechanism. Am. Mineral. 99, 531–538 (2014).

54. S. Mostefaoui, A. El Goresy, P. Hoppe, Ph. Gillet, U. Ott, Mode of occurrence, textural settings and nitrogen-isotopic compositions of in situ diamonds and other carbon phases in the Bencubbin meteorite. Earth Planet. Sci. Lett. 204, 89–100 (2002).

55. F. P. Bundy, J. S. Kasper, Hexagonal diamond–A new form of carbon. J. Chem. Phys. 46, 3437–3446 (1967).

56. P. Gillet, A. El Goresy, Shock events in the solar system: The message from minerals in terrestrial planets and asteroids. Annu. Rev. Earth Planet. Sci. 41, 257–285 (2013).

57. P. Michel et al., Selective sampling during catastrophic disruption: Mapping the location of reaccumulated fragments in the original parent body. Proceedings of the 8th Catastrophic Disruption Workshop. Planet. Space Sci. 107, 24–28 (2015).

58. C. Le Guillou, F. Brunet, T. Irifune, H. Ohfuji, J.-N. Rouzaud, Nanodiamond nucleation below 2273 K at 15 GPa from carbons with different structural organizations. Carbon 45, 636–648 (2007).

59. G. N. Bezrukov et al., "Kinetic features of diamond crystallization" in Growth of Crystals, N. N. Sheftal', E. I. Givargizov, Eds. (Consultants Bureau, New York,, 1975), Vol. 9, pp. 74–77.

60. T. D. Varfolomeeva, "Synthesis and investigation of polycrystalline diamond," PhD thesis, Institute for High Pressure Physics, USSR Academy of Sciences (1971), p. 154.

61. L. F. Trueb, An electron-microscope study of shock-synthesized diamond. J. Appl. Phys. 39, 4707–4716 (1968).

62. H. M. Strong, R. E. Hanneman, Crystallization of diamond and graphite. J. Chem. Phys. 45, 3668–3676 (1967).

63. I. I. Fedorov, A. A. Chepurov, J. M. Dereppe, Redox conditions of metal-carbon melts and natural diamond genesis. Geochem. J. 36, 247–253 (2002).

64. F. P. Bundy et al., The pressure-temperature phase and transformation diagram for carbon; updated through 1994. Carbon 34, 141–153 (1996).

65. C. A. Goodrich, R. D. Ash, J. A. Van Orman, K. Domanik, W. F. McDonough, Metallic phases and siderophile elements in main group ureilites: Implications for ureilite petrogenesis. Geochim. Cosmochim. Acta 112, 340–373 (2013).

66. C. A. Goodrich, J. L. Berkley, Primary magmatic carbon in ureilites: Evidence from cohenite-bearing metallic spherules. Geochim. Cosmochim. Acta 50, 681–691 (1986).

67. D. Stöffler, E. R. D. Klaus Keil, Scott, Shock metamorphism of ordinary chondrites. Geochim. Cosmochim. Acta 55, 3845–3867 (1991).

68. H. P. Bovenkerk, F. P. Bundy, H. M. Strong, R. H. Wentorf Jr., H. T. Hall, Preparation of diamond. Nature 184, 1094–1098 (1959).

69. D. J. Erskine, W. J. Nellis, Shock-induced martensitic phase transformation of oriented graphite to diamond. Nature 349, 317–319 (1991).

70. H. Ohfuji, M. Nakaya, A. P. Yelisseyev, V. P. Afanasiev, K. D. Litasov, Mineralogical and crystallographic features of polycrystalline yakutite diamond. J. Mineral. Petrol. Sci. 112, 46–51 (2017).

71. A. N. Dremin, O. N. Breusov, "Dynamic synthesis of superhard materials" in Shock Waves in Materials Science, A. B. Sawaoka, Ed. (Springer, Tokyo, 1993), pp. 17–34. 25318 |

CHAPTER 3

GRAPHITE-BASED GEOTHERMOMETRY ON ALMAHATA SITTA UREILITIC METEORITES

Anna Barbaro [1,*], M. Chiara Domeneghetti [1], Cyrena A. Goodrich [2], Moreno Meneghetti [3], Lucio Litti [3], Anna Maria Fioretti [4], Peter Jenniskens [5], Muawia H. Shaddad [6] and Fabrizio Nestola [7,8]

[1]Department of Earth and Environmental Sciences, University of Pavia, 27100 Pavia, Italy; [2] Lunar and Planetary Institute, Universities Space Research Association, Houston, TX 77058, USA; [3] Department of Chemical Sciences, University of Padova, 35131 Padova, Italy; [4] Institute of Geosciences and Earth Resources, National Research Council, 35131 Padova, Italy; [5] SETI Institute, Mountain View, CA 94043, USA; [6] Department of Physics and Astronomy, University of Khartoum, Khartoum 11111, Sudan; [7] Department of Geosciences, University of Padova, 35131 Padova, Italy; [8] Geoscience Institute, Goethe-University Frankfurt, 60323 Frankfurt, Germany
** Correspondence: anna.barbaro01@universitadipavia.it; Tel.: +39-3491548631*

Published version in Minerals 10, 1005 pp 1-14. Open Access.
Received: 13 October 2020; Accepted: 10 November 2020; Published: 12 November 2020

ABSTRACT

The thermal history of carbon phases, including graphite and diamond, in the ureilite meteorites has implications for the formation, igneous evolution, and impact disruption of their parent body early in the history of the Solar System. Geothermometry data were obtained by micro-Raman spectroscopy on graphite in Almahata Sitta (AhS) ureilites AhS 72, AhS 209b and AhS A135A from the University of Khartoum collection. In these samples, graphite shows G-band peak centers between 1578 and 1585 cm^{-1} and the full width at half maximum values correspond to a crystallization temperature of 1266 °C for graphite for AhS 209b, 1242 C for AhS 72, and 1332 C for AhS A135A. Recent work on AhS 72 and AhS 209b has shown graphite associated with nanodiamonds and argued that this assemblage formed due to an

impact-event. Our samples show disordered graphite with a crystalline domain size ranging between about 70 and 140 nm. The nanometric grain-size of the recrystallized graphite indicates that it records a shock event and thus argues that the temperatures we obtained are related to such an event, rather than the primary igneous processing of the ureilite parent body.

INTRODUCTION

Almahata Sitta (AhS) is the first meteorite to originate from a known asteroid, 2008 TC_3. This asteroid was discovered on 6 October 2008 and tracked for ~20 h before it hit Earth in the Nubian Desert, Sudan [1,2]. The AhS meteorites in the University of Khartoum (UoK) collection consist of >~700 cm-sized stones of diverse meteorite types [2–4]. Those studied so far are dominated by ureilites, which are a major group of achondrites, but also include several types of chondrites (enstatite, ordinary, carbonaceous and Rumuruti chondrites are a range of subtypes) [3].

AhS is classified as an "anomalous polymict ureilite" [1]. It is analogous to typical polymict ureilites, which are fragmental breccias dominated by ureilitic clasts, except that it disintegrated in the atmosphere with its clasts landing on Earth as individual stones [4]. The ureilitic clasts in polymict ureilites, including AhS, are essentially identical to main group ureilites, except possibly that a higher fraction of them are highly shocked [5–7].

Ureilites are ultramafic rocks mainly composed of olivine and pyroxene, with minor carbon phases, metals, and sulfides. The most common pyroxene in most ureilites is pigeonite. A few ureilites contain augite and orthopyroxene instead of or in addition to pigeonite [4]. They are interpreted to represent a single original ureilitic parent body (the UPB), which accreted within 1–2 Ma after CAI (Calcium Aluminum Inclusions) formation and shortly thereafter was partially differentiated, experiencing igneous processing at temperatures up to 1200–1300 °C [4]. It was then disrupted by a catastrophic impact at ~5 Ma after CAI, followed by reassembly of daughter bodies from which the known ureilites probably originate [4–8]. Various degrees of shock recorded in ureilite silicates (e.g., [7,9,10]) may result largely from this event, although the reassembled bodies likely experienced subsequent impact events as well, including the recent breakup events that brought fragments of them into Earth-crossing orbits. The carbon in ureilites occurs dominantly as graphite, in elongated masses along silicate grain boundaries. There is compelling evidence (from very low shock ureilites) that the primary form of graphite in all ureilites was mm sized crystals of well-crystalline graphite [11–13]. Diamonds in ureilites always occur embedded in the graphite masses.

Some recent studies [14,15] have proposed formation of diamonds at static pressures >20 GPa in a large planetary body, similar to the diamonds formed deep within the Earth's mantle. This would imply that the UPB was a large planetary embryo, the former existence of which is predicted by current planetary formation models [15]. In contrast, Goodrich et al. [16] and Nestola et al. [17] showed that there is no evidence supporting the requirement of long growth times at high static pressures and argued for the formation by shock transformation from originally larger graphite crystals. Understanding the origin of the diamonds critically depends on constraining the thermometric and shock history of the graphite in which they are embedded, which is the subject of this investigation. [17] showed that graphite can be nanometric in size in shocked ureilites.

In order to elucidate the nature of graphite in different ureilitic fragments of AhS, we applied a graphite-based geothermometer (recently applied to chondrites by [18], and to other AhS ureilites by [19]) on these fragments (two of which were studied by [17]). In addition, using published calibrations on the ratio of Raman D-bands and G-bands intensities [20,21], we were able to determine the crystallite size of graphite, which could add crucial information regarding the thermal and crystallization/re-crystallization history of the graphite.

MATERIAL AND METHODS

Our study was performed on Almahata Sitta (AhS) samples AhS 72, AhS 209b and AhS A135A, which are three stones from the Almahata Sitta meteorite that fell in the Nubian desert in 2008 [2]. These samples belong to the collection of the University of Khartoum, Sudan. The petrographic description was carried out on the AhS 209b and AhS 72 polished sections. We obtained backscattered electron images (BSE) of non-carbon-coated sections of AhS 209b, AhS 72 and of the main mass (embedded in epoxy) of AhS A135A. For the AhS A135A sample, the SEM analysis was performed on just a tiny mass embedded in epoxy, as this was the only available sample.

The investigation by SEM on carbon aggregates was conducted at the Astromaterials Research and Exploration Science Division at the Johnson Space Center in Houston, Texas (USA) using the JEOL 5910-LV SEM (JEOL Ltd., Tokyo, Japan) and at the Centro Analisi per la Certificazione (CEASC) at the University of Padova (Italy) using the FEI Quanta 200 (FEL, Brno, Czech Republic), low vacuum SEM. The observations using the JEOL 5910-LV SEM were made at 15 KeV accelerating potential in normal high vacuum mode, despite the lack of carbon coat, in order to allow higher beam currents (and hence greater BSE contrast). Under these conditions charging of silicates was observed, but carbon areas were sufficiently conductive to provide good images. The BSE images of AhS A135A were obtained using the FEI Quanta 200 SEM, using 20 KeV accelerating potential in low vacuum mode. Silicate mineral compositions were determined by electron microprobe analyses (EMPA) at the Johnson Space Center, with techniques and results described in [17].

The polishing and cutting procedure for preparing the samples can induce defects on graphite crystals [22]. As reported by these authors, the polishing procedure could induce an unpredictable increase in the ID/IG ratio [integrated intensity(D-band)/integrated intensity(G-band)], which in this work has been used to determine the crystallite size [20], while it does not affect the Full Width at Half Maximum (FWHM) of (G) parameter [18]. For this specific reason, we conducted our Raman spectroscopy on unpolished carbon-bearing samples. This non-destructive approach is crucial for providing reliable estimation of crystallite size by Raman spectroscopy of graphite.

Graphite-bearing fragments, with sizes ranging between 0.10 and 0.50 mm, were gently removed from the AhS ureilites and only non-polished volumes of such fragments were glued on top of 0.10 mm thick glass fibers (Figure 1).

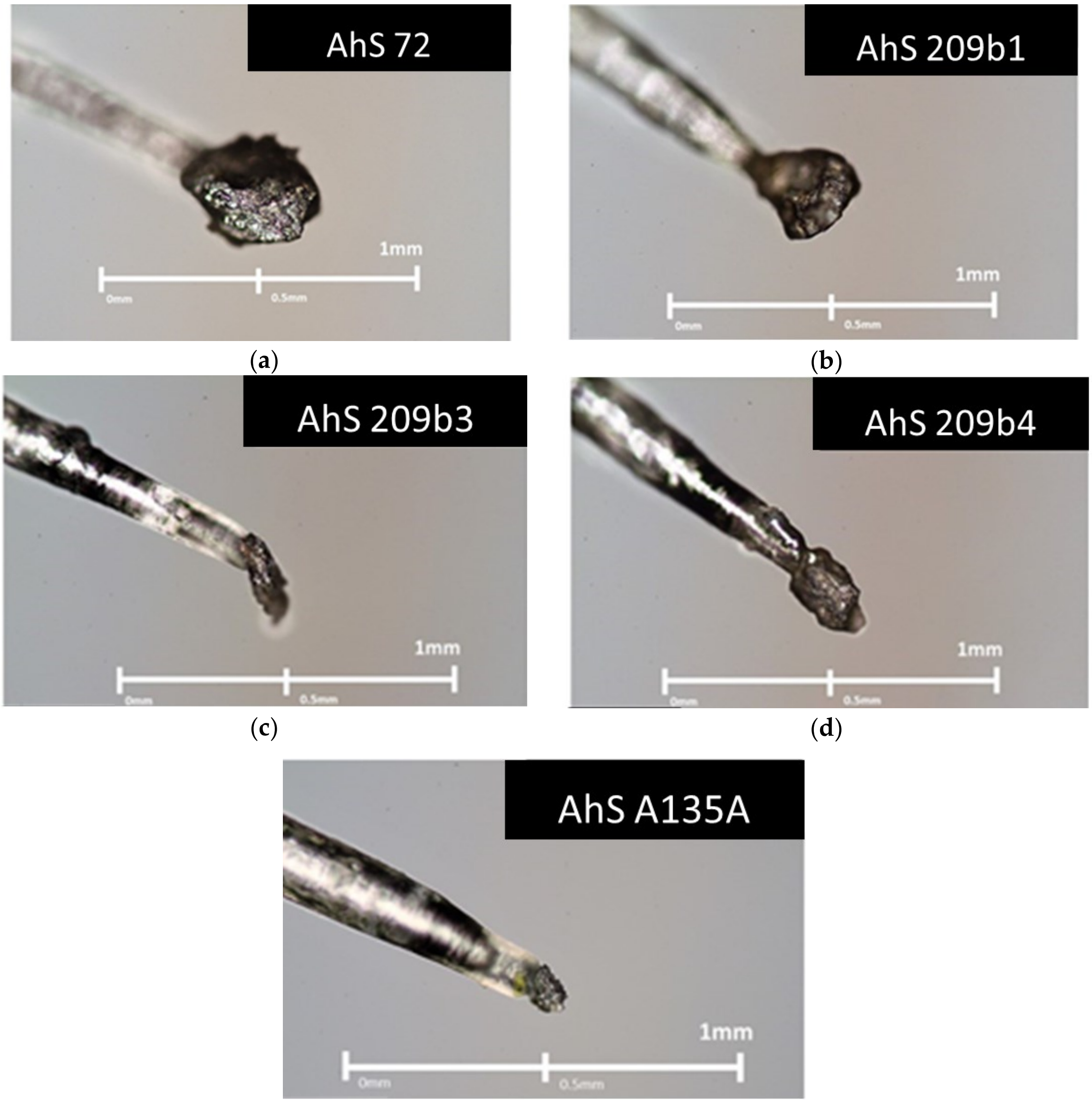

(**a**) (**b**) (**c**) (**d**) (**e**)

Fig. 1. Graphite-bearing fragments glued on top of glass fibers 0.1 mm thick. (a) Almahata Sitta (AhS) 72. (b) AhS 209b1. (c) AhS 209b2. (d) AhS 209b4. (e) AhS A135A.

Confocal micro-Raman Spectroscopy (MRS) analysis was conducted on the graphite fragments (e.g., Figure 1) using an inVia Renishaw micro-Raman spectrometer installed at the Department of Chemical Sciences of the University of Padova. We used a 514 nm laser excitation with an operating power of 1.3 mW, in order to avoid any graphite damage. A magnification of 50× was used for AhS 209b and AhS 72 samples while for AhS A135A we used a magnification of 100×. The spectral resolution was 1.5 cm^{-1}, the laser beam spot on the samples was about 1 μm. For each sample, we used a 30 s integration time with five accumulations for each spectrum. The spectra were always collected very far from the areas in contact with the fiber glass to avoid any Raman signal coming from the glue. A highquality octahedral gemstone lithospheric diamond was used as a standard material to obtain the instrumental broadening, following the same experimental procedure used in [19] (see section on geothermometry below). Curve fitting of the spectra was carried out using the software OMNICTM for dispersive Raman (Thermo Fisher Scientific, Waltham, WA, USA), adopting Gaussian and Lorentzian curves to obtain the best fit.

RESULTS

Petrographic Analysis: characterization of AhS Graphite phases

Fragments AhS 209b and AhS 72 (Figure 2) are fine-grained, porous ureilites showing various degrees of “impact-smelting” and shock metamorphism as previously described for fine-grained AhS ureilites and a few main group ureilites [23].

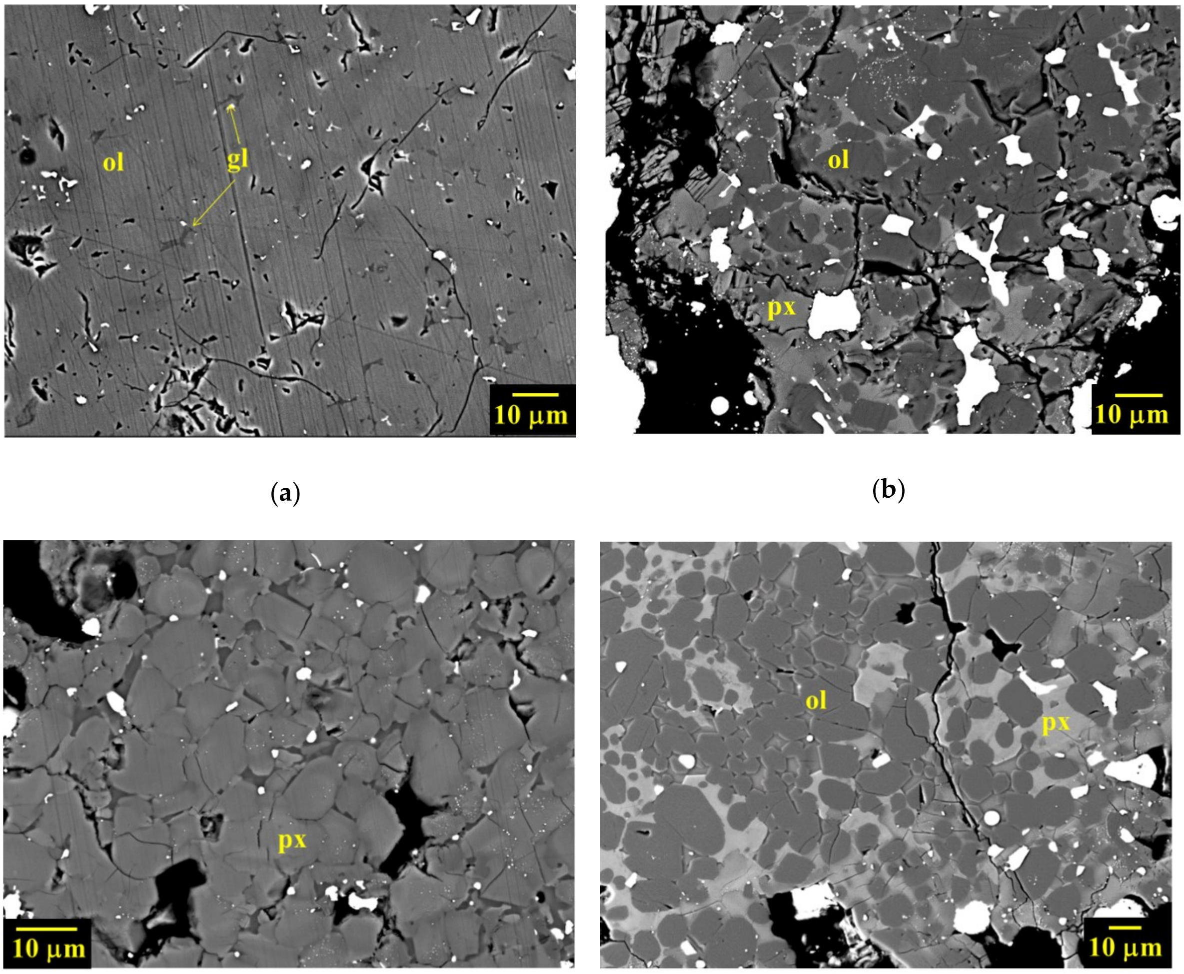

(a) (b) (c) (d)

Fig. 2. (a) Back-scattered electron image (BSE) of AhS #209b, showing the dominant texture of olivine areas (the parallel lines on the surface are polishing scratches). Original olivine (ol) crystals are completely mosaicized to ~5–20 μm sized equigranular tiles, with minor interstitial Si-Al-enriched glass (gl). (b) BSE of less common, impact-smelted olivine area in AhS 209b, μm sized equigranular, rounded, grains of interstitial pyroxenes (px). Metal and sulfide grains (bright) are common. (c) BSE of AhS #209b showing impact-smelted pyroxene, consisting of aggregates of ~5–10 μm sized subhedral grains, with small of interstitial Ca-enriched pyroxenes (px) and Si-Al-enriched glass. Pores and small grains of metal and sulfide (bright) are common. Pyroxenes are reduced relative to inferred primary compositions and show further-reduced outer rims. (d) BSE showing dominant lithology in AhS #72, similar to (b), of equigranular, rounded, highly reduced olivine with interstitial pyroxene.

It is evident in Figure 2 that olivine areas in AhS 209b are completely mosaicized. They consist of aggregates of ~5–20 μm sized equigranular tiles (adopting the terminology of [23]) with tiny amounts of interstitial pyroxene and Si-Al-rich glass. The outlines of the original larger (~mm sized) primary silicate grains are defined by cracks, aggregates of carbon phases and metal as seen in Figures 3 and 4.

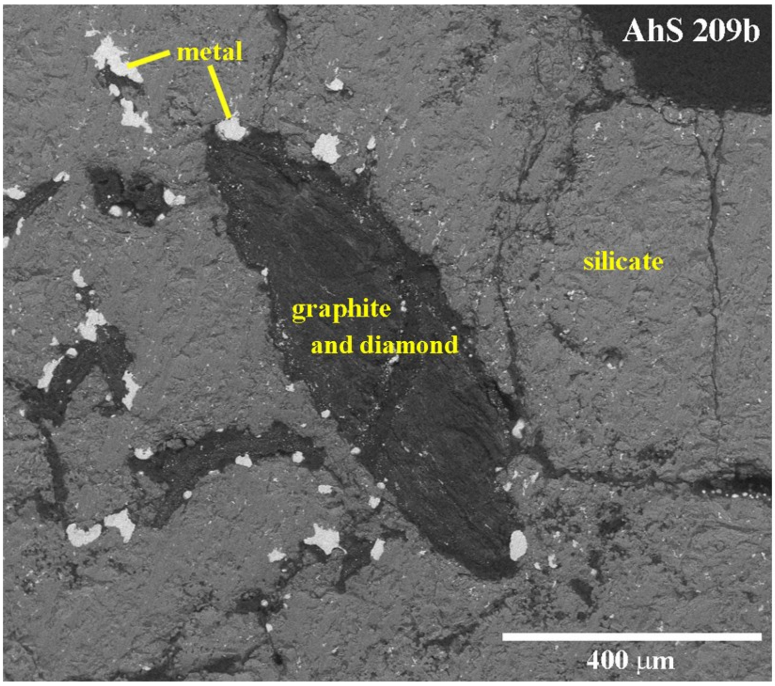

Fig. 3. Carbon area in polished sections of AhS 209b. Back-scattered electron image (BSE) of the noncarbon- coated section of AhS 209b collected in low-vacuum mode.

The olivine largely preserves a typical ureilite olivine core composition of Fo ~79, except in reduction rims near original grain boundaries and/or graphite aggregates. Reduction rim compositions range up to Fo ~93. Pigeonitic pyroxene areas in AhS 209b also show complete mosaicism with extensive in-situ reduction and porosity. They consist of aggregates of ~5–10 µm sized subhedral to anhedral grains, with varying amounts of interstitial Ca-enriched pyroxenes and Si-Al-enriched glass. Pores and small grains of metal and sulfide among the pyroxene grains are common. The pyroxene tiles show reverse zoning. Cores are reduced (core Mg#s up to ~93) relative to inferred primary compositions (~Mg# 81, such as would have been in equilibrium with Fo ~79 olivine) with varying Wo contents (~2–8). Dustings of very fine metal grains occur in some of the cores, indicating multiple episodes of reduction. Pyroxene textures such as these were described by [23] in several main groups and Almahata Sitta ureilites and were attributed to “impact smelting”.

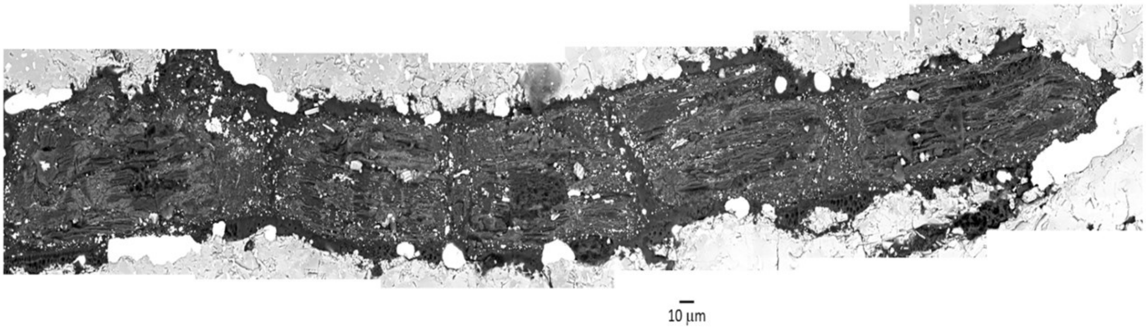

Fig. 4. Collage of six BSE images showing blade-shaped carbon area in AhS 209b.

The fragment of AhS 72 that we examined is dominated by olivine and shows a higher degree of shock metamorphism than AhS 209b. Olivine is completely re-crystallized to ~1–20 µm sized equigranular (anhedral to subhedral) grains in a groundmass (of varying proportions relative to the amount of olivine) of pyroxene. The olivine grains are highly reduced (Fo ~99) and nearly free of inclusions, suggesting re-crystallization from a melt (or at least at very high temperatures) under highly reducing conditions [17]. Interstitial pyroxene compositions range from Wo 0.8 to Wo 34 and are also reduced (Mg# 88–99). Pores, masses of graphite, and grains of metal are abundant and generally on a much larger scale (~20–100 µm) than the olivine grains. As also reported by [16,17], it is evident from Figures 3 and 4 that in samples AhS 209b and AhS 72, the carbon aggregates typically occur as elongated (blade-shaped), internally layered structures of up to 1 mm in length and 300 µm in width (Figure 2) located along original silicate grain boundaries. The lighter areas contain numerous tiny, bright grains of what appears to be mainly Fe-sulfides, based on the EDS spectra showing peaks for C, Fe, and S. The darker areas appear to be largely free of inclusions and have EDS spectra showing only C.

AhS A135A is composed of olivine and minor low Ca pyroxene and metal-sulfide blebs. AhS 135A is classified as a typical coarse-grained ureilite with a medium shock level. As in most ureilites, carbon masses occur principally in elongated shapes along silicate grain boundaries. Carbon phases are intermixed with minor Fe and Ni compounds and sulfides (Figure 5).

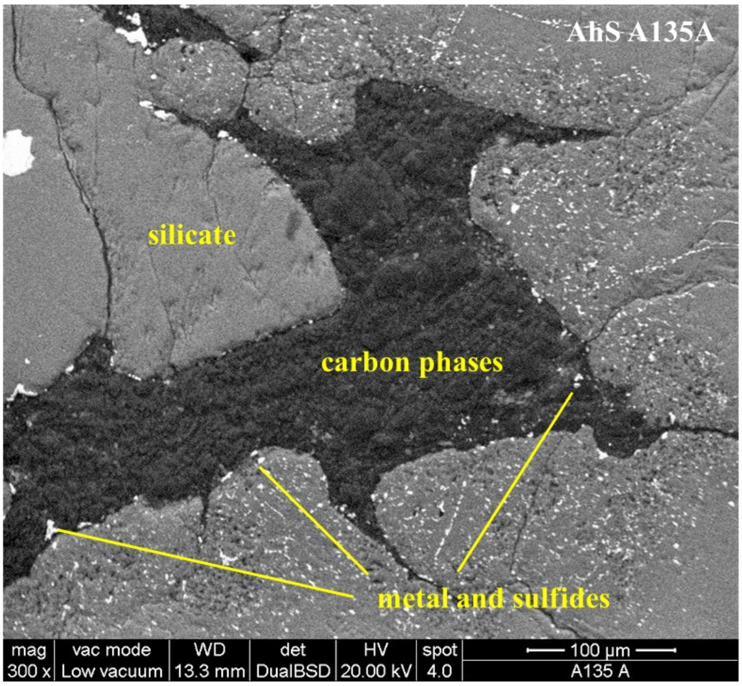

Fig. 5. Carbon area in AhS A135A. Back-scattered electron image (BSE) of the non-carbon-coated surface of AhS A135A collected in low-vacuum mode.

Micro-Raman Analysis: characterization of AhS graphite phases

Figure 6 shows a typical Raman spectrum of graphite in our AhS samples. The spectra off all the samples with the D’-band (following the same nomenclature used by [21]). The G-band is at around 1580 cm^{-1}, which is the main band of crystalline graphite; the D-band is at around 1355 cm^{-1}, which is defect-induced and is the band that refers to the disordered graphite [21]. In almost all samples, the D’-band at around 1620 cm^{-1} is detected as a shoulder of the G-band peaks.

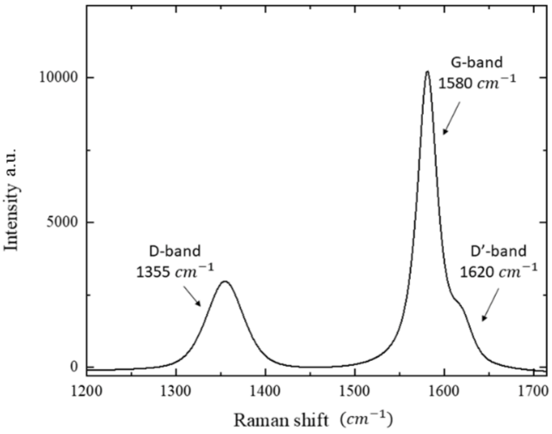

Fig. 6. A Raman spectrum of graphite in AhS 209b. The band positions are indicated in the spectrum: G-band at 1580 cm^{-1}, D-band at 1355 cm^{-1} and D'-band at 1620 cm^{-1}.

Table 1 shows the I(D)/I(G) ratio (where I = integrated intensity; D = D-band; G = G-band) for all the studied samples, representing the ratio of the integrated D- and G-band intensities. These values range between 0.3 and 0.9.

Table 1. Integrated intensities of the D- and G-bands, (I(D)/I(G) which is the ratio of the integrated intensities of the D and G band and the crystallite size of graphite (La) of all micro-Raman Spectroscopy (MRS) acquisitions of AhS samples. For the intensity ratios, I(D)/I(G), the standard deviation is 0.08. For La, the estimated uncertainty is in the order of 20 nm.

D-band	**G-band**	**I(D)/I(G)**	**L_a(nm)**
AhS 209 b1			
127900	399714	0.32	138
220935	479647	0.46	96
318675	710620	0.45	98
201393	397684	0.51	87
102706	351800	0.29	151
AhS 209b3			
338898	653892	0.52	84
360516	578409	0.62	70
206073	433157	0.48	92
321808	605128	0.53	83
280470	519306	0.54	81

AhS 209b4			
668370	1164605	0.57	77
203554	355261	0.57	77
282967	417484	0.68	65
211874	463592	0.46	96
287755	442705	0.65	68
AhS 72			
321884	550667	0.58	75
285483	476515	0.60	73
89546	127387	0.70	63
384023	491833	0.78	56
317754	479550	0.66	66
AhS A135A			
20946	37139	0.56	78
23887	35184	0.68	65
23911	44283	0.54	81
8174	18598	0.44	100
9394	21367	0.46	95

An important relationship between the ratio of the intensity of D-band and G-band [I(D)/I(G)] and the crystallite size of graphite (La) was noted by [20] and validated by [21] as follows [Equation (1)]:

$$\frac{I(D)}{I(G)} = \frac{C(\lambda_{\mathrm{L}})}{L_a} \tag{1}$$

The parameter C (λL = 514 nm), which corresponds to ~ 44 Å, represents the wavelength dependent prefactor. The wavelength dependency of C was considered by [24], who reported the following relation: C(λL) ≈C0 + λLC1, where C0 = =12.6 nm and C1 = 0.033, valid for 400 nm < λL < 700 nm [24,25].

The results obtained for our samples by applying Equation (1) are shown in Table 1. Our data show that graphite is nanometric with a crystallite size ranging from an average of 138(24) nm of AhS 209b to 67(8) nm of AhS 72 and 84(14) nm of AhS A135A.

Geothermometry Application to Graphite in AhS Ureilite

A geothermometer for determining the maximum temperature (Tmax) of the parent body of carbonaceous matter in chondrites was developed by [18]. In their study [18], they proposed that a unique spectroscopic feature identified by studying twenty-five different samples of meteoritic insoluble organic matter (IOM) through carbon X-ray absorption near edge structure (XANES) spectroscopy provided what these authors considered a good estimate of the parent body metamorphism.

Applying their approach to previously published micro-Raman data by [26], they were able to calibrate a new thermometric equation, which leads to a self-consistent organic derived temperature scale. [18] assumed that the error (2) associated with the use of GG is relatively large, as ±120 °C, is the uncertainty represented by the distribution of experimental points of their curve, see Equation (5) by [18]. Although the analytical uncertainty of this method is large, this geothermometer allows the determination of much higher temperatures than well-established methods used on terrestrial metamorphic graphite, which only permit the studying of samples of lower temperatures, e.g., 650 °C [27]. We also note that the temperature estimates made with this thermometer could be affected by defects induced during polishing. Thus, again, it is crucial that our data were obtained on non-polished graphite samples.

The equation of [18] is expressed in terms of Raman G-band full width at half maximum (hereafter GG) as follows [Equation (2)]:

$$T_{max}(°C) = 1594.4 - 20.4\Gamma_G - 5.8 \times 10^{-2}\Gamma_G^2 \tag{2}$$

Equation (2) was applied by [19] to non-polished graphite in AhS ureilite sample #7, resulting in an average temperature of 990 ± 120 °C.

Table 2 reports the positions of graphite peaks (G-band, D-band and D0 band) and the relevant GG values for all our studied samples and the T_{max} estimated temperature using Equation (2) of [19]. In order to compare our GG data with those published by [19], we corrected our data for the instrumental peak broadening using a high-quality gemstone lithospheric diamond, following the same procedure as in [19]. These authors reported for a lithospheric diamond a GG value equal to 3 cm^{-1}; our measurement on a lithospheric diamond provides a GG value equal to 6 cm^{-1}. Therefore, in Table 2, we report both uncorrected and corrected data. The T_{max} calculations were performed using corrected data (last column in Table 2).

Our calculations indicate an average temperature of 1266 °C for AhS 209b, 1242 °C for AhS 72 and 1332 °C for AhS A135A. The standard deviations of the measurements for these three average values are 77 °C, 46 °C and 28 °C, respectively. However, the analytical temperature uncertainties of ± 120 (2σ) °C estimated for this experimental approach by [18] are much higher.

Table 2. Center positions for G-, D- and D'-bands and GG (both in cm^{-1}) of all the studied samples. Calculated crystallization temperature, T_{max}, is reported in the last column and was obtained using Equation (2). The uncertainty (2σ) of T_{max} is ±120 °C.

G-band center	**G-band** Γ_G	**G-band** Γ_G **corrected**	**D-band center**	**D-band** Γ_G	**D′-band center**	**D′-band** Γ_G	T_{max} **(°C)**
AhS 209B							
b1							
1582	22	11	1356	41	1615	26	1360
1582	27	13	1354	49	1618	25	1310
1582	35	18	1352	47	1619	37	1212

1582	27	13	1355	46	1618	40	1309
1582	29	15	1355	47	1618	29	1285
b3							
1585	45	23	1354	55	1618	31	1103
1583	33	17	1354	50	1620	28	1237
1581	28	14	1355	50	1620	28	1300
1583	29	15	1355	48	1620	27	1284
1583	32	16	1355	57	1621	28	1254
b4							
1581	43	22	1355	60	1613	44	1122
1582	26	13	1355	49	1619	31	1313
1582	25	12	1354	47	1618	30	1332
1580	35	17	1353	51	1619	24	1219
1580	22	11	1353	52	1611	58	1357
AhS 72							
1577	33	13	1352	53	1616	37	1245
1579	40	16	1351	54	1616	31	1166
1581	29	20	1353	51	1606	68	1283
1584	32	15	1352	50	1619	33	1246
1583	30	14	1353	50	1620	29	1274
AhS A135A							
1582	25	13	1355	48	1619	20	1320
1583	28	14	1356	51	1618	26	1288
1582	22	10	1357	41	1620	25	1350
1580	21	12	1353	57	1614	30	1361
1582	23	11	1357	38	1620	23	1340

DISCUSSION

Comparing our results with the previous temperature estimate on AhS ureilite #7, obtained using the same technique [19], it is evident that our temperature data are higher by at least two uncertainty intervals, i.e., ~1240–1330 °C for our samples vs. 990 °C for AhS #7 [19]. Our temperature data are within the range of peak equilibration temperatures of ureilites recorded by pyroxene geothermometry [7,28,29], whereas the AhS #7 temperature [19] is lower.

The apparent agreement between the temperatures obtained on graphite by micro-Raman spectroscopy in this work and those obtained by pyroxene geothermometry in ureilites suggests the possibility that the graphite temperatures could record the temperature of the UPB due to internal heating/differentiation. However, our Raman data not only provide a temperature estimate recorded by graphite, but at the same time they also tell us that graphite is nanometric, which strongly suggests that this graphite is the product of some transformation from an original carbon compound. In detail, the geo-thermometer by [18] is based on graphite's G-band FWHM, which cannot be the same for recrystallized nanographite and original crystalline graphite in the ureilitic parent body. Consequently, as nanographite was reduced in size by the shock, the temperature recorded by this nanographite can be ascribed to the shock itself. For this reason, the temperatures we have estimated could represent the temperature recorded by graphite during a shock event. Graphite existing within the mantle of a planetesimal under conditions of high static pressure and temperature for millions of years, as inferred for the igneous stage of ureilite evolution [30,31], would not be expected to be nanometric in grain size, but rather to develop into much coarser crystals. Indeed, mm sized crystals of well-crystalline graphite, such as in very low-shock ureilites, are inferred to have been the primary igneous form of graphite in all ureilites [12], whereas the graphite in all shocked ureilites has been found to be internally polycrystalline and fine-grained [32]. In our samples, which have undergone a significant shock event [17], these primary graphite grains have been internally recrystallized to much smaller grain sizes, presumably during the shock process. This is also supported by the findings of [16] and [17] that this graphite is intimately associated with nanodiamonds, which were demonstrated to have plausibly formed by transformation from a pristine form of carbon (likely larger, well-crystalline graphite crystals) due to a shock event. Therefore, it seems unlikely that the temperatures recorded by nanometric graphite in our study correspond to the temperatures of pristine UPB. Although high shock pressures could also be accompanied by high-temperature regimes, our temperatures (e.g., 1200–1300 °C) are consistent with a shock event characterized by pressures as low as 15–20 GPa (determined by the AhS 72 and AhS 209b samples based on olivine mosaicism [17,33]). The evidence that high pressure could be accompanied by high-temperature regimes is well explained by [34] in their Figure 5, in which they reported the P-T Hugoniot curve for some rocks (e.g., gabbros, basalt, mare basalt, granite). Among them, there is also the Murchison carbonaceous chondrite (CC) (composed of olivine, pyroxenes and carbon phases), with a mineral association similar to that of an ureilite but with a considerably higher porosity in a larger matrix in respect to an ureilite. Using the data by [34], for our average temperatures between 1242 and 1332 °C, the returned shock pressure is between 21 and 23 GPa, respectively. However, it is known that a higher porosity and matrix of the carbonaceous chondrites [35, 36] could increase the temperature during a shock event. Therefore, if we consider these rheological differences between Murchison CC and ureilites, the pressures that refer to our estimated temperatures are underestimated. However, these are still consistent with the pressures derived from olivine mosaicism, which we observed in our meteorites (≥15 GPa) [17,33].

If our interpretation is correct, however, it begs the question as to why the graphite in AhS #7 [19] records a lower temperature than our samples, when AhS #7 appears to be of the same, high-shock level as AhS 72 and AhS 209b [37]. This question would require further investigation of the grain size of graphite in AhS #7 and a detailed comparison of shock features. Indeed, a comprehensive MRS study of graphite in ureilitic samples of a wide range of shock levels, including the least-shocked, is needed to fully understand the process of the resetting of MRS graphite temperatures by shock. In addition, it could be possible to compare the temperature recorded by graphite with the temperature estimated on pyroxenes using other geo-thermometric approaches [7]. Our results clearly suggest that this would be a fruitful area for future work and could have applications in other graphite-bearing meteorites.

An alternative mechanism is that the nanometric graphite could have formed from back-transformation of diamonds after the pressure was released. Based on recent works that have focused on the thermal stability of diamonds [38–40], it is proposed that nanodiamonds start to graphitize above 800 °C; however, such a process, analyzed by high-resolution transmission electron microscopy, is characterized by the presence of an "onion graphite structure". Such a structure was not observed by TEM in our samples, see [17]. A second scenario of diamond graphitization could refer to graphitization from a large pristine microdiamond but the temperatures recorded by the graphite of our samples were close to 1200–1300°C and this range of temperature, according to [39], is not enough to induce graphitization on a microdiamond, and for this process temperatures above 1500 °C are required. The temperature obtained in this work on graphite, close to 1240–1330 °C (±120 °C), could represent the temperature related to the shock event or, following [34], it could be the post-shock temperature.

CONCLUSIONS

In this work, we investigated, by Raman spectroscopy, unpolished fragments of graphite in ureilites AhS 209b, AhS 72 and AhS A135A. AhS 209b and AhS 72 were recently studied by [16], who characterized them by X-ray diffraction and determined that these fragments consisted mainly of intimately associated nanodiamond and nanographite. Graphite in our AhS ureilite samples is nanometric with a crystallite size ranging between about 70 and 140 nm.

Our micro-Raman study on graphite provided the following results: all samples showed homogeneous values of G-band centers (between 1577 and 1585 cm^{-1}) and D-band centers (between 1351 and 1357 cm^{-1}); the GG values of graphite for the G-band provided temperatures between 1242 and 1332 °C (±120 °C), which is two sigma higher than previous temperature estimates.

The mineral association of nanodiamonds and nanographite in ureilites points to the production of an impact event. Although the obtained temperature is similar to the reported igneous equilibration temperatures of ureilites [7], the observation that graphite in our sample is nanometric suggests the temperature recorded in the crystallization structure of the graphite is imprinted by the shock wave. This imprinting likely occurred during the strongest impact event it experienced during its history, which was probably the one disrupting the ureilite parent body.

Aknoledgments

Funding: This research was funded by PNRA 2018 (COMMANDER project, grant number PNRA18 00247 – A to F. Nestola) and NASA EW program (grant numbers 80NSSC17K0165, NNX17AH09GS03, and 80NSSC19K0507 to C. A. Goodrich).

Acknowledgments: The authors thank the anonymous reviewers for the helpful suggestions which improved the manuscript.

References

1. Jenniskens, P.; Shaddad, M.H.; Numan, D.; Elsir, S.; Kudoda, A.M.; Zolensky, M.E.; Le, L.; Robinson, G.A.; Friedrich, J.M.; Rumble, D.; et al. The impact and recovery of asteroid 2008 TC3. Nature 2009, 458, 485–488.

2. Shaddad, M.H.; Jenniskens, P.; Numan, D.; Kudoda, A.M.; Elsir, S.; Riyah, I.F.; Ali, A.E.; Alameen, M.; Alameen, N.M.; Eid, O.; et al. The recovery of asteroid 2008 TC3. Meteorit. Planet. Sci. 2010, 45, 1618–1637.

3. Horstmann, M.; Bischoff, A. The Almahata Sitta polymict breccia and the late accretion of asteroid 2008 TC_3. Geochemistry 2014, 74, 149–183.

4. Goodrich, C.A.; Hartmann, W.K.; O'Brien, D.P.; Weidenschilling, S.J.; Wilson, L.; Michel, P.; Jutzi, M. Origin and history of ureilitic material in the solar system: The view from asteroid 2008 TC3 and the Almahata Sitta meteorite. Meteorit. Planet. Sci. 2015, 50, 782–809.

5. Downes, H.; Mittlefehldt, D.W.; Kita, N.T.; Valley, J.W. Evidence from polymict ureilite meteorites for a disrupted and re-accreted single ureilite parent asteroid gardened by several distinct impactors. Geochim. Cosmochim. Acta 2008, 72, 4825–4844.

6. Goodrich, A.C.; Scott, E.R.D.; Fioretti, A.M. Ureilitic breccias: Clues to the petrologic structure and impact disruption of the ureilite parent asteroid. Geochemistry 2004, 64, 283–327.

7. Herrin, J.S.; Zolensky, M.E.; Ito, M.; Le, L.; Mittlefehldt,D.W.; Jenniskens, P.; Ross, A.J.; Shaddad, M.H. Thermal and fragmentation history of ureilitic asteroids: Insights from the Almahata Sitta fall. Meteorit. Planet. Sci. 2010, 45, 1789–1803.

8. Michel, P.; Jutzi, M.; Richardson, D.C.; Goodrich, C.A.; Hartmann,W.K.; Brien, D.P.O. Selective sampling during catastrophic disruption: Mapping the location of reaccumulated fragments in the original parent body. Planet. Space Sci. 2015, 107, 24–28.

9. Mikouchi, T.; Zolensky, M.E.; Ohnishi, I.; Suzuki, T.; Takeda, H.; Jenniskens, P.; Shaddad, M.H. Electron microscopy of pyroxene in the Almahata Sitta ureilite. Meteorit. Planet. Sci. 2010, 1820, 1812–1820.

10. Nakamuta, Y.; Kitajima, F.; Shimada, K. In situ observation, X–ray diffraction and Raman analyses of carbon minerals in ureilites: Origin and formation mechanisms of diamond in ureilites. J. Petrol. Sci. 2016, 111, 252–269.

11. Berkley, J.L.; Taylor, G.J.; Keil, K.; Harlow,G.E.; Prinz, M. The nature and origin of ureilites. Geochim. Cosmochim. Acta 1980, 44, 1579–1597.

12. Berkley, J.L.; Jones, J.H. Primary igneous carbon in ureilites: Petrological implications. J. Geophys. Res. 1982, 87, A353–A364.

13. Treiman, A.H.; Berkley, L. Igneous petrology of the new ureilites Nova 001 and Nullarbor 010. Meteorit. Planet. Sci. 1994, 848, 843–848.

14. Miyahara, M.; Ohtani, E.; El Goresy, A.; Lin, Y.; Feng, L.; Zhang, J.; Gillet, P.; Nagase, T.; Muto, J.; Nishijima, M. Unique large diamonds in a ureilite from Almahata Sitta 2008 TC_3 asteroid. Geochim. Cosmochim. Acta 2015, 163, 14–26.

15. Nabiei, F.; Badro, J.; Dennenwaldt, T.; Oveisi, E.; Cantoni, M.; Hèbert, C.; El Goresy, A.; Barrat, J.; Gillet, P. A large planetary body inferred from diamond inclusions in an ureilite meteorite. Nat. Commun. 2018, 9, 1–6.

16. Goodrich, C.A.; Nestola, F.; Jakubek, R.; Erickson, T.; Fries, M.; Fioretti, A.M.; Ross, D.K.; Brenker, F.E. The origin of diamonds in ureilites. In Proceedings of the 51st Lunar and Planetary Science Conference, Houston, TX, USA, 16–20 March 2020.

17. Nestola, F.; Goodrich, C.A.; Morana, M.; Barbaro, A.; Christ, O.; Brenker, F.E.; Domeneghetti, M.D.; Dalconi, M.C.; Alvaro, M.; Fioretti, A.M.; et al. Impact shock origin of diamonds in ureilite meteorites. Proc. Natl. Acad. Sci. USA 2020.

18. Cody, G.D.; Alexander, C.M.O.D.; Yabuta, H.; Kilcoyne, A.L.D.; Araki, T.; Ade, H.; Dera, P.; Fogel, M.; Militzer, B.; Mysen, B.O. Organic thermometry for chondritic parent bodies. Earth Planet. Sci. Lett. 2008, 272, 446–455.

19. Ross, A.J.; Steele, A.; Fries, M.D.; Kater, L.; Downes, H.; Jones, A.P.; Smith, C.L.; Jenniskens, P.; Zolensky, M.E.; Shaddad, M.H. MicroRaman spectroscopy of diamond and graphite in Almahata Sitta and comparison with other ureilites. Meteorit. Planet. Sci. 2011, 46, 364–378.

20. Tuinstra, F.; Koenig, J.L. Raman Spectrum of Graphite. J. Chem. Phys. 1970, 53, 1126–1130.

21. Ferrari, A.C.; Roberson, J. Interpretation of Raman spectra of disordered and amorphous carbon. Phys. Rev. B 2000, 61, 14095–14107.

22. Ammar, M.R.; Galy, N.; Rouzaud, J.N.; Toulhoat, N.; Vaudey, C.E.; Simon, P.; Moncoffre, N. Characterizing various types of defects in nuclear graphite using Raman scattering: Heat treatment, ion irradiation and polishing. Carbon 2015, 95, 364–373.

23. Warren, P.H.; Rubin, A.E. Pyroxene -selective impact smelting in ureilites. Geochim. Cosmochim. Acta 2010, 74, 5109–5133.

24. Matthews, M.J.; Pimenta, M.A. Origin of dispersive effects of the Raman D band in carbon materials. Phys. Rev. B 1999, 59, 6585–6588.

25. Zickler, G.A.; Smarsly, B.; Gierlinger, N.; Peterlik, H.; Paris, O. A reconsideration of the relationship between the crystallite size La of carbons determined by X-ray diffraction and Raman spectroscopy. Carbon 2006, 44, 3239–3246.

26. Busemann, H.; Alexander, C.M.O.; Nittler, L.R. Characterization of insoluble organic matter in primitive meteorites by microRaman spectroscopy. Meteorit. Planet. Sci. 2007, 42, 1387–1416.

27. Beyssac, O.; Goe, B.; Chopin, C.; Rouzaud, J.N. Raman spectra of carbonaceous material in metasediments: A new geothermometer. J. Metamorphic. Geol. 2012, 20, 859–871.

28. Goodrich, C.A.;Wilson, L.; Van Orman, J.A.; Michel, P. Comment on "Parent body depth-pressure-temperature relationships and the style of the ureilite anatexis" by P. H. Warren (MAPS 47:209-227). Meteorit. Planet. Sci. 2013, 48, 1096–1106.

29. Warren, P.H. Parent body depth-pressure-temperature relationships and the style of the ureilite anatexis. Meteorit. Planet. Sci. 2012, 47, 209–227.

30. Goodrich, C.A.; Van Orman, J.A.; Wilson, L. Fractional melting and smelting of the ureilite parent body. Geochim. Cosmochim. Acta 2007, 71, 2876–2895.

31. Collinet, M.; Grove, T. Incremental melting in the ureilite parent body: Initial composition, melting temperatures, and compositions. Meteorit. Planet. Sci. 2020, 4, 832–856.

32. Mittlefehldt, D.W.; McCoy, T.J.; Goodrich, C.A.; Kracher, A. Non-chondritic meteorites from asteroidal bodies. Planet. Mater. 1998, 36, 1–195.

33. Stöer, D.; Hamann, C.; Metzlet, K. Shock metamorphism of planetary silicate rocks and sediments: Proposal for an updated classification system. Meteorit. Planet. Sci. 2018, 53, 5–49.

34. Gillet, P.; El Goresy, A. Shock Events in the Solar System: The message from minerals in Terrestrial Planets and Asteroids. Annu. Rev. Earth Planet. Sci. 2013, 41, 247–285.

35. Flynn, G.J.; Moore, L.B.; Klöck, W. Density and Porosity of Stone Meteorites: Implication for the Density, Porosity, Cratering, and Collisional Disruption of Asteroids. Icarus 1999, 142, 97–105.

36. Corrigan, C.M.; Zolensky, M.E.; Long, M.;Weir, J. Comparison of Porosity and Permeability in Chondritic Materials. Meteorit. Planet. Sci. 1996, 31, A32.

37. Zolensky, M.E.; Herrin, J.S.; Mikouchi, T.; Ohsumi, K.; Friedrich, J.; Steele, A.; Rumble, D.; Fries, M.; Sandford, S.; Milam, S.; et al. Mineralogy and petrography of the Almahata Sitta ureilite. Meteorit. Planet. Sci. 2010, 45, 1618–1637.

38. Efremov, V.P.; Zakatilova, E.I.; Maklashova, I.V.; Shevchenko, N.V. Thermal stability of detonation-produced micro and nanodiamonds. J. Phys. Conf. Ser. 2018, 946, 012107.

39. Efremov, V.P.; Zakatilova, E.I. Spectroscopic methods of investigation and the thermal stability of detonation nanodiamonds. J. Phys. Conf. Ser. 2019, 1238, 012013.

40. Popov, V.A.; Egorov, A.V.; Savilov, S.V.; Lunin, V.V.; Kirichenko, A.N.; Denisov, V.N.; Blank, V.D.; Vyaselev, O.M.; Sagalova, T.B. Features of the transformation of detonation nanodiamonds into onion-like carbon nanoparticles. J. Surf. Invest. X-ray Synchrotron Neutron Tech. 2013, 7, 1034–1043.

CHAPTER 4

CHARACTERIZATION OF CARBON PHASES IN YAMATO 74123 UREILITE TO CONSTRAIN THE METEORITE SHOCK HISTORY

[1] Anna Barbaro, [2,3] Fabrizio Nestola, [4] Lidia Pittarello, [4] Ludovic Ferrière, [5] Mara Murri,
[6] Konstantin D. Litasov, [2] Oliver Christ, [1] Matteo Alvaro and [1] Maria C. Domeneghetti

[1] Department of Earth and Environmental Sciences, University of Pavia, Via A. Ferrata 1, I-27100, Pavia, Italy; [2] Department of Geosciences, University of Padova, Via Gradenigo 6, 35131, Padova, Italy; [3] Geoscience Institute, Goethe-University Frankfurt, Altenhöferallee 1, 60323, Frankfurt, Germany ; [4] Natural History Museum, Department of Mineralogy and Petrography, Burgring 7, 1010, Vienna, Austria; [5] Department of Earth and Environmental Sciences, University of Milano-Bicocca, I-20126, Milano, Italy; [6] Vereshchagin Institute for High Pressure Physics RAS, Troitsk, Moscow, 108840, Russia

Published version in press in American Mineralogist journal (https://doi.org/10.2138/am-2021-7856). American Geophysical Union. All Rights Reserved.
Submitted on November 21st, 2021, accepted on March 3rd, 2021 and now in press.

ABSTRACT

The formation and shock history of ureilite meteorites, a relatively abundant type of primitive achondrites, has been debated since decades. For this purpose, the characterization of carbon phases can provide further information on diamond and graphite formation in ureilites, shedding light on the origin and history of this meteorite group. In this work, we present X-ray diffraction and micro-Raman spectroscopy analyses performed on diamond and graphite occurring in the ureilite Yamato 74123 (Y-74123). The results show that nano- and micro-diamonds coexist with nano-graphite aggregates. This, together with the shock-deformation features observed in olivine, such as mosaicism and planar fractures, suggest that diamond grains formed by a shock event (≥ 15 GPa) on the Ureilitic Parent Body (UPB). Our results on Y-74123 are consistent with those obtained on the NWA 7983 ureilite and further support the hypothesis that the simultaneous formation of nano- and micro-diamonds with the assistance of a Fe-Ni melt catalysis may be related to the heterogeneous propagation and local scattering

of the shock wave. Graphite geothermometry revealed an average recorded temperature (T_{max}) of 1314°C (± 120°C) in agreement with previously estimated crystallization temperatures reported for graphite in Almahata Sitta ureilite.

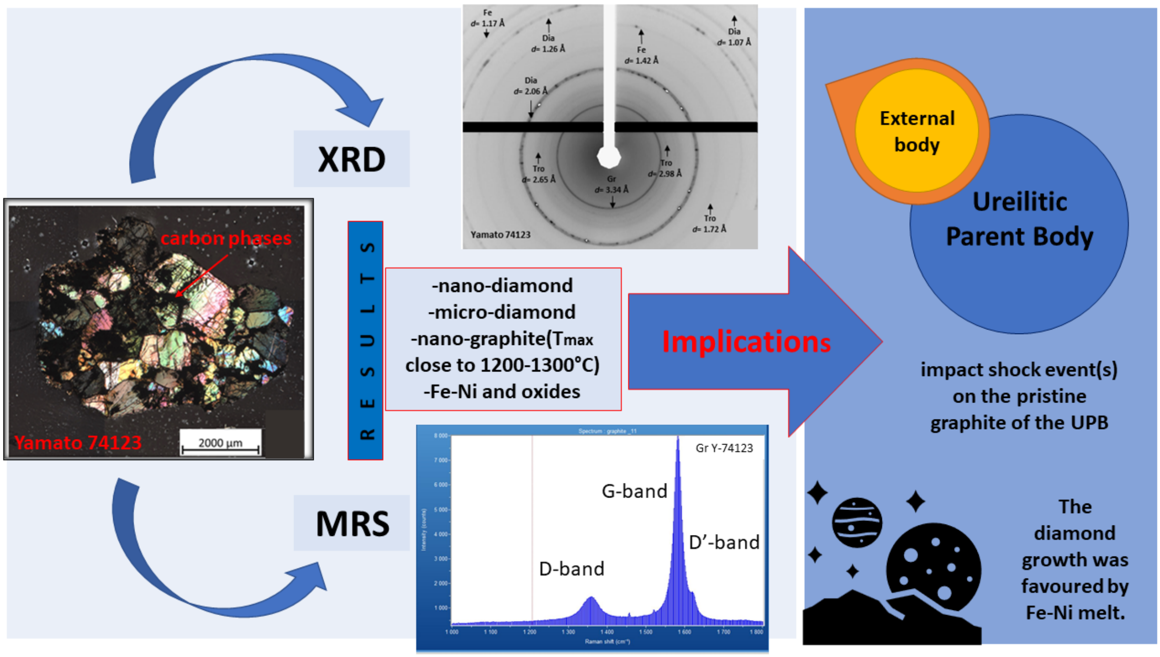

Graphical abstract of "CHARACTERIZATION OF CARBON PHASES IN YAMATO 74123 UREILITE TO CONSTRAIN THE METEORITE SHOCK HISTORY"

INTRODUCTION

Ureilites represent the second largest group of achondrite meteorites (Goodrich et al. 1992), with about 570 individuals with distinct names but only 6 observed falls (Meteoritical Bulletin Database 2020). Their formation, origin, and history are still under discussion among the scientific community. The debate about the formation of carbon phases contained in these meteorites has been going on for 80 years (see Nestola et al. 2020, and references therein).

As reported by Goodrich et al. (1992), ureilites appear to be fractionated ultramafic igneous rocks, either magmatic cumulates (Berkley et al. 1980; Goodrich et al. 1987) or partial melt residues (Boynton et al. 1976; Scott et al. 1992) and, thus, the products of planetary differentiation processes. These conclusions were based on mineralogy, textures, fabrics, lithophile element chemistry, and on some aspects of Sm-Nd isotopic systematics (Berkley et al. 1976) observed in these meteorites (Goodrich et al. 1992). Ureilites strongly differ from the other groups of stony meteorites (i.e., due to a high content of carbon phases and distinct oxygen isotopic composition) and, compared to chondrites, they are enriched in Mg, but depleted in metal, troilite, and alkalis. Ureilites typically contain large olivine grains and a few smaller low Ca-clinopyroxene (pigeonite) aggregates in a fine-grained, carbon-rich, matrix. Minor phases are kamacite (1-3 vol% with the Ni content up to 7.3 %), troilite (1-2%), chromite (1-2%), and carbon material (up to 8.5%) (Cloutis et al. 2010; Goodrich et al. 2015). Carbon is present as diamond, usually with stacking disorder and nanotwins (Németh et al. 2014, 2020a, 2020b; Salzmann et al. 2015; Murri et al. 2019), graphite, and organic material (e.g., Sabbah et al. 2010).

The different shock levels observed in ureilites are very important for constraining their history. Shock level determination in meteorites was first proposed by Stöffler et al. (1991, 2018) and is subdivided in six stages of shock for ordinary chondrites, from low (S1) to high (S6) level of shock, based on (i) shock effects in olivine and plagioclase (e.g., extinction, fractures, planar elements) and (ii) the presence of glass and/or of high-pressure silicate phases. Recently, Nakamuta et al. (2016) adapted the shock classification based on olivine in chondrites to the observations in ureilites. For this reason, we will apply this classification in this work.

The occurrence of diamonds in ureilites poses the question of how this high-pressure mineral formed and whether diamonds in ureilites are similar or not to those formed by shock in terrestrial impact structures (e.g., Masaitis 1998; Hough et al. 1995; Koeberl et al. 1997; Ohfuji et al. 2015; Murri et al. 2019). Three main hypotheses have been proposed for the formation of diamonds in ureilites: (i) static high-pressure conditions in the deep interior of large parent bodies (Urey 1956), (ii) direct transformation from graphite due to shock (e.g., Lipschutz et al. 1964; Bischoff et al. 1999; Grund and Bischoff 1999; Nakamuta et al. 2000, 2016; Hezel et al. 2008; Le Guillou et al. 2010; Ross et al. 2011; Lorentz 2019), also strongly supported by De Carli et al. (1995; 2002), and (iii) growth from a dilute gas phase, i.e., at low pressure in the solar nebula by a chemical vapor deposition (CVD) process (Fukunaga et al. 1987). The hypothesis of formation under static high-pressure conditions was recently supported by Miyahara et al. (2015) and Nabiei et al. (2018), who concluded that the size of a hypothetical Ureilitic Parent Body (UPB) could be comparable to the size of Mars, since static high-pressure conditions would be required for the formation of micrometer-scaled-diamond crystallites. The shock hypothesis was instead supported by the results obtained by Nakamuta et al. (2016). Indeed, these authors proposed that diamonds in ureilites could have formed at high-pressure (above 12 GPa) by spontaneous shock transformation from graphite, and at low pressure (6-10 GPa) by a solid-state catalytic transformation from graphite in presence of a Fe-Ni melt. Additional support to the shock hypothesis is provided in a recent work by Nestola et al. (2020) on Almahata Sitta samples (AhS 72 and AhS 209b), as well as on NWA 7983. In their study, graphite associated with nano- and (in NWA 7983) micro-diamonds was reported, suggesting that the conversion from graphite to diamond was triggered by an impact event and was favored by the catalytic effect of Fe-Ni melts.

Yamato 74123 (Y-74123) ureilite is a meteorite that was found in Antarctic in 1974 by the Japanese expedition on the Yamato mountains. The first detailed study of Y-74123 dates back to 1978, when Hintenberger et al. (1978) measured its noble gases contents as well as several major and minor elements bulk rock abundances. Takeda et al. (1980) have reported the petrological description and a chemical characterization of pyroxenes, which revealed Fe-bearing augite compositions ($En_{75}Fs_{18}Wo_{7}$). In addition, the magnetic properties of Y-74123 were studied by Nagata (1980). Moreover, Grady et al. (1985) carried out a C-isotopic study on Y-74123 reporting values of about $\delta^{13}C_{PDB}$=-1.7, well inside the range of ureilites. However, the carbon phases of Y-74123 have not been extensively studied yet.

In this work, we present the results of a multi-methodological study carried out on diamond and graphite aggregates observed in Yamato 74123, to understand the carbon phases formation in ureilites. In addition, a comparison with similar carbon phases in other meteorites, based on a literature survey, and a discussion on their possible formation hypothesis are also presented.

METHODS

The fragment of Y-74123 (NHMV-#7636_A) and a corresponding polished thin section (NHMV-L9822) investigated in this study were kindly provided by the Natural History Museum Vienna (Austria). The thin section was investigated by optical and electron microscopy at the Department of Earth and Environmental Science, University of Pavia (Italy). Scanning electron microscopy (SEM) of the uncoated fragment of Y-74123 was performed using a FEI Quanta 200 SEM equipped with an Energy Dispersive X-ray Spectrometry (EDS) in low vacuum mode at the CEASC (Centro di Analisi e Servizi per la Certificazione) of the University of Padova (Italy). Backscattered electron (BSE) images of Y-74123 were obtained in low vacuum mode analytical conditions, at the working distance of 10.6 mm, with an emission current of 93 mA, and a voltage of 20 kV, with the aim to identify the graphite beds in which diamonds were probably located. The BSE images collected by SEM were merged and analyzed with ImageJ and MultiSpec software to estimate the relative percentages of each phase of interest observed on the surface of the investigated meteorite fragment.

Carbon phases were manually extracted from the fragment and mounted on the tip of a 100 µm thick glass fiber (Fig. 1) and investigated using micro-Raman spectroscopy (MRS) followed by X-ray diffraction (XRD).

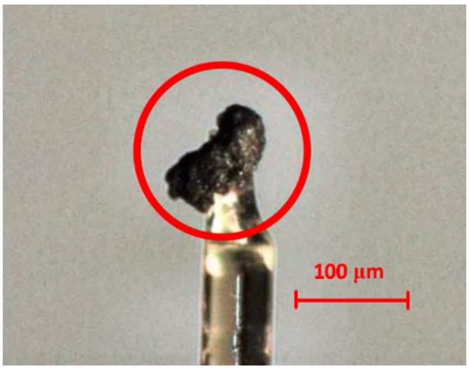

Fig. 1. Carbon-bearing subsample of Y-74123 attached at the top of a glass fiber. Micro-Raman spectroscopy and XRD analyses were performed on this subsample.

Micro-Raman spectroscopy analyses were performed on the graphite material occurring in the extracted carbon-bearing subsample of Fig. 1 to estimate the recorded temperature using the geothermometer of Cody et al. (2008), modified by Ross et al. (2011). The analysis of Y-74123 graphite was performed by high-resolution MRS using a Horiba LabRam HR Evolution spectrometer equipped with an Olympus BX41 confocal microscope at the controlled temperature of 20 (±1) °C at the Department of Earth and Environmental Science of the University of Pavia. A 532 nm laser excitation with an operating power of 1-2 mW (in order to prevent damage of the graphite), a grating of 600 g/mm, and a magnification of 50x was used. The spectrometer was calibrated using the silicon Raman peak at 520.5 cm^{-1}. The spectral resolution was 2 cm^{-1} and the acquisition time for each spectrum was 30 seconds with four accumulations. Curve fitting of the spectra was carried out using the OMNIC^{TM} software for dispersive Raman (Thermo Fisher Scientific) adopting Gaussian + Lorentzian curves to obtain the best fit. XRD analyses were then performed on the same carbon-bearing subsample (Fig. 1) using a Rigaku-Oxford Diffraction Supernova kappa-geometry goniometer with an X-ray Mo micro-source equipped with a Pilatus 200K Dectris detector in transmission mode, controlled by the Crysalis-Pro™ software at the Department of Earth and Environmental Science in University of Pavia. Line profile analysis fitting of the obtained diffraction pattern was performed using the High Score Plus Software package (Panalytical) to estimate the crystallite size.

RESULTS

Petrographic description and observation by Scanning Electron Microscopy

The investigated polished thin section of Y-74123 consists of aggregates of subhedral to anhedral olivine mineral grains, with varying amounts of interstitial pyroxenes and Si-Al-rich glass. The sample contains coarse-grained olivine and minor pigeonite crystals, ranging from 0.1 to 1.5 mm in size, surrounded by a large amount of opaque material (Fig. 2), composed of carbon mixed with different sulfides and metal phases. Pores and small grains of metal and sulfide (≤100 µm in size) commonly occur in the interstitial space between pyroxene and olivine grains.

The shock level of Y-74123 was determined using optical microscope observations on shock microstructures in olivine crystals in transmitted light and following the criteria of Stöffler et al. (1991, 2018) and Nakamuta et al. (2016). Olivine crystals show undulate extinction, planar fractures, and locally, mosaicism. The concurrent observation of undulate extinction and mosaicism in olivine indicates a pressure in the range of 15-20 GPa, corresponding to shock level S4 (Stöffler et al. 2018). In addition, both silicates, i.e., olivine and clinopyroxene, show darkening, caused by the dispersion of Fe-Ni metal and sulfides within the grains, which is commonly associated to shock metamorphism (e.g., Rubin 2006).

In the investigated sample, even after a careful inspection by optical and electron microscopy, high-pressure polymorphs of olivine, such as wadsleyite or ringwoodite, were not found.

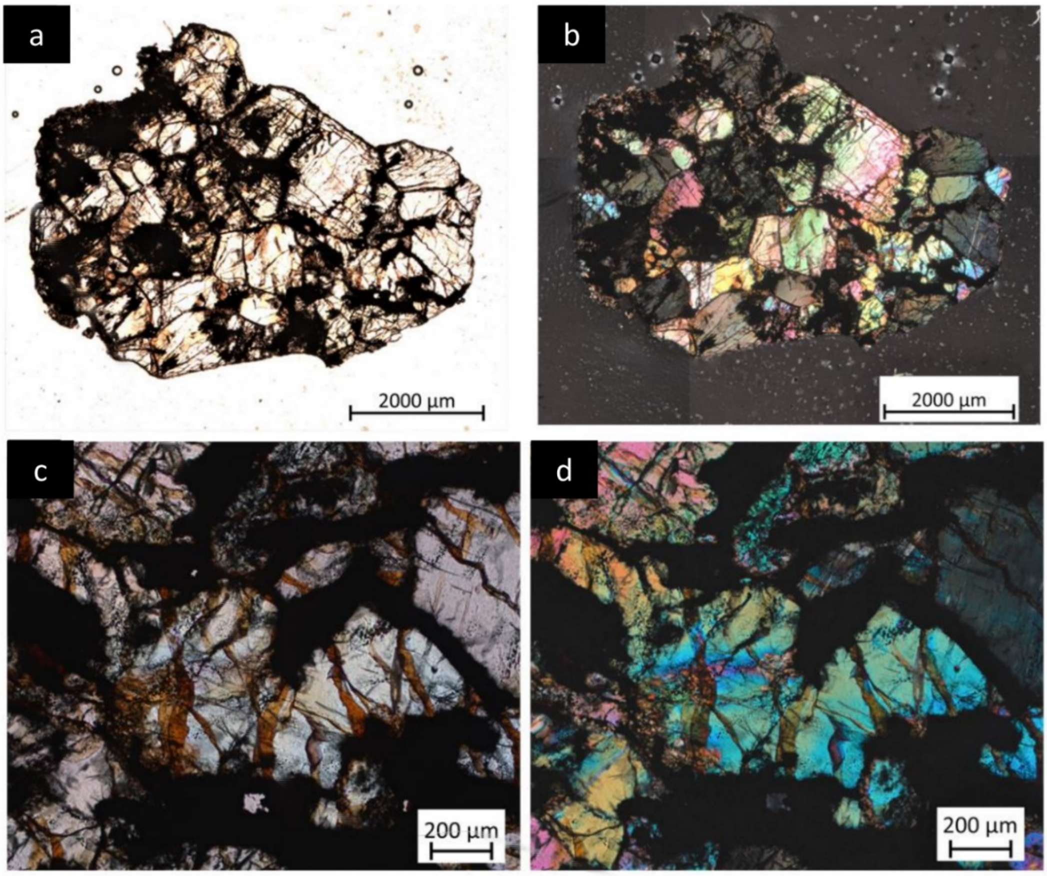

Fig. 2. Yamato 74123 polished thin section (NHMV-L9822) overview in plane-polarized light (a) and between crossed polarizers (b); detailed structure of olivine grains in Y-74123 in plane-polarized light (c) and between crossed polarizers (d) are also presented. Note the presence of interstitial opaque material and the size of olivine grains, which dominate the thin section.

A fragment of Y-74123, about 8 x 5 x 5 mm in size, was analyzed by SEM. Figure 3a shows a BSE image of a typical carbon aggregate which occurs as interstitial phase in silicates. The size of the carbon phases in Y-74123 is evident in Fig. 3b, where carbon phases are about 10 µm wide.

In Fig. 3a, it is possible to see that locally, metal phases, indicated as “Fe-Ni metal”, occur next to silicates. These metal phases are extremely fine-grained, partly mixed with the carbon phases.

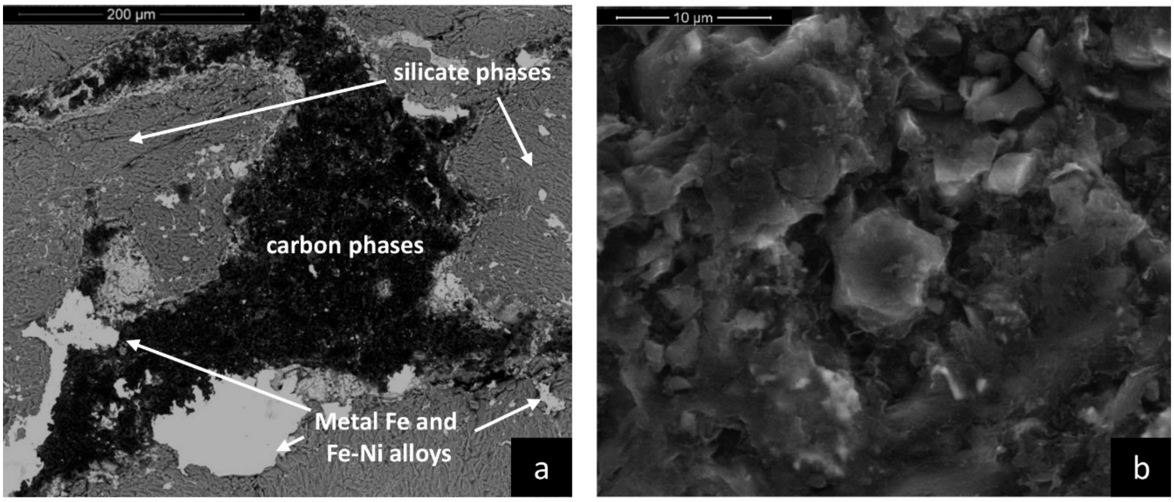

Fig. 3. (a) BSE image of a carbon aggregate from which the investigated carbon-bearing subsample was extracted. Also note the presence of silicate phases and Fe-Ni metal and alloys (metal + troilite + oxide); (b) detail of (a) in secondary electron (SE). As visible on this image, the aggregates in the carbon phases beds are not larger than 10 µm in size.

The relative abundances, expressed in percentages, of the main mineralogical components present on the surface of the investigated sample of Y-74123 are: 91% of silicate phases (olivine and pyroxene), 7% of carbon phases, and 2% of Fe-Ni metal and alloys, respectively (Fig. 4). The image analysis performed on the surface of the fragment of Y-74123 was important to evidence the best carbon aggregate zone from which to extract the carbon-bearing aggregate to be analyzed by MRS and XRD. The investigated fragment of Y- 74123 turned out to be relatively easy to be cut and polished in comparison with many other studied ureilites, indicating a relatively low amount of diamonds.

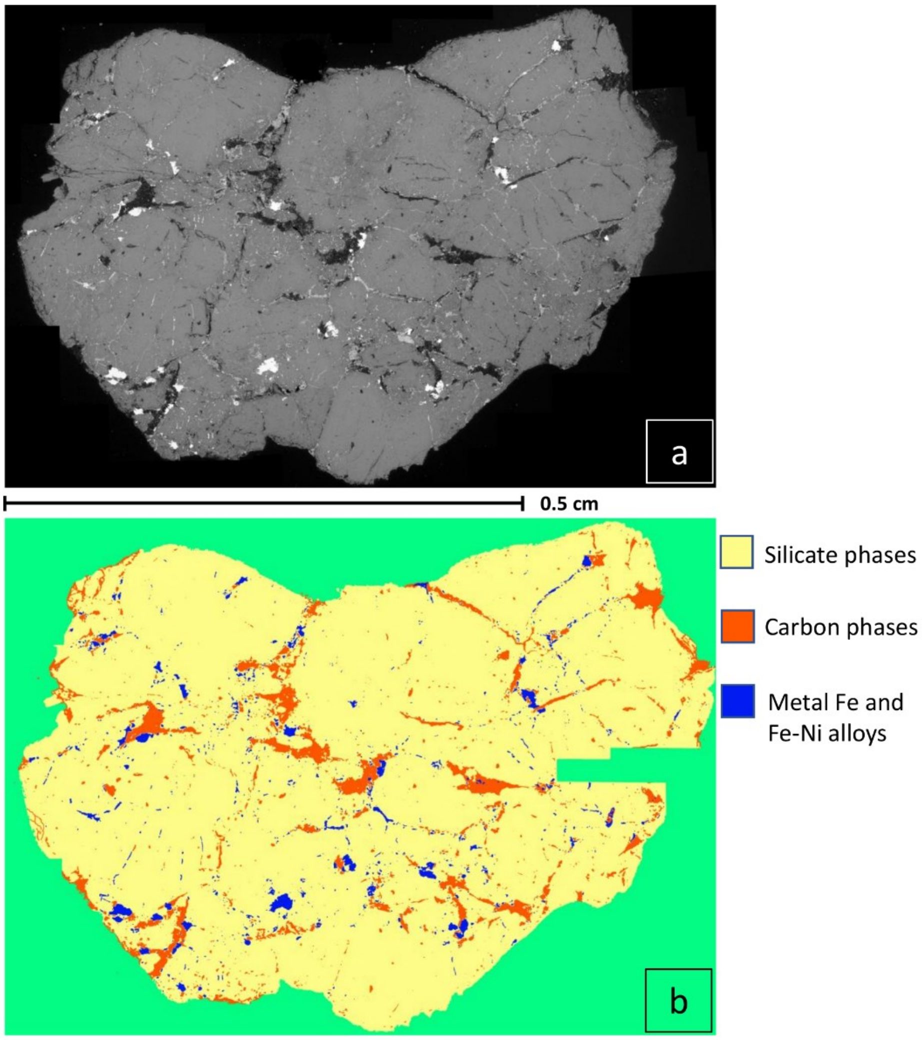

Fig. 4. (a) BSE mosaic of the Yamato 74123 fragment (NHMV-#7636_A) showing the typical texture of the meteorite; (b) image analysis applied to (a) with the percentage referred to silicate phases, carbon phases, Fe-Ni metal, Fe-Ni alloys and Fe-oxides.

X-Ray Diffraction

The reconstructed XRD image of the carbon-bearing aggregate of Yamato 74123 and its powder diffraction pattern are shown in Figs. 5a and b. Instead, Fig. 5c clearly shows the presence of spots referred to micrometer sized diamond.

In particular, Fig. 5a shows both rings and spots at d-spacing characteristic of cubic diamond (d-spacing at 2.06 Å, 1.26 Å, and 1.07 Å) and hexagonal graphite (highest peak at d-spacing at 3.34 Å, while the peaks at d-spacing 2.03 Å and 1.15 Å are overlapped by the diamond peaks). In Fig. 5b the highest peak of diamond (at d-spacing 2.06 Å) shows an asymmetry. This asymmetry could be ascribed, at higher d-spacing (d≈2.18 Å), to the presence of cubic and hexagonal sp^3 stacked layers or nanotwins (Murri et al. 2019) and, at lower d-spacing (d≈2.02 Å), to the main peak of Fe metal (which also shows peaks at d- spacing 1.42 Å and 1.17 Å). In addition to diamond, graphite, and Fe metal, a few other peaks can be assigned to troilite (d-spacing at 2.99 Å, 2.66 Å, 1.72 Å, and 1.68 Å), and also to minor silicate matrix components. The presence of cubic Ni, common in ureilites, cannot be excluded, as its peaks overlap those of metallic Fe and troilite.

To estimate the crystallite size of the carbon phases, we applied line profile analysis fitting to the diffraction pattern reported in Fig. 5b. The integral breadth values, which were obtained by this method, were then inserted into the Scherrer equation (Eq. 1 and 2, Scherrer 1918) to estimate the crystallite size, as follows:

$$(1) \qquad \beta(2\theta) = \frac{K_\beta \times \lambda}{<D>_V \; cos\theta_{hkl}}$$

$$(2) \qquad \frac{D_V}{K_\beta} = \frac{\lambda}{cos\theta_{hkl} \times \beta(2\theta)}$$

Scherrer equation provides a correlation between peaks broadening β, the dimension of diffracted domain, and the crystallite size (DV). K is a constant value ranging between 0.5 and 1, describing the contribution of crystallites shape and dependent upon the relative orientation of the scattering vector with respect to the external shape of the crystallite (Scherrer 1918).

For diamond, in order to obtain a reliable estimate of the crystallite size, we only used the two peaks at d-spacing 1.26 Å and 1.07 Å, as they do not exhibit any overlap with peaks of other phases within the analyzed carbon fragment. A similar approach was used to estimate the crystallite size of graphite, using the peak at d-spacing 3.34 Å (see Table 1). The results are reported in Table 1 along with the unit cell parameters and the space group for the diamond single crystal found in Y-74123. The possibility to estimate the unit-cell parameters for the investigated diamond in Y-74123 implies that micrometer-sized diamonds (i.e., spots in the diffraction image) are present. As it appears from the XRD images (Figs. 5a and c), i.e., on the basis of the presence of spots and rings, we can state that nano-graphite coexists with micro- and nano-diamonds in Y-74123, as also observed by Goodrich et al. (2020) and Nestola et al. (2020) in the NWA 7983 ureilite.

Table 1. The unit cell parameters for the micrometer-sized cubic diamond single crystal found in Y-74123. Mo $\lambda \approx 0.71$. 2θ° positions of the graphite and diamond diffraction peaks, d spacings, and the crystallite size (D_v) are reported. The crystallite size was calculated using the most intense peak of graphite at 3.34 Å, and the two peaks of diamond at 1.26 Å and 1.07 Å.

single crystal micrometer-sized diamond

$a = 3.569(1)$ Å

$V = 45.46(2)$ Å^3

polycrystalline diamond

Pos. [2θ°]	***d*-spacing (Å)**	**D_v (nm)**
32.65	1.26	15
38.50	1.07	11

polycrystalline graphite

Pos. [2θ°]	***d*-spacing (Å)**	**D_v (nm)**
12.10	3.34	8

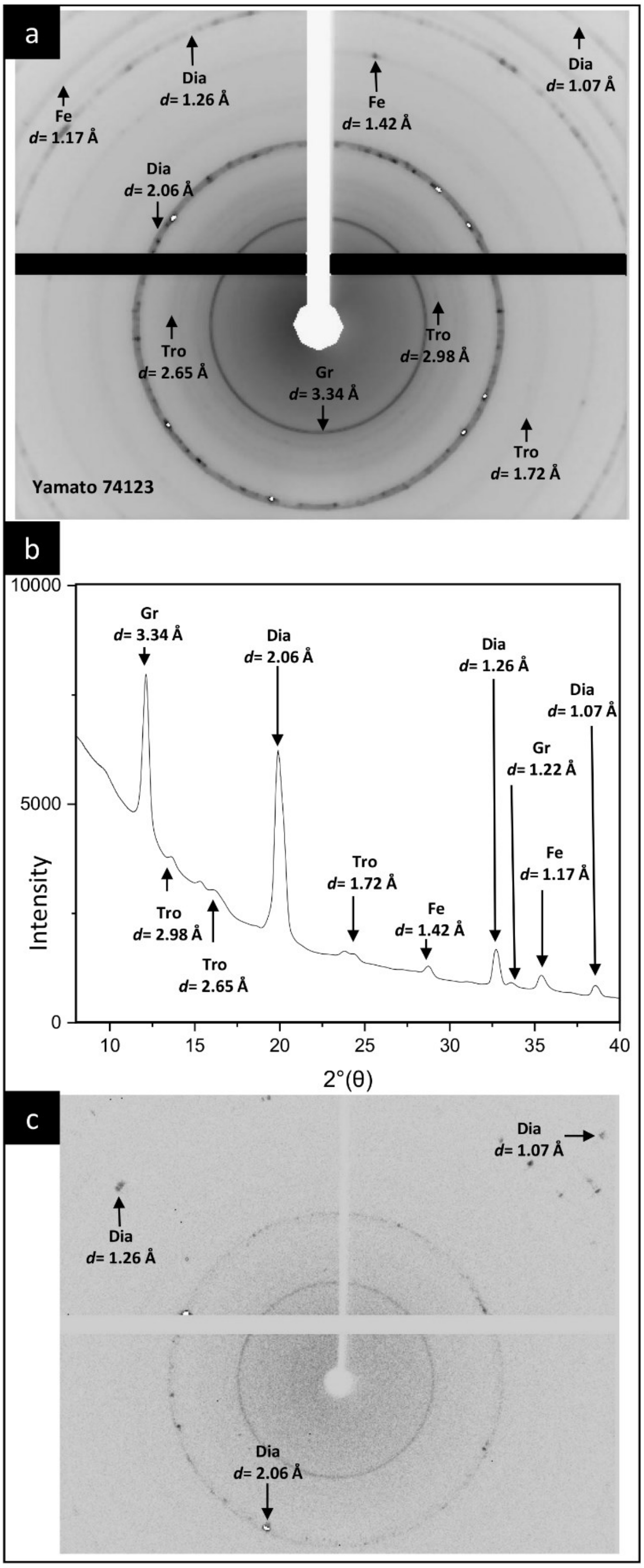

Fig. 5 X-ray diffraction images of the carbon-bearing subsample from Y-74123. In (a) reconstructed powder diffraction image and in (b) X-ray diffraction pattern of the investigated sample, analyzed by micro X-ray powder diffraction, are shown. The most abundant phases found in the carbon-bearing aggregate are diamond (Dia), graphite (Gr), Fe metal (Fe), and troilite (Tro). In (c) a diffraction image shows the spots corresponding to micrometer-sized diamonds.

Micro-Raman spectroscopy

We applied the geothermometric approach by Cody et al. (2008) and Ross et al. (2011), following the same procedure as reported in Barbaro et al. (2020a, 2020b) for Almahata Sitta samples (AhS 209b, AhS 72, and AhS A135A), to determine the T_{max} recorded by graphite. The temperature was estimated using Eq. 3, expressed in terms of Raman G-band full width at half maximum (FWHM) (Γ_G):

$$(3) \qquad T_{max}(°C) = 1594.4 - 20.4\Gamma_G - 5.8 \times 10^{-2}\Gamma_G^2$$

In Table 2, we list the graphite peaks positions (G-band, D-band, and D' band), the relevant Γ_G values (G, D, and D' bands FWHM) for Y-74123, as well as the T_{max} estimated using Eq. 3.

In order to compare our Γ_G data with those published by Ross et al. (2011) and Barbaro et al. (2020b), we corrected our data for the instrumental peak broadening using a high-quality gemstone lithospheric diamond (with $\Gamma_G = 5$ cm^{-1}), following the same procedure as in Ross et al. (2011) (see Table 2). In Table 2, for each set of acquisition, the values of Γ_G used in Eq. 3 to obtain the T_{max}, are reported. T_{max} values range between 1265 and 1334 (± 228 120) °C. These temperatures are slightly higher than those obtained by Ross et al. (2011) on graphite in AhS #7 ureilitic fragment (T_{max} of 990 ± 120 °C), whereas they are very similar to those obtained by Barbaro et al. (2020b) on other Almahata Sitta samples (average T_{max} of 1266 °C for graphite in AhS 209b, 1242 °C in AhS 72, and 1332 °C in AhS A135A). A comparison between the average temperatures recorded by graphite on the above quoted ureilitic samples is presented in Table 3.

Table 2. Center positions for G, D, and D′ bands and FWHM (both in cm^{-1}) of Y-74123. Calculated crystallization temperature, T_{max}, is reported in the last column and was obtained using the Equation 3. The uncertainty on T_{max} is (2σ) ± 120 °C.

G-band center	**G-band FWHM**	**G-band FWHM corrected**	**D-band center**	**D-band FWHM**	**D2-band center**	**D2-band FWHM**	**T_{max} (°C)**
Y-74123							
1582	24	15	1356	49	1618	21	1286
1580	22	13	1354	46	1618	19	1310
1579	21	13	1349	37	1611	22	1329
1579	18	11	1356	22	1618	17	1365
1579	20	12	1351	40	1616	23	1334
1581	25	16	1350	50	1617	22	1265

Table 3. Comparison among the T_{max} recorded by graphite in different ureilites using the geothermometer by Cody et al. (2008)*.

	AhS #7 (Ross et al. 2011)	**AhS 209** (Barbaro et al. 2020b)	**AhS 72** (Barbaro et al. 2020b)	**AhS A135A** (Barbaro et al. 2020b)	**Y-74123** (this work)
average T_{max} (°C)	990 ±120	1266 ±120	1242 ±120	1332 ±120	1314 ±120

DISCUSSION

Micro-Raman spectroscopy and XRD analyses in Y-74123 revealed the presence of diamond and graphite aggregates in the interstitial space between silicate grains, as commonly observed in other ureilites (e.g., Hanneman et al. 1967; Vdovykin 1971). Our results from the XRD analysis on Y-74123 confirm the coexistence of nano- and micro-diamonds associated with nano-graphite. In the carbon-bearing aggregates, we also detected Fe metal and troilite, which fill the interstitial space between graphite-diamond crystals or occur at the border of the carbon aggregates (Fig. 4).

The observed local differences in size of the newly formed diamonds, i.e., nano- to micro-metric, may result from heterogeneous shock distribution within a heterogeneous sample. The heterogeneous distribution of shock effects is mainly ascribed to shock impedance contrast between contiguous phases. For greater contrast, the shock impedance is amplified (Ogilvie et al. 2011), as in the case of large, “rigid”, olivine crystals, separated by interstitial, relatively “soft”, carbon-bearing matrix. This implies that the shock pressure locally experienced by the carbon phases might have been higher than that recorded by the adjacent olivine crystal, thus, explaining the local occurrence of relatively coarse-grained diamonds. Conversely, for cases of low contrast between phases, the shock impedance would have been suppressed. Furthermore, we cannot exclude that Y-74123 suffered multiple impact events with different P-T conditions.

Our study provides further evidence in support of the diamond formation mechanism in ureilites proposed for NWA 7983 ureilite by Nestola et al. (2020). According to this mechanism, the formation of micrometer-sized diamond crystals from graphite observed in Y-74123 is likely due to the combined effect of highly heterogeneous P-T-conditions due to shock wave propagation and immediate penetration of Fe-Ni melt into carbon aggregates, whereas the formation of nano-diamonds resulted from direct transformation from graphite (i.e., even without the catalytic Fe-Ni melt). The occurrence of Fe compounds, as observed in Y-74123, could explain the formation of diamonds at pressures ≥15-20 GPa (Nestola et al. 2020), which is lower than the pressure of 30-60 GPa estimated for diamonds formed in impact cratering processes on Earth (see, e.g., Koeberl et al. 1997, and references therein). In Nestola et al. (2020) it is clearly reported how the catalyzed formation of diamonds by metallic melts during a shock event can also account for simultaneous formation of micro- and nanodiamonds in ureilites. These authors, with the aim to explain this process, reported an example of a pulsed heating experiment performed on a graphite-metal charge in a static high-pressure apparatus (Varfolomeeva 1971). This apparatus simulates natural impact processes (De Carli et al. 2002; Bundy et al. 1967) which produced diamonds up to 10-µm- sized, found near to the catalyst, and nanodiamonds occurring in other parts of the experimental charge (Nestola et al. 2020 and references therein).

The proposed scenario is further supported by the average value of the temperatures determined for Y-74123 graphite [T_{max}=1314°C (±120 °C)], which is similar to the values reported by Barbaro et al. (2020a; 2020b) for Almahata Sitta samples (e.g., AhS 209b, AhS 72, and AhS A135A), even though slightly higher than the values reported by Ross et al. (2011) for the AhS #7 sample. As reported by Gillet and El Goresy (2013), the shock peak temperature determination for a sample with different mineral composition should also account for the effect of the porosity, grain boundaries, and heterogeneous composition of the rock. In addition, it is important to consider that the shock waves do not propagate at the same speed in all different minerals of a polymineralic rock, as explained above. However, even if it is difficult to estimate the exact peak shock pressure values of the impact event(s), we can argue that the temperature recorded by graphite may correspond to the shock-induced temperature or to a subsequent post-shock thermal event, as hypothesized by Gillet and El Goresy (2013). We exclude that our estimated temperature values could be a pre-shock temperature, because our estimation is determined on newly crystallized nano-graphite. Such nano-graphite cannot be the pristine graphite of the UPB, which should have been micrometer-sized, due to the long residence time spent in the UPB deep interior. Therefore, as reported by Barbaro et al. (2020b) for three AhS ureilitic fragments, nano-graphite formed by shock.

IMPLICATIONS

Our study on carbon phases in Yamato 74123 provides hints on the shock history of this specific meteorite, and generally, of the UPB. The XRD analysis carried out on Y-74123 showed that nano-diamonds coexist together with micro-diamonds and nano-graphite, in agreement with observations by Nestola et al. (2020) on the NWA 7983 ureilite meteorite. In addition, by means of MRS analyses of graphite, we were able to show that (i) the investigated sample exhibits homogeneous values of G-band centers (between 1579 and 1582 cm^{-1}) and D-band centers (between 1349 and 1356 cm^{-1}) and that (ii) the Γ_G of graphite for the G-band range between 11 and 16 cm^{-1}. These values were used to estimate an average T_{max} of 1314°C (±120 °C).

Our results support that micrometer-sized diamonds in Y-74123, as also suggested by Nestola et al. (2020) for NWA 7983, formed with the assistance of the catalytic effect of metallic melts, without requiring static high-pressures conditions within a large Mars-sized parent body. The formation of micro- and nano-diamonds and nano-graphite is likely to be the result of an impact event or multiple impact events. We assume that the temperature recorded by graphite, close to 1200-1300°C, likely represents the shock-induced temperature excursion or corresponds to a subsequent post-shock temperature. The temperature values obtained in our sample Y-74123, together with further studies on ureilites, using the same approach as presented here, will contribute to widen our knowledge of the graphite resetting temperatures by shock.

In conclusion, the results from our combined SEM, XRD, and MRS study in Y-74123 suggest that one or multiple shock event(s), with the contribution of metallic melts catalysis, is likely responsible for the formation of diamond, both nano- and micro-diamonds. Moreover, heterogeneity in the peak shock pressure that affected the UPB during the impact event(s) may also explain the coexistence of diamonds with notable different sizes.

Acknoledgments

This paper is dedicated to the memory of Heinrich Hintenberger (1910–1990) who donated to the NHM Vienna collection the Yamato 74123 sample used for this study. C.A. Goodrich is acknowledged for interesting discussions. S. Jaret and an anonymous reviewer are thanked for their comments, which greatly contributed improving this manuscript. S. Redfern is thanked for editorial handling. This work was supported by PNRA 2018 grant number PNRA18 00247 – A to F. N.; A.B., M.C.D., M.M., and M.A. were funded by the IMPACt project (R164WEJAHH) to M. Alvaro.

References

Barbaro, A., Domeneghetti, M. C., Goodrich, C. A., Meneghetti, M., Litti, L., Fioretti, A. M., Shaddad, M. H., Alvaro, M., and Nestola, F. (2020a) Shock temperature recorded by graphite in ureilites from Almahata Sitta. 51st Lunar and Planetary Science Conference, abstract #1480.

Barbaro, A., Domeneghetti, M. C., Goodrich, C., Meneghetti, M., Litti, L., Fioretti, A. M., Jenniskens, P., Shaddad, M. H., Alvaro, M., and others. (2020b) Graphite based geothermometry on Almahata Sitta ureilites meteorites. Minerals, submitted.

Berkley, J.L., Brown, IV, H.G., Keil, K., Carter, N.L., Mercier, J.-C.C., and Huss, G. (1976) The Kenna ureilite: an ultramafic rock with evidence for igneous, metamorphic, and shock origin. Geochimica et Cosmochimica Acta, 40, 1429–1437.

Berkley, J. L., Taylor, G. J., Keil, K., Harlow, G. E., and Prinz, M. (1980) The nature and origin of ureilites. Geochimica et Cosmochimica Acta, 44, 1579–1597.

Bischoff, A., Goodrich, C.A., and Grund T. (1999) Shock-induced origin of diamond in ureilites. 30st Lunar and Planetary Science Conference, abstract #1100.

Boynton, W. V, Starzyk, P. M., and Schmitt, R. A. (1976) Chemical evidence for the genesis of the ureilites, the achondrite Chassigny and the nakhlites. Geochimica et Cosmochimica Acta, 40, 1439–1447.

Bundy, F. P., and Kasper J. S. (1967) Hexagonal diamond–A new form of carbon. Journal of Chemical Physics, 46, 3437–3446.

Cloutis, E. A., Hudon, P., Romanek, C. S., Bishop, J. L., Reddy, V., Gaffey, M. J., and Hardersen, P. S. (2010) Spectral reflectance properties of ureilites. Meteoritics & Planetary Science 45, 10–11.

Cody, G. D., Alexander, C. M. O'D., Yabuta, H., Kilcoyne, A. L. D., Araki, T., Ade, H., Dera, P., Fogel, M., Militzer, B., and Mysen, B. O. (2008) Organic thermometry for chondritic parent bodies. Earth and Planetary Science Letters, 272, 446–455.

De Carli, P.S. (1995) Shock wave synthesis of diamond and other phases. Material Research and Society Symposium Proceedings, 383, 21–31.

De Carli, P. S., Bowden, E., Jones, A. P., and Price, G. D. (2002) Laboratory impact experiments versus natural impact events. In Catastrophic Events and Mass Extinctions: Impacts and Beyond, Geological Society of America Special Paper, p. 595–605. Lunar and Planetary Institute, Houston, Texas.

Frondel, C. and Marvin, U. B. (1967) Lonsdaleite, a hexagonal polymorph of diamond. Nature, 214, 587–589.

Fukunaga, K., Matsuda, J., Nagao, K., Miyamoto, M., and Ito, K. (1987) Noble-gas enrichment in vapour-growth diamonds and the origin of diamond in ureilites. Nature, 328, 141–143.

Gillet, P. and El Goresy, A. (2013) Shock events in the Solar System: The message from minerals in terrestrial planets and asteroids. Annual Review of Earth and Planetary Sciences, 41, 247–285.

Goodrich, C. A., and Jones, J. H. (1987) Origin and evolution of the ureilite parent magmas: Multi-stage igneous activity on a large parent body. Geochimica et Cosmochimica Acta, 51, 2255–366 2273.

Goodrich, C. A. (1992) Ureilites: A critical review. Meteoritics & Planetary Science, 27, 327–352.

Goodrich, C. A., Hartmann, W. K., O'Brien, D.P., Weidenschilling, S. J., Wilson, L., Michel, P., and Jutzi, M. (2015) Origin and history of ureilitic material in the solar system: The view from asteroid 2008 TC_3 and the Almahata Sitta meteorite. Meteoritic & Planetary Science, 50, 782–809.

Goodrich, C. A., Nestola, F., Jakubek, R., Erickson, T., Fries, M., Fioretti, A. M., Ross, D. K., and Brenker, F. E. (2020) The origin of diamond in ureilites. 51st Lunar and Planetary Science Conference, abstract #1411.

Grady, M. M., Wright, I. P., Swart, P. K., and Rllinger, C. T. (1985) The carbon and nitrogen isotopic composition of ureilites: implications for their genesis. Geochimica et Cosmochimica Acta, 49, 903–915.

Grund, T. and Bischoff, A. (1999) Cathodoluminescence properties of diamonds in ureilites: further evidences for a shock-induced origin. 62nd Annual Meteoritical Society Meeting, abstract #5074.

Hanneman, R. E., Strong, H. M., and Bundy, F. P. (1967) Hexagonal diamonds in meteorites: Implications. Science, 155, 995–997.

Hezel, D. C., Dubrovinsky, L., Nasdala, L., Cauzid, J., Simionovici, A., Gellissen, M., and Schonbeck, T. (2008) In situ micro-Raman and X-ray diffraction study of diamonds and petrology of the new ureilite UAE 001 from the United Arab Emirates. Meteoritics & Planaetary Sciences, 43, 1127–1136.

Hintenberger, H., Jochum, K.P., Braun, O., Christ, P., and Martin, W. (1978) The Antarctic meteorite Yamato 74123 — a new ureilite. Earth and Planetary Science Letters, 40, 187–193.

Hough, R. M., Gilmour, I., Pillinger, C. T., Arden, J.W., Gilkess, K. W. R., Yuan, J., and Milledge, H. J. (1995) Diamond and silicon carbide in impact melt rock from the Ries impact crater. Nature 378,41–44.

Koeberl, C., Masaitis, V. L., Shafranovsky, G. I., Gilmour, I., Langenhorst, F., and Schrauder, M. (1997) Diamonds from the Popigai impact structure, Russia. Geology, 25, 967–970.

Le Guillou, C., Rouzaud, J. N., Remusat, L., and Bourot-Denise, A. (2010) Structures, origin and evolution of various carbon phases in the ureilite Northwest Africa 4742 compared with laboratory-shocked graphite. Geochimica et Cosmochimica Acta, 74, 4167–4185.

Lipschutz, M. E. (1964) Origin of Diamonds in the Ureilites. Science, 143, 1431–1434.

Lorentz, C.A., Shiryaev, A. A., Vlasov, I. I., and Borisovsky, S. E. (2019) Metamorphism of four desert ureilites and luminescence spectroscopy of defects in ureilitic diamonds. Meteoritics and Planetary Science, 54, 1197–1214.

Masaitis, V. L. (1998) Popigai crater: Origin and distribution of diamond-bearing impactites. Meteoritics and Planetary Science, 33, 349–359.

Meteoritical Bulletin Database (2020). Available: https://www.lpi.usra.edu/meteor/

Miyahara, M., Ohtani, E., El, A., Lin, Y., Feng, L., Zhang, J., Gillet, P., Nagase, T., and Muto, J. (2015) Unique large diamonds in a ureilite from Almahata Sitta 2008 TC 3 asteroid. Geochimica et Cosmochimica Acta, 163, 14–26.

Murri, M., Smith, R. L., McColl, K., Hart, M., Alvaro, M., Jones, A. P., Németh, P., Salzmann, C. G., Corà, F. and others. (2019) Quantifying hexagonal stacking in diamond. Scientific Reports 9, 10334. https://doi.org/10.1038/s41598-019-46556-3

Nabiei, F., Badro J., Dennenwaldt T., Oveisi E., Cantoni M., Hébert C., Goresy A. El, Barrat J., and Gillet P. (2018) A large planetary body inferred from diamond inclusions in a ureilite meteorite. Nature Communications, 9, 1–6.

Nagata, T. (1980) Magnetic classification of Antarctic meteorites. Proceedings of the 21st Lunar and Planetary Science Conference, p. 1789–1799. Lunar and Planetary Science Institute, Houston, Textas.
Nakamuta, Y., and Aoiko, Y. (2000) Mineralogical evidence for the origin of diamond in ureilites. Meteoritics and Planetary Science, 35, 487–493.

Nakamuta, Y., Kitajima, F., and Shimada, K. (2016) In situ observation, X–ray diffraction and Raman analyses of carbon minerals in ureilites: Origin and formation mechanisms of diamond in ureilites. Journal of Mineralogical and Petrological Sciences, 111, 252–269.

Nèmeth, P., Garve, L. A. J., Aoki, T., Dubrovinskaia, N., Dubrovinsky, L., and Buseck, P. R. (2014) Lonsdaleite is faulted and twinned cubic diamond and does not exist as a discrete material. Nature Communications, 5, 5447, 1–5.

Németh, P., McColl, K., Smith, R. L., Murri, M., Garvie, L. A. J., Alvaro, M., Pécz, B., Jones, A. P., Corà, F., Salzmann and others. (2020a) Diamond-graphene composite nanostructures. 426 Nanoletters, 20, 3611–3619.

Németh P., McColl, K., Garvie L. A. J., Salzmann C. G., Murri M., McMillan P. F. (2020b) Complex nanostructures in diamond. Nature Materials, 1–6. https://doi.org/10.1038/s41563-020-0759-8

Nestola, F., Goodrich, C. A., Morana, M., Barbaro, A., Jakubek, R. S., Chris, O., Brenker, F. E., Domeneghetti, M. C., Dalconi, M. C. and others. (2020) Impact shock origin of diamond in ureilite meteorites. Proocedings of the National Academy of Sciences of the United States of 432 America, 1-9. https://doi.org/10.1073/pnas.1919067117

Ogilvie, P., Gibson, R. L., Reimold, W. U., Deutsch, A., and Hornemann, U. (2011) Experimental investigation of shock metamorphic effects in a metapelitic granulite: The importance of shock impedance contrast between components. Meteoritics & Planetary Science, 46, 1565–1586.

Ohfuji, H., Itifune, T., Litasov, K. D., Yamashite, T., Isobe, F., Afanasiev V. P., and Pokhilenko N. P. (2015) Natural occurrence of pure nano-polycrystalline diamond from impact crater. Scientific Reports, 5, 14702, 1–8.

Ross, A. J., Steele, A., Fries, M. D., Kater, L., Downes, H., Jones, A. P., Smith, C. L., Jenniskens, P. M., Zolensky, M. E., and Shaddad, M. H. (2011) MicroRaman spectroscopy of diamond and graphite in Almahata Sitta and comparison with other ureilites. Meteoritics & Planetary Science, 46, 364–378.

Rubin, A. (2006) Shock, post-shock annealing, and post-annealing shock in ureilites. Meteoritics & Planetary Science, 41, 125–133

Sabbah, H., Morrow, A. L., Jenniskens, P., Shaddad, M. H., and Zare, R. N. (2010) Polycyclic aromatic hydrocarbons in asteroid 2008 TC3: Dispersion of organic compounds inside asteroids. Meteoritics & Planetary Science, 45, 1710–1717.

Salzmann, C. G., Murray, B. J., and Shephard, J. J. (2015) Extent of stacking disorder in diamond. Diamond and Related Materials, 59, 69–72.

Scherrer, P. (1918) Estimation of the size and internal structure of colloidal particles by means of röntgen. Journal of Mathematical Physics, 2, 98–100.

Scott E. R. D., Keil K., and Taylor G. J. (1992) Origin of ureilites by partial melting and explosive volcanism on carbon-rich asteroids. Proceedings of the 23rd Lunar and Planetary Science Conference, pp. 1253–1254.

Stöffler, D., Keil, K., and Edward, R. D. S. (1991) Shock metamorphism of ordinary chondrites. Geochimica et Cosmochimica Acta, 55, 3845–3867.

Stöffler, D., Hamann, C., and Metzler, K. (2018) Invited Review Shock metamorphism of planetary silicate rocks and sediments: Proposal for an updated classification system. Meteoritics & Planetary Science, 49, 5–49.

Takeda, H., Mori, H., Keizo, Y., and Shiraishi, K. (1980) Mineralogical examination of the Allan Hills achondrites and their bearing on the parent bodies. Memoirs of National Institute of Polar Reasearch. Special issue, 17, 119–144.

Urey, H. C. (1956) Diamond, meteorites, and the origin of the solar system. American Astronomical Society, 623–637.

Varfolomeeva, T. D. (1971) Synthesis and investigation of polycrystalline diamond. PhD thesis, Institute for High Pressure Physics, USSR Academy of Sciences, 154.

Vdovykin, G. (1970) Ureilites. Space Science Reviews, 10, 483–510.

CHAPTER 5

ORIGIN OF MICROMETER-SIZED IMPACT DIAMOND IN UREILITES BY CATALYTIC GROWTH INVOLVING FE-NI-SILICIDE: THE EXAMPLE OF KENNA METEORITE

Anna Barbaro [a,*], Maria Chiara Domeneghetti [a], Konstantin D. Litasov [b,c], Ludovic Ferrière [d], Lidia Pittarello [d], Oliver Christ [e], Sofia Lorenzon [e], Matteo Alvaro [a], Fabrizio Nestola [e,f]

[a] Dipartimento di Scienze della Terra e dell'Ambiente, Universita` degli Studi di Pavia, Via Ferrata 1, I-27100 Pavia, Italy; [b] Vereshchagin Institute for High Pressure Physics RAS, Troitsk, Moscow 108840, Russia; [c] Fersman Mineralogical Museum RAS, Moscow 115162, Russia; [d] Natural History Museum, Department of Mineralogy and Petrography, Burgring 7, 1010 Vienna, Austria; [e] Dipartimento di Geoscienze, Universita` degli Studi di Padova, Via G. Gradenigo 6, I-35131 Padova, Italy; [f] Geoscience Institute, Goethe-University Frankfurt, Altenho¨feralee 1, 60323 Frankfurt.

*Corresponding author at: Dipartimento di Scienze della Terra e dell'Ambiente, Universita` degli Studi di Pavia, Via Ferrata 1, I-27100 Pavia, Italy. E-mail address: anna.barbaro01@universitadipavia.it (A.Barbaro).

Published version in Geochimica et Cosmochimica Acta journal. ® 2021 Elsevier Ltd. All rights reserved. Received 5 March 2021; accepted in revised form 16 June 2021; available online 24 June 2021 and published on 15 September 2021.

ABSTRACT

The occurrence of shock-induced diamonds in ureilite meteorites is common and is used to constrain the history of the ureilite parent bodies. We have investigated a fragment of the Kenna ureilite by micro-X-ray diffraction, micro-Raman spectroscopy and scanning electron microscopy to characterize its carbon phases. In addition to olivine and pigeonite, within the carbon-bearing areas, we identified microdiamonds (up to about 10 µm in size), nanographite and magnetite. The shock features observed in the silicate minerals and the presence of microdiamonds and nanographite indicate that Kenna underwent a shock event with a peak pressure of at least 15 GPa. Temperatures estimated using a graphite geothermometer are close to 1180 °C. Thus, Kenna is a medium-shocked ureilite, yet it contains microdiamonds, which are typically found in highly shocked carbon-bearing meteorites, instead of the more common

nanodiamonds. This can be explained by a relatively long shock event duration (in the order of 4–5 s) and/or by the catalytic effect of Fe-Ni alloys known to favour the crystallization of diamonds. For the first time in a ureilite, carletonmooreite with formula Ni_3Si and grain size near 4–7 nm, was found. The presence of nanocrystalline carletonmooreite provides further evidence to support the hypothesis of the catalytic involvement of Fe-Ni bearing phases into the growth process of diamond from graphite during shock events in the ureilite parent body, enabling the formation of micrometer-sized diamond crystals.

INTRODUCTION

Ureilites are achondritic meteorites, which consist of ultramafic rocks mainly composed of olivine and pigeonite (an exhaustive review about the ureilite group can be found in Goodrich, 1992). Ureilites contain up to ~8 wt% of carbon (e.g. Cloutis et al., 2010; Goodrich et al., 2015), which is mostly present as diamond and graphite, located in the interstitial space between silicate grains. Diamond and graphite are commonly accompanied by iron-nickel metal, troilite and other accessory phases (e.g. Berkley et al., 1976).

The origin of diamonds in ureilites is still debated within the scientific community. Lipschutz (1964) proposed that diamonds were formed by shock conversion of graphite during the catastrophic breakup of the ureilitic parent body (UPB), while Fukunaga et al. (1987) suggested that diamonds could grow from a dilute gas phase by chemical vapour deposition process (CVD). Another hypothesis by Urey (1956) excludes the shock origin of diamond and instead proposes a process similar to that observed for Earth's mantle diamonds, which is that diamonds are formed under high static pressure conditions in the deep interior of the UPB. This last hypothesis was re-evaluated in some works on the Almahata Sitta ureilite by Miyahara et al. (2015) and Nabiei et al. (2018).

On the other hand, a recent study by Nestola et al. (2020), based on combined data obtained by micro X-ray diffraction (XRD) and transmission electron microscopy (TEM) on three highly-shocked ureilitic samples, Almahata Sitta 209b and 72, and NWA 7983, suggests that diamond formation in ureilites is most likely related to shock, probably characterized by a peak pressure of at least 15 GPa. These authors report on the coexistence of both nanodiamonds and microdiamonds (with single crystals up to 100 lm in size) as well as nanographite intergrown with iron-nickel alloys. According to these authors, the cooccurrence of large monocrystalline diamonds and nanodiamonds can be explained by transformation from graphite during an impact event due to peak pressure with a local duration of up to a few seconds (De Carli et al. 2002). The formation of such ‘‘large” diamonds have been favoured by the catalytic effect of metallic Fe-Ni-C liquid interacting with graphite during impact events.

The Kenna ureilite meteorite (Berkley et al., 1976) had a mass of 10.9 kg. Several studies on Kenna have provided data on petrography (Berkley, et al. 1976), noble gases and fossil particles tracks (Wilkening and Marti,1976), magnetism (Brecher and Fuhrman, 1979), oxygen isotope composition (Clayton et al., 1976), reflectance properties (Cloutis et al., 2010) and carbon content (Nakamuta and Aoki 2000). The occurrence of diamond and graphite, reported by Nakamuta and Aoki (2000) based on X-ray powder diffraction data, showed an intimate coexistence of diamond and graphite, similar to that reported for other ureilites by Nestola et al. (2020) and Barbaro et al. (2021).

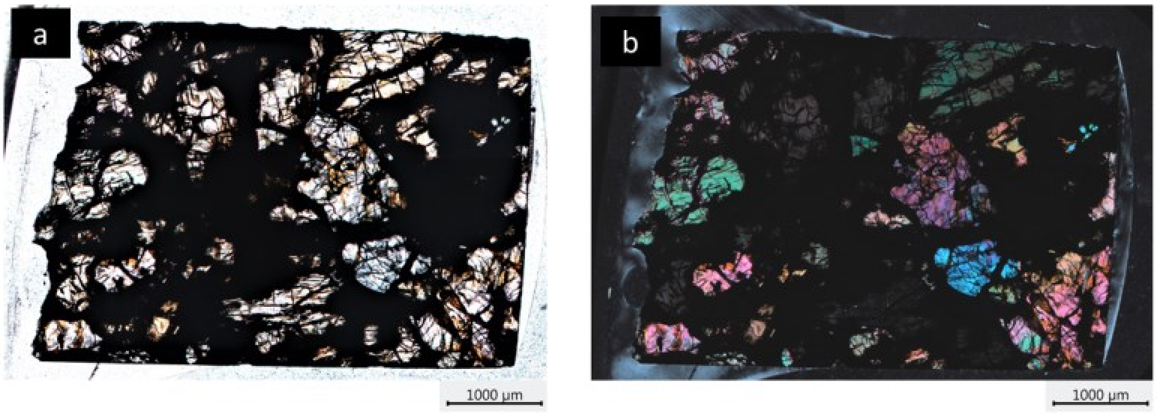

Fig. 1. Thin section of Kenna ureilite in (a) plane polarized light and (b) cross polarized light; the opaque material (mainly composed by carbon material, Fe-Ni alloys and fine silicate crystals) around the large silicate crystals of olivine and pigeonite is shown.

Concerning carbon phases, Nakamuta and Aoki (2000) reported on the occurrence of diamond and graphite based on X-ray powder diffraction data obtained using a Gandolfi camera and showed an intimate coexistence of diamond and graphite. Similar intimate coexistence was reported by Nestola et al. (2020) for Almahata Sitta and NWA 6873, and by Barbaro et al. (2021) for Yamato 74123 ureilite. The aim of this study is the analysis of carbon-bearing aggregates (diamond, graphite and other minor phases) in Kenna ureilite in order to understand their origin, following the same experimental approaches adopted by Nestola et al. (2020) and Barbaro et al. (2021). During our investigations, we found, for the first time in an ureilite (and the second occurrence in a natural sample), a recently discovered Ni_3Si phase called carletonmooreite (IMA 2018-068; Garvie et al., 2021), originally reported by Ma et al. (2018) within the Norton County aubrite meteorite. Using a multimethods approach [by scanning electron microscopy (SEM), energy dispersive X-ray spectroscopy (EDS), Xray diffraction (XRD) and micro-Raman spectroscopy (MRS)] we have characterized the carbon phases and estimated the shock pressure and temperature experienced by the Kenna meteorite. Our new observations are discussed in terms of shock metamorphism and compared with observations reported from other ureilites.

MATERIALS AND ANALYTICAL PROCEDURES

The polished thin section NHMW-O1972 (Fig. 1) and fragment of Kenna (Fig. 2) here investigated are from the Natural History Museum, Vienna (NHMW, Austria) meteorite collection (note that thin section NHMW-O1972 was prepared from the fragment of Kenna investigated here). Petrographic characterization of the thin section (Fig. 1) was carried out at the ‘‘Fiorenzo Mazzi” Experimental Mineralogy Lab at the Earth and Environmental Department of University of Pavia (Italy) using a conventional petrographic microscope in transmitted light.

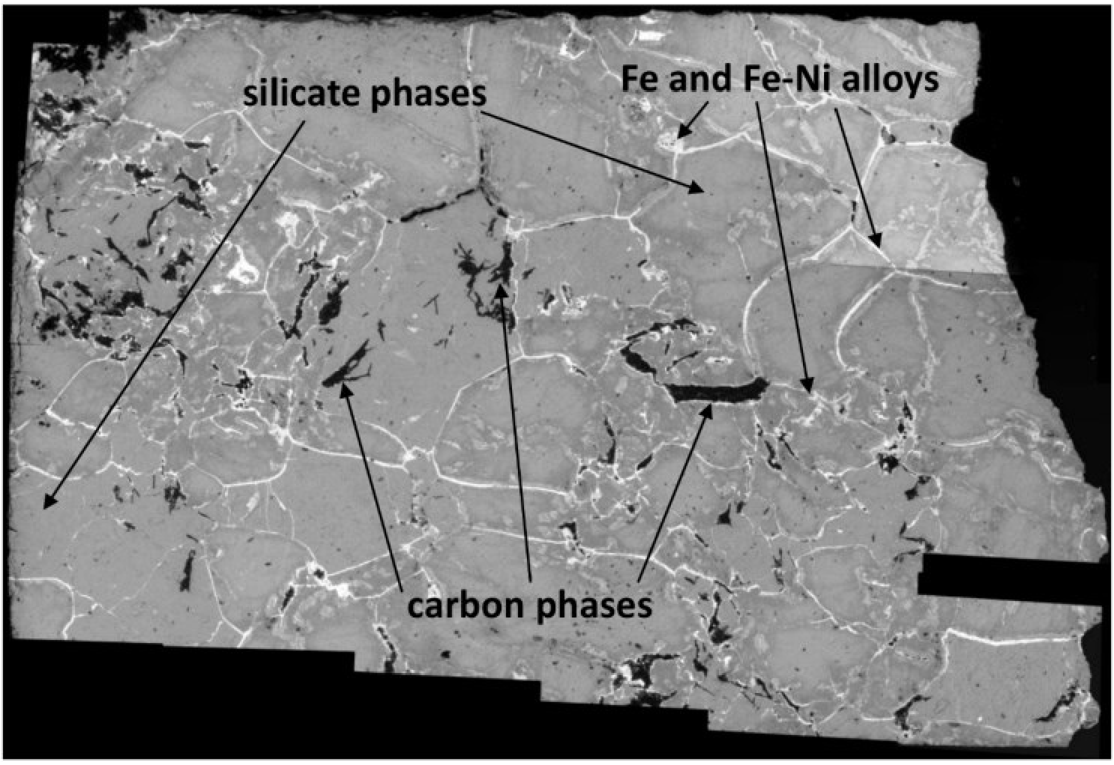

Fig. 2. Mosaic of BSE images of a Kenna ureilitic fragment. Silicate phases (light grey 91%), carbon phases (black 4%) and Fe, Fe-Ni alloys and Fe oxides (white 5%) are easily distinguishable. Relative abundance estimated by image analysis.

The non-carbon coated fragment of Fig. 2 was analysed using low vacuum FEI Quanta 200 equipped with an EDS, at CEASC (Centro di Analisi e Servizi per la Certificazione) at the

University of Padova (Italy). The working distance was 14 mm, with an emission current of 93 mA, and a voltage of 20 kV. From this fragment we gently removed a small grain from the dark areas in Fig. 2. This grain was then mounted at the tip of a glass fibre for EDS, SEM, micro-XRD and MRS analyses. Unfortunately, we could not perform electron microprobe analysis on the carbon-bearing aggregate sample due to the softness of the material that prevented embedding it in epoxy and subsequent polishing.

A back-scattered electron (BSE) image (collected with a working distance of 13.8 mm, emission current of ca. 100 mA and voltage of about 20 kV) of the grain is shown in Fig. 3. The grain, an aggregate fragment, with its longest dimension reaching about 100 μm, was investigated using a Rigaku-Oxford Diffraction Supernova kappa-geometry diffractometer (at the Department of Geosciences, University of Padova) equipped with an X-ray Mo micro-source and a Pilatus 200 K Dectris detector, controlled with the CrysAlis-Pro^{TM} software. Diffraction profile of the powder pattern was analysed using the High Score Plus Software package (from Panalytical). We also performed line profile analysis fitting to the diffraction pattern obtained on the carbon-bearing aggregate with the aim to estimate the crystallite size of the carletonmooreite (Ni_3Si) present in this sample using the same High Score Plus software.
To estimate the crystallite size of graphite and carletonmooreite, we applied line profile analysis fitting to the diffation pattern obtained on the carbon bearing samples of Fig. 3. The crystallite size is different from grain size, a grain may be made up of different crystallites. According to Scherrer (1918) crystallite size represents the crystal domain which produces diffraction. The values of the integral breadth, which were obtained by line profile analysis method, were inserted into the Scherrer equation (Eqs. (1) and (2), Scherrer 1918) to estimate the crystallite size, as follows:

$$\beta(2\theta) = \frac{K_\beta \times \lambda}{<D>_V \cos\theta_{hkl}} \qquad [1]$$

$$\frac{D_V}{K_\beta} = \frac{\lambda}{\cos\theta_{hkl}\, x\, \beta(2\theta)} \qquad [2]$$

Scherrer equation provides a correlation between peaks broadening b, the dimension of diffracted domain and the crystallite size (D_V). K is a constant value ranging between 0.5 and 1, describing the contribution of crystallites shape and dependent upon the relative orientation of the scattering vector with respect to the external shape of the crystallite (Scherrer 1918).

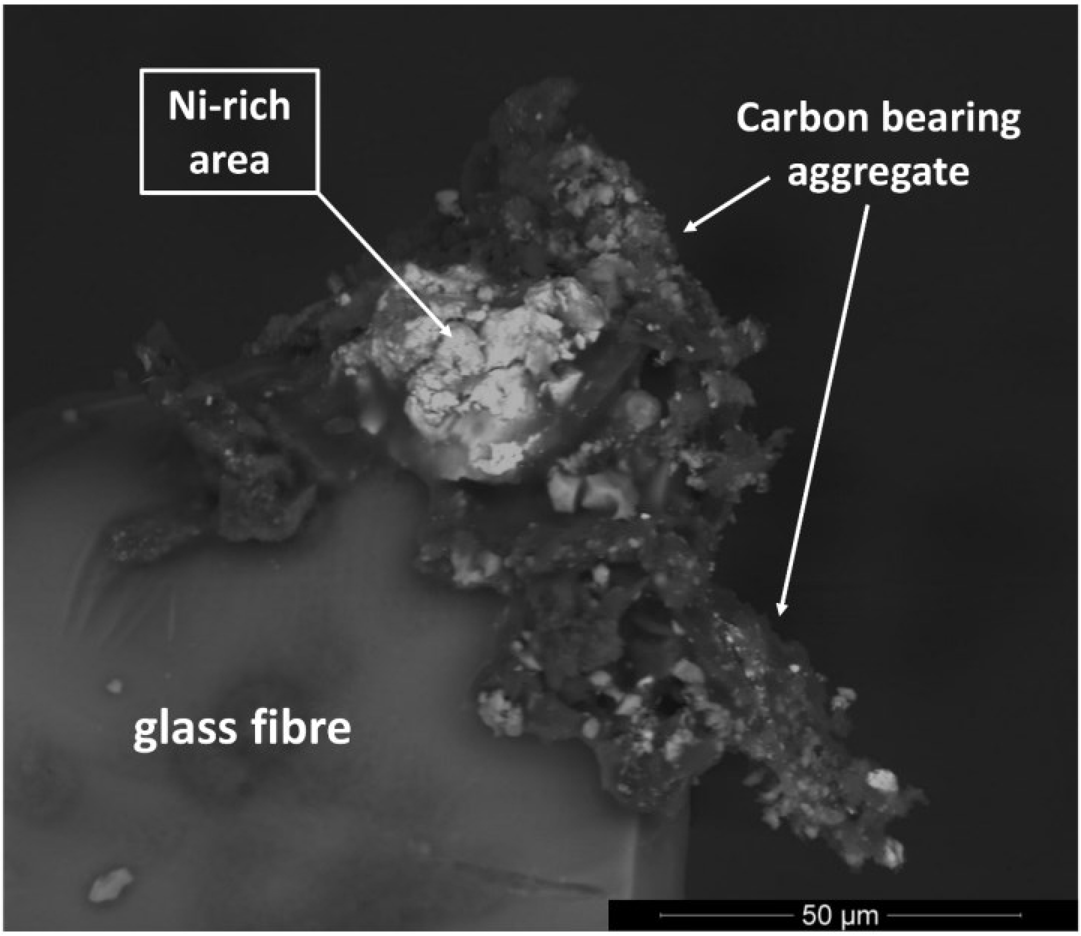

Fig. 3. Backscattered electron image of carbon bearing sample of Kenna ureilite on which we performed EDS, XRD and MRS analyses. In the middle of the sample, it is possible to observe light-grey/white coloured areas, referred to high content of nickel.

The same fragment of Fig. 3 studied by XRD was also analysed by MRS using a Horiba LabRam HR Evolution spectrometer equipped with an Olympus BX41 confocal microscope at the controlled temperature of 20(1) °C at the ‘‘Fiorenzo Mazzi” Experimental Mineralogy Lab at the Department of Earth and Environmental Science of the University of Pavia. We used a laser excitation of 532 nm with an operating low power of 1–2 mW (in order to avoid any graphite damage), a grating of 600 and a 50x objective magnification. The spectrometer was calibrated to the silicon Raman peak at 520.7 cm $^{-1}$. The spectral resolution was 2 cm^{-1} and we used a 30 s integration time with four accumulations for each spectrum. Curve fitting of the spectra was carried out using the software OMNIC for dispersive Raman (from Thermo Fisher Scientific) adopting Gaussian + Lorentzian curves to obtain the best fit.

The carbon-bearing fragment on which we performed all the analyses was detached from the glass fibre, was carbon-coated and then analysed in high vacuum mode using a CamScan MX3000 electron microscope equipped with a LaB_6 four-quadrant solid-state backscattered-electron detector and an EDAX EDS system for micro-analysis (at the Department of Geosciences, University of Padova).

RESULTS

Petrographic description and SEM characterization

The petrographic analysis of the thin section of Fig. 1 shows that silicates in Kenna meteorite are mainly olivine and low-Ca pyroxene. The olivine crystals in the investigated fragment of Kenna ranges from 0.2 to 2 mm in size. In general, anhedral grains display triple junctions. Anhedral pyroxenes, with size ranging from 0.1 to 1.4 mm, are homogeneously distributed throughout the studied thin section, in agreement with observations made on another thin section of Kenna as reported in Berkley et al. (1976). Possible shock-induced features in Kenna silicates include fracturing and local (weak) mosaicism. In particular, in some olivine grains, it is possible to observe undulatory extinction and kinking due to a slip parallel to [001] (Berkley et al. 1976). As already reported by these authors, twin and translation gliding parallel to (100) were observed in clinopyroxene. In some silicates, it is possible to observe darkening due to the dispersion of metallic Fe-Ni and sulphides within the grains, which is commonly associated to shock effects (Rubin, 2006). All these observations on silicates suggest that Kenna ureilite recorded a medium shock level which could be ascribed to a shock level S3-S4, according to the shock classification by Stöffler et al. (1991, 2018). This assignment to a medium shock level agrees with the shock level as reported by Berkley et al. (1976), who provided a detailed study of the petrography of Kenna. All our observations agree with those reported by these authors in their petrographic description. In Fig. 4, SEM images of the analysed fragment (Fig. 2) show that carbon phases mixed together with Fe-Ni phases occur in the interstitial space between silicate grains. The carbon phases are present as relatively thin vein-like aggregates of micrometer-sized, but also, more or less regularly, they are found as elongated laths with thickness around 0.3 mm and length up to 0.7 mm (Fig. 4). Pores and small grains of metal and sulphide localized in the interstitial spaces are relatively abundant. Secondary electron (SE) images collected in the central portion of the carbon aggregates of Fig. 4a at progressively higher magnification (Fig. 4b, c) clearly show that the carbon aggregate is made of an assemblage of individual grains, likely not larger than 10 μm in size.

The SEM-EDS analysis of the non-carbon-coated Kenna fragment of Fig. 2 confirmed the presence of olivine, pigeonite, interstitial carbon phases intermixed with Fe-Ni metals and minor magnetite. The presence of magnetite indicates the oxidation of Fe metal dispersed within the carbon material and is likely related to terrestrial weathering (Lee and Bland, 2004). Furthermore, we have also analysed by SEM-EDS (low vacuum mode) the carbon-bearing aggregate of Fig. 3. In addition to the carbon phases, we unexpectedly detected the presence of high Ni content often associated with Si peaks (Fig. 5). With the aim to totally exclude the possibility that the detected Si content was from the glass fibre on which the grain was mounted, we detached the carbon-bearing aggregate and analysed it again, after carbon coating,

by EDS (in high vacuum mode) (Fig. 6a). During the detachment procedure, the carbon-bearing aggregate was accidentally broken into three fragments (Fig. 6b). The EDS spectrum collected on fragment 1 (Fig. 6c) definitively confirmed our previous observation of the presence of Si, with an Ni/Si ratio close to 3, and a minor amount of Fe.

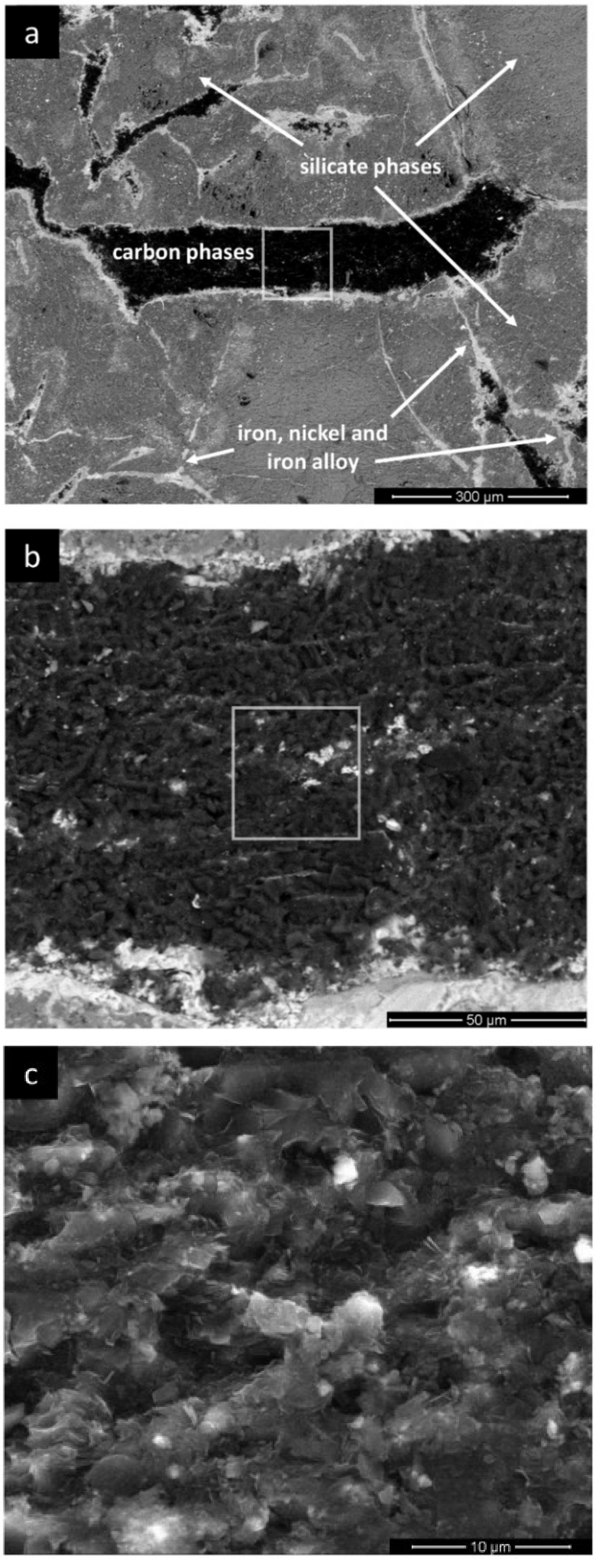

Fig. 4. The carbon material of Kenna ureilite fragments (represented by the dark grey portions). In (a) the carbon aggregate from which we gently removed the carbon bearing sample, that we used for XRD and MRS analyses, is shown (Fig. 3); in (b) a detail from (a) in BSE is shown; in (c) a detail from (b) in SE is reported, showing that the grain size is not larger than 10 μm.

In order to further characterize the above-mentioned carbon phases and to understand the origin of the anomalous high Ni content detected during EDS analysis of the carbon-bearing fragments of Fig. 3, we investigated the same grain by micro-XRD.

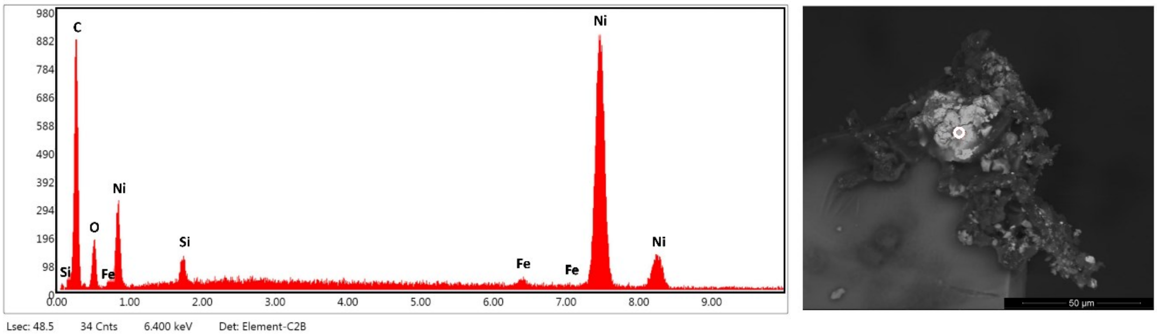

Fig. 5. EDS spectrum collected on the carbon bearing sample of Fig. 3 extracted from Kenna ureilite and attached at the top of the glass fibre. The EDS spectrum corresponds to the spot on the right side of the image (BSE image). This spectrum shows a high content of Ni and the presence of C, Si, Fe, O. The ratio between Ni and Si intensities is close to 3:1.

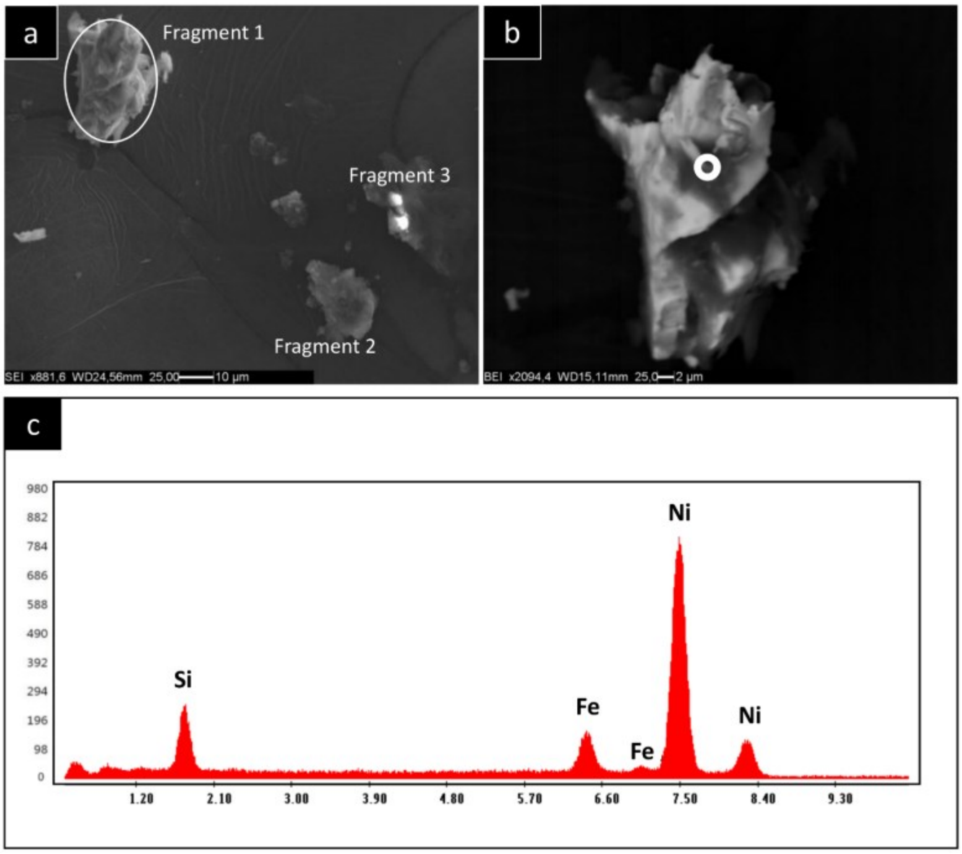

Fig. 6. In (a) three carbon bearing fragments removed from the original carbon bearing aggregate of Fig. 3 are shown; in (b), it is possible to observe the spot on Fragment 1 on which we performed the EDS analysis; in (c) the spectrum collected on the spot reported in (b) is shown.

MICRO-X-RAY DIFFRACTION

Micro X-ray diffraction of the Kenna fragment mounted on glass fibre (see Fig. 3) confirmed the presence of monocrystalline diamonds, as indicated by the presence of an intense peak at 2.06 Å and the two further less intense peaks at 1.26 and 1.07 Å (see spots in Fig. 7). Combining such information with the SEM images from Fig. 4b, c, we can further assess that the monocrystalline diamonds in the investigated fragment are not larger than 10 μm in size.

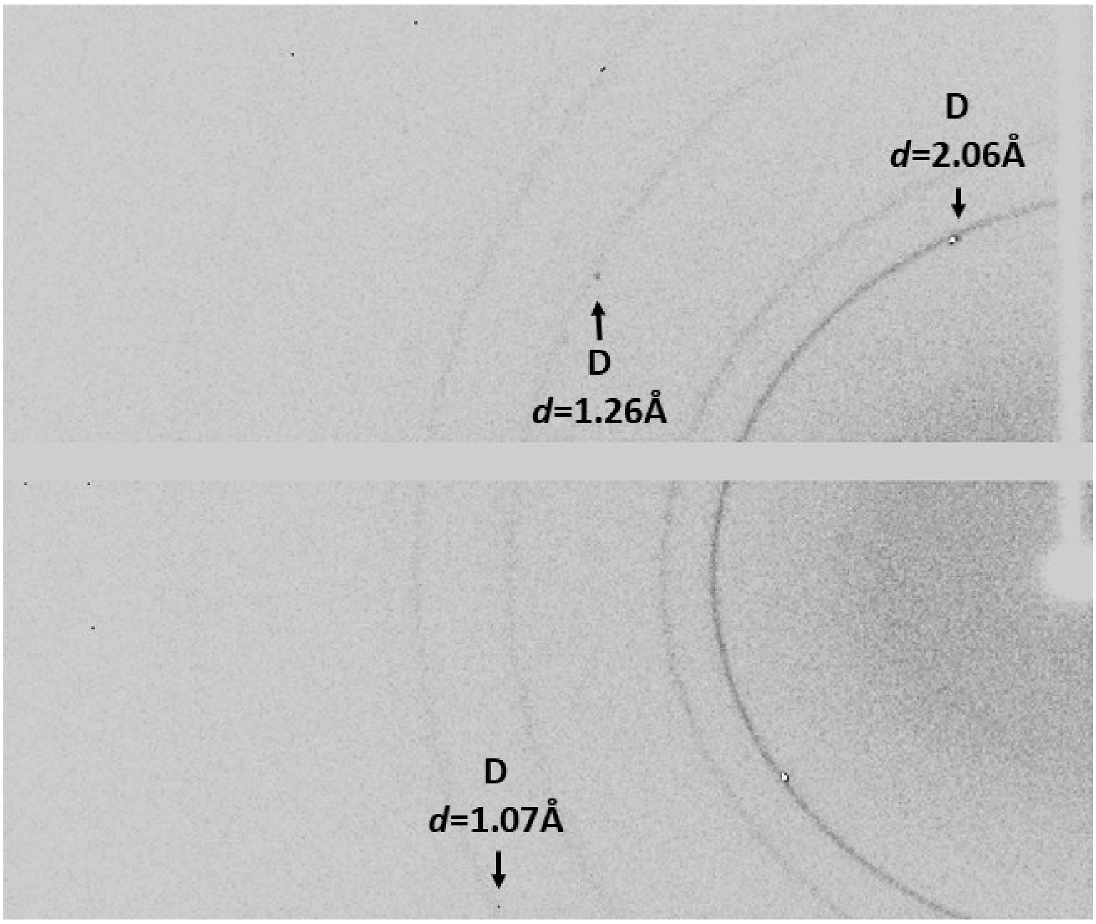

Fig. 7. Diffraction image for the carbon-bearing fragment of Kenna ureilite of Fig. 3, showing diffraction spots (marked with arrows) typical of a monocrystalline diamond and a few diffraction rings typical of polycrystalline materials (see the text).

In addition to the diamond spots, Fig. 7 also shows diffraction rings, which at first seem to overlap with the d-spacings of diamonds, but their position indicates d-spacing values systematically shorter. In order to assign such shorter *d*-spacings, we analysed the reconstructed powder diffraction pattern (Fig. 8) collected over 0–360° phi rotation of the grain in Fig. 3. The pattern shows the main peak of graphite (d = 3.34 Å) which indeed looks strongly asymmetric. Based on the diffraction pattern peak profile broadening from Fig. 8, we can ascertain that graphite in our sample is definitively nanometric in size. In addition to graphite, the powder pattern indicates the presence of minor magnetite (its main peak is at d = 2.56 Å), whose occurrence is also supported by SEM observations and EDS results (see Fe and O in Fig. 5). As reported before, the *d*-spacings observed in the powder diffraction profile do not match those of diamond. Indeed, as it is possible to observe on Fig. 8, the *d*-spacings (in Å) are at 2.03, 1.76, 1.24, 1.06, 1.01, 0.81 and 0.78. The mineralogical phases ascribed to these d-spacings could be either metallic Ni (ICDS 98- 006-2897, Fm-3m) or carletonmooreite Ni_3Si (Pm-3m, Ma et al., 2018). However, it was also possible to identify in the diffraction powder data a low intensity peak at *d*-spacing 1.17Å, which is indexed as (3 0 0) and ascribed to Ni3Si. Indeed, as metal Ni belongs to the Fm-3m space group, we can exclude that the d-spacing at 1.17 Å, ‘‘forbidden den” in this space group, together with those reported above could refer to metallic Ni. In addition, according to Nash and Nash (1987) if we consider the EDS analysis, the homogeneity range obtained for Si is of 20.3 at% which, if we exclude the presence of Fe, is of 22.0 at%. This value of Si at% homogeneity range is not ascribable to either Ni (0.0–15.8 Si at%) phase or to Ni_3Si β_1 (22.8–24.5Si at%) phase, but it is closer to the second one.

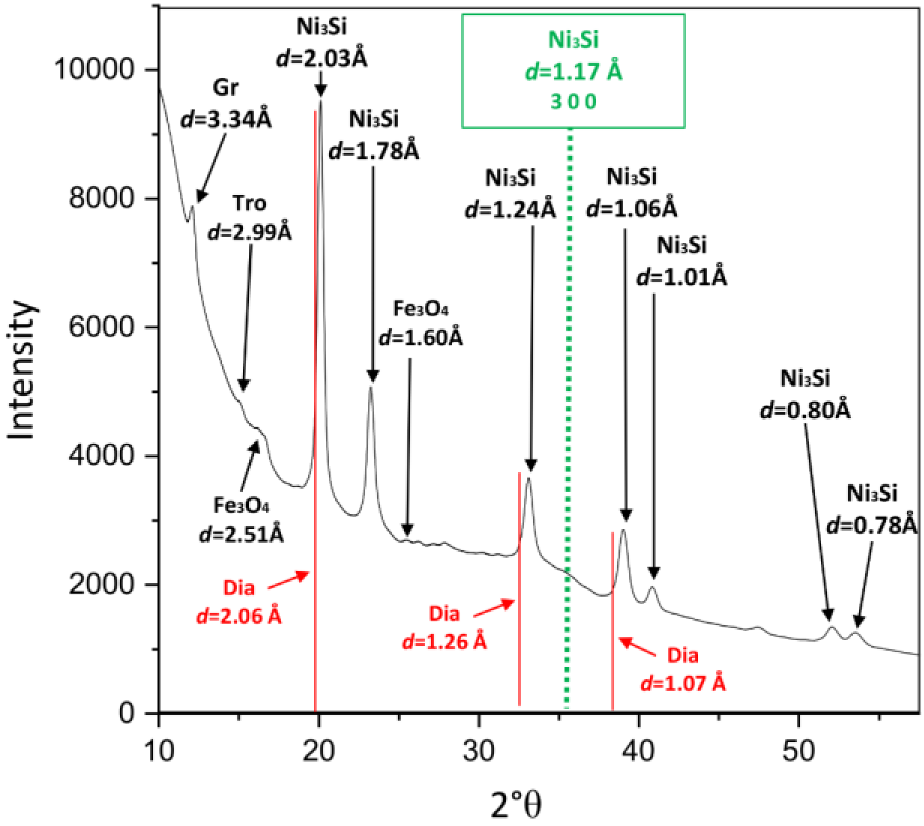

Fig. 8. X-ray powder diffraction patterns reconstructed from the XRD data of Fig. 7 (using the Crysalis software). The diffractogram shows the presence of carletonmooreite (Ni3Si), and the occurrence of graphite (Gr), magnetite (Fe$_3$O$_4$) and troilite (Tro). The other minor peaks are referred to minor Ni sulphides. The dotted green line highlights the presence of a minor peak at *d*-spacing 1.17Å, which is referred to Ni$_3$Si phase. The red lines point out the difference of the d-spacings position in the diffraction pattern with respect to those of diamond (Dia).

The combination of semiquantitative EDS analyses and the diffraction data support the identification of carletonmooreite (Ni$_3$Si), with minor Fe, in the investigated sample. Raghavan (2010) reported that the solubility of Fe in Ni$_3$Siβ$_1$ is up to 7.6 at%, which is the same value as obtained for Fe in our EDS analysis (Fig. 6). We refined the lattice parameter for carletonmooreite and, as reported in Table 1, the obtained value is a = 3.527 Å with a volume of 43.87 Å^3. The peak line profile analysis of the carletonmooreite diffraction pattern shows that such phase is definitively nanometric in size, with a crystallite size of around 4–7 nm.

MICRO-RAMAN SPECTROSCOPY

Results of micro-Raman investigations are reported in Tables 1 and 2. In Fig. 9, a typical Raman spectrum obtained for graphite is shown. Table 1 shows the I(D)/I(G) ratio (where I = integrated intensity; D = D-band; G = G-band), which represents the ratio of the integrated D- and G-band intensities.

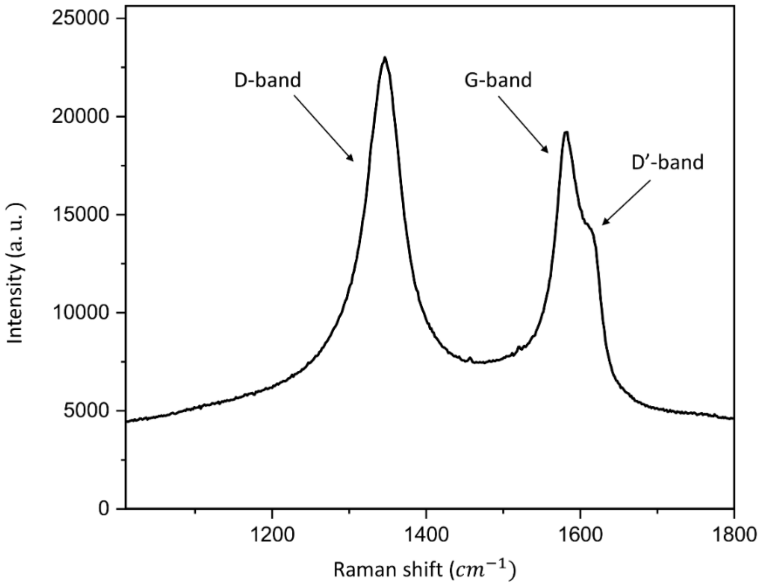

Fig. 9. A typical Raman spectrum of graphite of Kenna ureilite. The G-band (close to 1580 cm^{-1}), D-band (close to 1350 cm^{-1}) and the D0-band (close to 1620 cm^{-1}) are indicated in the figure. The intensity and the positions of the peaks are expressed in arbitrary units (a.u.) and Raman shift (cm^{-1}), respectively.

Tuinstra and Koenig (1970) observed an important relationship between the ratio of the intensity of D-band and G-band [I(D)/I(G)] and crystallite size of graphite (La). This relationship was then validated by Ferrari and Roberson (2000) as follows:

$$\frac{\mathrm{I(D)}}{\mathrm{I(G)}} = \frac{\mathrm{C}(\lambda_{\mathrm{L}})}{\mathrm{L_a}} \tag{1}$$

The wavelength-dependent prefactor parameter $C(k_L)$ is equal to $C_0 + k_L C_1$, where $C_0 = -12.6$ nm and $C_1 = 0.033$, is valid for 400 nm < k_L < 700 nm. The wavelength dependency of C parameter is expressed by Eq. (1) (Barbaro et al. 2020 and references therein). The C ($k_L = 532$

nm) parameter corresponds to ~44 Å. The crystallite size results obtained for our sample by applying Eq. (1) are reported in Table 1. The average crystallite size is 84 nm, with a range between 43 and 177 nm. Such data are consistent with the XRD data collected on graphite, which also exhibits a nanometric size.

Table 1. Integrated intensities of the D- and G-bands, I(D)/I(G) ratio of the integrated D- and G-bands and the crystallite size of graphite (La) of all MRS acquisition of Kenna sample. For the intensity ratios, I (D)/I(G), the standard deviation is 0.08. For La, the estimated uncertainty is in the order of 20 nm.

D-band	**G-band**	**I(D)/I(G)**	**L_a(nm)**
	Kenna		
263589	255746	1.03	43
141757	318349	0.44	99
1093290	630303	1.73	25
52855	117656	0.45	98
62323	162959	0.38	115
200743	805442	0.25	177

We applied the geothermometer by Ross et al. (2011) based on the Raman G-band full width at half maximum of graphite [Γ_G] as follows:

$$T_{max}(°C) = 1594.4 - 20.4\Gamma_G - 5.8 \times 10^{-2}\Gamma_G^2 \qquad (2)$$

In Table 2 we report the graphite Raman peaks positions (G-band, D-band and D_0-band), the relevant Γ_G values for all studied samples and the Tmax estimated using Eq. (2). In order to compare obtained Γ_G data with those published by Ross et al. (2011) and Barbaro et al. (2020, 2021), we corrected our data for the instrumental peak broadening using a high-quality gemstone natural diamond (which resulted in Γ_G = 5 cm^{-1}), following the same procedure as in Ross et al. (2011) (Table 2). In the same Table 2, the values of Γ_G used in Eq. (2) to obtain the T_{max} are reported for each acquirement. The obtained temperature values range between 1102 and 1300 °C, with an uncertainty of ±120 °C (this is a 2σ uncertainty as indicated by Cody et al., 2008).

Table 2 Centre positions for G, D and D$_0$ bands and FWHM (both in cm^{-1}) of Kenna ureilite. Calculated crystallization temperature, T_{max}, is reported in the last column and was obtained using Eq. (2). The uncertainty on T_{max} is ±120 °C.

G-band center	G-band FWHM	G-band FWHM corrected	D-band center	D-band FWHM	D′-band center	D′-band FWHM	T_{max} (°C)
Kenna							
1579	36	23	1346	49	1614	27	1102
1573	28	18	1346	45	1609	23	1215
1582	37	23	1346	53	1615	27	1090
1572	27	17	1345	50	1607	20	1228
1573	25	16	1342	52	1608	20	1256
1571	31	19	1350	40	1609	20	1175

DISCUSSION

Comparison with other ureilites: The origin of carbon phases

Unlike in the case of recent XRD studies on diamond in ureilites (Nestola et al., 2020; Barbaro et al., 2021), Kenna only contains μm-size diamonds. Indeed, in the fragments studied by these authors, namely, Almahata Sitta 209b and 72, NWA 7983 and Y-74123, the presence of only nm-diamond (for Almahata Sitta samples) or the coexistence of both μm and nano-diamonds (in NWA 7983 and Y-74123) was observed. It is noteworthy that, even if Kenna was classified as a medium shock level ureilite (this work and Berkley et al., 1976), similarly to Yamato 74123, it contains only μm-size diamonds, whereas Y- 74123 contains both μm- and nano-diamonds. In the conditions of a natural shock event (with a shock pulse duration up to 4–5 s, as reported by De Carli et al. 2002) the formation of micrometer-sized diamond could either result from higher shock pressure in the graphite due to shock impedance contrast between contiguous olivine and graphite (e.g. Ogilvie et al., 2011; Gillet and El Goresy, 2013) and/or to the catalytic effect of Fe-Ni-bearing phases, which are particularly abundant in Kenna (compared to the above mentioned ureilites) and could favour the growth of larger diamonds.

In the XRD pattern obtained for Kenna meteorite, graphite highest peak shows the same asymmetry as that observed in the carbon-bearing samples studied in Nestola et al. (2020) and Barbaro et al. (2021) in Almahata Sitta, NWA 7983 and Y-74123 samples, respectively. This graphite was defined as ‘‘compressed graphite”, which usually occurs at the initial stage of the direct transformation from graphite to diamond during shock compression. The presence of this type of graphite and the shock-formation hypothesis of diamond for Kenna was proposed for the first time by Nakamuta and Aoki (2000), who interpreted it as a typical indicator of shock event.

The temperature range we estimated on graphite from Kenna, averaging at about 1180 °C, is higher than the values reported by Ross et al. (2011) for graphite in Almahata Sitta #7 ureilitic fragment (T_{max} of 990 ± 120 °C), but slightly lower than values by Barbaro et al. (2020, 2021) for Almahata Sitta (209b, 72 and A135A) and Y-74123 ureilites, which provided an average T_{max} of 1275 ± 120 °C and 1314 ± 120 °C, respectively. Considering that our method is affected by about ±120 °C uncertainty, it is evident that the T-values measured on the above mentioned five samples is very close, providing an average value at about 1200 °C. Such similar temperature could suggest that all these ureilites of medium shock level recorded a common event, such as the UPB breakup. It is unlikely that this T-value can refer to pre-shock temperature as it was measured on nano-sized compressed graphite, which must result from an impact event and cannot be pristine graphite from the UPB.

The occurrence of carletonmooreite

The results from XRD measurements carried out on the carbon-bearing aggregates show the presence of micrometer-sized diamond (up to 10 µm), nanographite (average crystal size around 80 nm as determined by micro-Raman spectroscopy), nanocrystals of carletonmooreite, and minor magnetite. In Table 3, some a lattice parameter values for synthetic Ni_3Si, natural Ni_3Si and metallic Ni are reported to make a comparison with our estimated value for carletonmooreite (see references in Table 3). The a and V parameters we obtained appear to be slightly larger than those reported by Garvie et al. (2021). These authors reported on the chemical composition of (Ni_3Si) in Norton County aubrite, as obtained with electron-microprobe, which is Ni 82.8 ± 0.4, Fe 4.92 ± 0.09 and Si 13.08 ± 0.08 wt.%. Garvie et al. (2021) also reported on carletonmooreite grains with an average composition of Ni 81.44 ± 0.82, Fe 5.92 ± 0.93, Cu 0.13 ± 0.02 and Si 13.01 ± 0.1 wt.%. Considering that in our EDS spectrum of Fig. 6c the presence of Fe together with Ni is evident, we can assume that carletonmooreite in the Kenna meteorite contains higher amounts of Fe replacing Ni, compared to carletonmooreite characterized by Garvie et al. (2021). This could justify the slight difference between our cell volume and that reported for carletonmooreite by Ma et al. (2018) and Garvie et al. (2021).

The analyses by SEM revealed an intimate textural association between the carbon aggregates and the Fe-Ni compounds (Fe-Ni metal, carletonmooreite and magnetite) as reported for other ureilitic fragments in the recent studies by Nestola et al. (2020) and Barbaro et al. (2021). These authors did not report on the presence of carletonmooreite or of other silicides (Ross et al., 2019), but reiterated the fundamental role played by Fe-Ni phases in the shock transformation from graphite to diamond of different sizes in ureilites. In particular, the debated formation process of lm-sized diamond crystals present in ureilites was ascribed by Nestola et al. (2020), for diamonds found in NWA 7983, to shock event with the catalytic involvement of Fe-Ni phases and long duration peak pressure stage (up to 4–5 s). Even if the effective duration of a typical laboratory shock experiment for diamond formation is too short to allow the growth of diamonds beyond a few µm sizes (De Carli, 1995), a catastrophic impact event is expected to ensure a sufficient duration of high-pressure conditions (De Carli et al., 2002; Fritz et al., 2017). However, it has been established (Dremin and Breusov, 1993) that the formation of diamonds catalysed by metal-bearing (Fe,Ni, Co)-C melts proceeds at lower pressures and higher reaction rates compared to those in absence of these phases, as reported in many studies on industrial synthesis of diamonds (e.g. Bundy et al., 1996; Fedorov et al., 2002). In particular, a description of how the catalysed formation of diamonds by metallic melts during a shock event can also account for simultaneous formation of micro- and nanodiamonds in ureilites is well explained in Nestola et al. (2020).

Table 3. Comparison of the value of the a-cell parameter for b1-Ni_3Si and metal Ni.

β1-Ni_3Si *a*-cell (Å)	**References**	**Ni metal *a*-cell (Å)**	**References**
3.482-3.500	Zhou and Bakker (1994) (milled) Ackerbauer et al. (2009) (Fe = 4 at%)		
3.496	Osawa and Okamoto (1938)	3.516	Osawa and Okamoto (1938)
3.497	Ohira et al. (2005)		
3.506	Oya and Suzuki (1983)		
3.506	Pigozzi et al. (2006)		
3.507-3.510	Suzuki et al. (1984)	3.523	Suzuki et al. (1984)
3.51	Zhang et al. (2009)	3.45	Zhang et al. (2009)
3.51	Garvie et al. (2021) (aubrite) (cell volume = 43.24 Å^3)		
3.512	Connetable and Thomas (2011) (ab initio)		
3.516	Cao et al. (2013) (ab initio)		
3.52	This work (ureilite, nano) (cell volume = 43.87 Å^3)	3.5186	ICDS 98-006-2897
		3.5231	Jovic et al. (2006) (nano)
		3.528-3.541	Wei et al. (2007) (nano)

Notes: nano – nanocrystalline; milled – ball milled (deformed structures); ab initio – calculated from ab initio; other – experimental synthesis.

In this work the pulsed heating experiments performed by Varfolomeeva (1971) on a graphite-metal charge in a static high-pressure apparatus, which roughly simulates natural impact processes (De Carli et al. 2002; Bundy and Kasper, 1967), are discussed. In these experiments diamonds up to 10 µm-sized were produced near to the catalyst, while nanodiamonds occurred in other parts of the experimental charge (Fig. S14 of Nestola et al. 2020). The use of Ni as a catalyst for the formation of diamonds is widely discussed in the literature (e.g. Strong, 1963;

Tsuzuki et al., 1985) and the anomalous content of Ni in this meteorite, due to the presence of an Ni-rich mineral as carletonmooreite (Ni_3Si) in our interpretation can favour the growth process of diamond from graphite during a shock event, thus also enabling the formation of micrometer-sized diamonds. Indeed, in Kenna carbon aggregates, we observed by XRD analysis micrometer-sized diamond alone, in contrast with what is observed in others ureilites (e.g. Yamato 74123 by Barbaro et al. 2021 and NWA 7983 by Nestola et al. 2020), where both micro- and nano-diamonds are present and a lower Ni content was measured.

At any rate, according to static experiments, very reduced conditions at which this silicide Ni_3Si can form (silicide would be few log units below Fe-FeO buffer) would not be compatible with diamond crystallization, which is commonly associated to relatively oxidizing (Fe-FeO) conditions (see Litasov et al., 2013, their Table 2.1). However, in the case of Kenna ureilite, the formation of diamond is ascribed to shock and is not coeval with the formation of Ni_3Si silicide.

Garvie et al. (2021) reported that in Norton County aubrite, carletonmooreite occurred as euhedral to subhedral crystals of 1–14 mm in size. Furthermore, these authors did not emphasize any shock feature in this meteorite. On the contrary, in Kenna, carletonmooreite occurs as nanometric sized grains, associated with nanographite and diamond, thus indicating that its nanometric size could be related to shock event(s), similarity to nanographite as it is unlikely that nanometric Ni_3Si is of pristine origin.

The iron analogue of carletonmooreite, suessite (Fe_3Si), has been already found in ureilites (Ross et al., 2019 and references therein), suggesting that silicides are not so rare in ureilites. Suessite (I m-3m) was discovered for the first time in the North Haig ureilite (Keil et al., 1982). As reported by Ikeda (2007), suessite was produced at temperatures around 1200 and 1100 °C and oxygen fugacity of 10^{-18} -10^{-20} bars from FeO-bearing olivine and Ni-bearing kamacite. Suessite can contain very low amounts of Ni (<5.6 wt.%) compared to carletonmooreite.

Based on one of the hypotheses proposed by Ross et al. (2019) for the formation of natural suessite, carletonmooreite could also have formed in ureilite in a very reduced environment, with fO_2 significantly below iron-wustite buffer. Such conditions are quite common in extraterrestrial material and consistent with the general redox state of ureilites.

On the other hand, it is hard to expect such reduced conditions in terrestrial environments. However, some unusual findings of Fe- and Mn-silicides were reported. There are several locations where Fe-silicides were identified along with other super-reduced phases, including: (a) in chromitite and peridotite from Luobusa (Tibet) (e.g. Nicheng et al., 2012); (b) in the Yakutian kimberlites (Shiryaev et al., 2011); (c) in the alluvial rocks near Mt. Carmel (Israel) (Griffin et al., 2016); (d) in mantle xenoliths from Kamchatka volcanics (Ishimaru et al., 2009); and (e) in fulgurites (Stefano et al., 2020). Mn-silicides are additionally reported in lamproite from Uzbekistan (Yusupov et al., 2009) and as inclusions in polycrystalline diamond aggregates from Kamchatka placers (Kaminsky et al., 2020). The origin of terrestrial Fe-silicides is, in some cases, questionable, because in the reported locations, a contamination by industrial abrasive or slag materials cannot be excluded (e.g. Litasov et al., 2019, 2020).

In summary, the small size of the carletonmooreite reported here in Kenna, its occurrence in close relationship with carbon phases, and the natural reducing conditions typical for ureilites, other than the rare occurrence of similar reduced phases in terrestrial environments, allow us to exclude that the observed carletonmooreite derives from terrestrial contamination.

CONCLUSIONS

Microdiamonds (up to about 10 µm in size), nanographite and magnetite were found within the carbon-bearing areas in the Kenna meteorite. The temperature (T_{max}) recorded by nanographite using the geothermometer by Cody et al. (2008) is close to 1180 °C. This temperature is ascribable to a shock event which reduced graphite to nanometric in size. In addition to these phases, we identified nanocrystalline carletonmooreite (Ni_3Si). This rare phase, reported for the first time in a ureilite, could be formed, in agreement with Ikeda (2007) and Ross et al. (2019), under extreme reducing condition by reaction of Fe-Ni melt, with silicate as a source of silicon (Ikeda, 2007), and graphite as a reducing agent. The shock features observed in olivine and in pyroxene (S3-S4), together with the presence of microdiamonds and nanographite indicate that the Kenna meteorite underwent a shock event with a peak pressure of at least 15 GPa, which could have reduced to nanometric size both pristine graphite and carletonmooreite.

Our results further demonstrate how the role of Fe-Ni metals (and eventually their compounds) is crucial in favouring diamond to grow directly from graphite during a shock event. It is well established that a direct graphite to- diamond transformation, in absence of any catalytic process, would require very high pressure and temperature conditions. In addition, it is expected that for shock event of limited magnitude (15–20 GPa, as supported by textural features observed in the silicates) such direct transformation could only produce diamonds of nanometric size (Nestola et al. 2020 and references therein).

Here we show that, combining a long shock pulse with the presence of Fe-Ni phases, in particular Ni as demonstrated by carletonmooreite, diamond growing from graphite can reach micrometer-size even for relatively low shock pressures (ca. 15–20 GPa).

Acknoledgments

We wish to thank H. Downes and an anonymous reviewer for their constructive reviews, as well as C. Koeberl for further suggestions and editorial handling. This work was supported by PNRA 2018 grant number PNRA18 00247 – A to F. Nestola. A.B. and M.A. were funded by the IMPACt project (R164WEJAHH) to M. Alvaro. M.C.D. has been funded by the PNRA 2016 to L. Folco.

References

Ackerbauer S., Krendelsberger N., Weitzer F., Hiebl K. and Schuster J. C. (2009) The constitution of the ternary system Fe– Ni–Si. Intermetallics 17(6), 414–420.

Barbaro A., Domeneghetti M. C., Goodrich A. C., Meneghetti M., Litti L., Fioretti A. M., Jenniskens P., Shaddad M. H., Alvaro M. and Nestola F. (2020) Graphite based geothermometry on Almahata Sitta ureilites meteorites. Minerals 10(11), 1005.

Barbaro A., Nestola F., Pittarello L., Ferrie`re L., Murri M., Litasov D. K., Christ O., Alvaro M. and Domeneghetti M. C. (2021) Characterization of carbon phases in Yamato 74123 ureilite to constrain the meteorite shock history. Am. Mineral. doi.10.2138/am 2021 7856 (in Press).

Berkley J. L., Brown, IV, H. G., Keil K., Carter N. L., Mercier J.- C. C. and Huss G. (1976) The Kenna ureilite: an ultramafic rock with evidence for igneous, metamorphic, and shock origin. Geochim. Cosmochim. Acta 40, 1429–1437.

Brecher A. and Fuhrman M. (1979) The magnetic effects of brecciation and shock in meteorites: II. The ureilites and evidence for strong nebular magnetic fields. Moon Planets 20(3), 251–263.

Bundy F. P., Bassett W. A., Weathers M. S., Hemley R. J., Mao H. U. and Goncharov A. F. (1996) The pressure-temperature phase and transformation diagram for carbon; updated through 1994.. Carbon 34(2), 141–153.

Bundy F. P. and Kasper J. S. (1967) Hexagonal diamond–A new form of carbon. J. Chem. Phys. 46, 3437–3446.

Cao Y., Zhu J., Liu Y., Nong Z. and Lai Z. (2013) First-principles studies of the structural, elastic, electronic and thermal properties of Ni3Si. Comput. Mater. Sci. 69, 40–45.

Ackerbauer et al., 2009 S. Ackerbauer, N. Krendelsberger, F. Weitzer, K. Hiebl, J.C. Schuster. The constitution of the ternary system Fe–Ni–Si. Intermetallics, 17 (6) (2009), pp. 414-420.

Clayton R. N., Mayeda T. K., Onuma N. and Shearer J. (1976) Oxygen isotopic composition of minerals in the Kenna ureilite. Geochim. Cosmochim. Acta 40(12), 1475–1476.

Cloutis E. A., Hudon P., Romanek C. S., Bishop J. L., Reddy V., Gaffey M. J. and Hardersen P. S. (2010) Spectral reflectance properties of ureilites. Meteorit. Planet. Sci. 45, 10–11.

Cody G. D., Alexander C. M. O'. D., Yabuta H., Kilcoyne A. L. D., Araki T., Ade H., Dera P., Fogel M., Militzer B. and Mysen B. O. (2008) Organic thermometry for chondritic parent bodies. Earth Planet. Sci. Lett. 272, 446–455.

Connétable D. and Thomas O. (2011) First-principles study of nickel-silicides ordered phases. J. Alloys Compd. 509(6), 2639– 2644.

De Carli P. S. (1995) Shock wave synthesis of diamond and other phases. Mat. Res. Soc. Symp. Proc. 383, 21–31.

De Carli P. S., Bowden E., Jones A. P. and Price G. D. (2002) Laboratory impact experiments versus natural impact events.

In Catastrophic Events and Mass Extinctions: Impacts and Beyond, Geological Society of America Special Paper 356, 595– 605.

Dremin A. N. and Breusov O. N. (1993) Dynamic synthesis of superhard materials. In Shock Waves in Materials Science (ed.

A. B. Sawaoka). Springer, Tokyo, pp. 17–34. Fukunaga K., Matsuda J., Nagao K., Miyamoto M. and Ito K. (1987) Noble-gas enrichment in vapour-growth diamonds and the origin of diamond in ureilites. Nature 328, 141–143.

Fedorov I. I., Chepurov A. A. and Dereppe J. M. (2002) Redox conditions of metal-carbon melts and natural diamond genesis. Geochem. J. 36, 247–253.

Ferrari A. C. and Roberson J. (2000) Interpretation of Raman spectra of disordered and amorphous carbon. Phys. Rev. B 61, 14095–14107.

Fritz J., Greshake A. and Fernandes V. A. (2017) Revising the shock classification of meteorites. Meteorit. Planet. Sci. 52(6), 1216–1232.

Garvie L. A. J., Ma C., Ray S., Domanik K., Wittman A. and Wadhwa M. (2021) Carletonmooreite, Ni3Si, a new silicide from the Norton County, aubrite meteorite. Am. Mineral. doi.10.2138/am-2021-7645 (in press).

Goodrich C. A. (1992) Ureilites: A critical review. Meteorit. Planet. Sci. 27, 327–352.

Goodrich C. A., Hartmann W. K., O'Brien D. P., Weidenschilling S. J., Wilson L., Michel P. and Jutzi M. (2015) Origin and history of ureilitic material in the solar system: The view from asteroid 2008 TC3 and the Almahata Sitta meteorite. Meteorit. Planet. Sci. 50, 782–809.

Gillet P. and El Goresy A. (2013) Shock Events in the Solar System: The message from minerals in Terrestrial Planets and Asteroids. Annu. Rev. Earth Planet. Sci. 41, 247–285.

Griffin W. L., Gain S. E. M., Adams D. T., Huang J.-X., Saunders M., Toledo V., Pearson N. J. and O'Reilly S. Y. (2016) First terrestrial occurrence of tistarite (Ti2O3): ultra-low oxygen fugacity in the upper mantle beneath Mount Carmel, Israel. Geology 44, 815–818.

Ikeda Y. (2007) Petrology of an unusual ureilite NWA 1241. Polar. Sci. 1, 45–53.

Ishimaru S., Arai S. and Shukuno H. (2009) Metal-saturated peridotite in the mantle wedge inferred from metal-bearing peridotite xenoliths from Avacha volcano, Kamchatka. Earth Planet. Sci. Lett. 284, 352–360.

Jovic´ V. D., Maksimovic´ V., Pavlovic´ M. G. and Popov K. I. (2006) Morphology, internal structure and growth mechanism of electrodeposited Ni and Co powders. J. Solid State Electrochem. 10(6), 373–379.

Lee M. R. and Bland P. A. (2004) Mechanisms of weathering of meteorites recovered from hot and cold deserts and theformation of phyllosilicates. Geochim. Cosmochim. Acta 68(4), 893–916.

Litasov K. D., Bekker T. B. and Kagi H. (2020) ‘‘Kamchatite” diamond aggregate from northern Kamchatka, Russia: New find of diamond formed by gas phase condensation or chemical vapor deposition – Discussion. Am. Mineral. 105, 144–145.

Litasov K. D., Kagi H. and Bekker T. B. (2019) Enigmatic superreduced phases in corundum from natural rocks: Possible contamination from artificial abrasive materials or metallurgical slags. Lithos 340–341, 181–190.

Litasov K. D., Shatskiy A. and Ohtani E. (2013) Earth's mantle melting in the presence of COH-bearing fluid. Physics and chemistry of the deep Earth. Shun-ichiro Karato, pp. 38–65.

Lipschutz M. E. (1964) Origin of Diamonds in the Ureilites. Science 143, 1431–1434.

Kaminsky F. V., Wirth R., Anikin L. P. and Schreiber A. (2020) On ''Kamchatite" diamond aggregate from northern Kamchatka,

Russia: New find of CVD-formed diamond in nature— Reply to KD Litasov, TB Bekker and H. Kagi. Am. Mineral. 105(1), 144–145.

Keil K., Berkley J. L. and Fuchs L. H. (1982) Suessite, Fe3Si: a new mineral in the North Haig ureilite. Am. Mineral. 67(1–2), 126– 131.

Ma C., Garvie L. A. J. and Wittmann A. (2018) Carletonmooreite, IMA 2018-068. CNMNC Newsletter No. 45, October (2018), page 1042. Europ. J. Mineral. 30, 1037–1043.

Miyahara M., Ohtani E., El A., Lin Y., Feng L., Zhang J., Gillet P., Nagase T. and Muto J. (2015) Unique large diamonds in a ureilite from Almahata Sitta 2008 TC3 asteroid. Geochim. Cosmochim. Acta 163, 14–26.

Nabiei F., Badro J., Dennenwaldt T., Oveisi E., Cantoni M., He´bert C., El Goresy A., El Barrat J. and Gillet P. (2018) A large planetary body inferred from diamond inclusions in a ureilite meteorite. Nat. Commun. 9, 1–6.

Nakamuta Y. and Aoki Y. (2000) Mineralogical evidence for the origin of diamond in ureilites. Meteorit. Planet. Sci. 35, 487– 493.

Nash P. and Nash A. (1987) The Ni–Si (Nickel-Silicon) system. Bull. Alloy Phase Diagrams 8(1), 6–14.

Nestola F., Goodrich C. A., Morana M., Barbaro A., Jakubek R. S., Chris O., Brenker F. E., Domeneghetti M. C., Dalconi M. C., Alvaro M., Fioretti A. M., Litasov K. D., Fries M. D., Leoni M., Casati N. P. M., Jenniskens P. and Shadad M. H. (2020) Impact shock origin of diamond in ureilite meteorites. PNAS 117(41), 25310–25318.

Nicheng S., Wenji B. A. I., Guowu L. I., Ming X. I. O. N. G., Jingsu Y. A. N. G., Zhesheng M. A. and He R. (2012) Naquite, FeSi, a new mineral species from Luobusha, Tibet, western China. Acta Geolog. Sinica – English Ed. 86(3), 533–538.

Ogilvie P., Gibson R. L., Reimold W. U., Deutsch A. and Hornemann U. (2011) Experimental investigation of shock metamorphic effects in a metapelitic granulite: The importance of shock impedance contrast between components. Meteorit. Planet. Sci. 46, 1565–1586.

Ohira K., Kaneno Y. and Takasugi T. (2005) Microstructure, mechanical property and oxidation property in Ni3Si–Ni3Ti– Ni3Nb multi-phase intermetallic alloys. Mater. Sci. Eng. 399(1–2), 332–343.

Osawa A. and Okamoto M. (1938) An X-ray analysis of the alloys of the nickel-silicon system. Nippon Kinzoku. Gakkai-Shi 2, 378–388 (in Japanese).

Oya Y. and Suzuki T. (1983) The nickel-rich portion of the Ni-Si phase diagram. Z. Metallkd. 74(1), 21–24.

Pigozzi G., Mukherji D., Gilles R., Barbier B. and Kostorz G. (2006) Ni3Si (Al)/a-SiOx core-shell nanoparticles: characteriza-tion, shell formation, and stability. Nanotechnology 17, 4195– 4203.

Raghavan V. (2010) Fe-Ni-Si (iron-nickel-silicon). J. Phase Equilibria Diffus. 31(2), 184–185.

Ross A. J., Steele A., Fries M. D., Kater L., Downes H., Jones A. P., Smith C. L., Jenniskens P. M., Zolensky M. E. and Shaddad M. H. (2011) MicroRaman spectroscopy of diamond and graphite in Almahata Sitta and comparison with other ureilites. Meteorit. Planet. Sci. 46, 364–378.

Ross A. J., Downes H., Herrin J. S., Mittlefehldt D. W., Humayun M. and Smith C. (2019) The origin of iron silicides in ureilite meteorites. Geochemistry 79(4) 125539.

Rubin A. (2006) Shock, post-shock annealing, and post-annealing shock in ureilites. Meteorit. Planet. Sci. 41, 125–133.

Scherrer P. (1918) Estimation of the size and internal structure of colloidal particles by means of ro¨ntgen. J. Math. Phys. 2, 98–100.

Shiryaev A. A., Griffin W. L. and Stoyanov E. (2011) Moissanite (SiC) from kimberlites: polytypes, trace elements, inclusions and speculations on origin. Lithos 122, 152–164.

Stefano C. J., Hackney S. A. and Kampf A. R. (2020) The occurrence of iron silicides in a fulgurite: implication for fulgurite genesis. Can. Mineral. 58(1), 115–123.

Stöffler D., Keil K. and Scott E. R. D. (1991) Shock metamorphism of ordinary chondrites. Geochim. Cosmochim. Acta 55(12), 3845–3867.

Stöffler D., Hamann C. and Metzler K. (2018) Shock metamorphism of planetary silicate rocks and sediments: Proposal for an updated classification system. Meteorit. Planet. Sci. 53(1), 5–49.

Strong H. M. (1963) Catalytic effects in the transformation of graphite to diamond. J. Chem. Phys. 39(8), 2057–2062.

Suzuki T., Oya Y. and Ochiai S. (1984) The mechanical behavior of nonstoichiometric compounds Ni3Si, Ni3Ge, and Fe3Ga. Metall. Trans. A 15(1), 173–181.

Tsuzuki A., Hirano S. I. and Naka S. (1985) Influencing factors for diamond formation from several starting carbons. J. Mater. Sci. 20(6), 2260–2264.

Tuinstra F. and Koenig J. L. (1970) Raman spectrum of graphite. J. Chem. Phys. 53, 1126–1130.

Urey H. C. (1956) Diamond, meteorites, and the origin of the solar system. American Astronom. Soc. 124, 623–637.

Varfolomeeva T. D. (1971) Synthesis and investigation of polycrystalline diamond, PhD thesis. Institute for High Pressure Physics, USSR Academy of Sciences. p. 154.

Wei Z., Xia T., Ma J., Feng W., Dai J., Wang Q. and Yan P. (2007) Investigation of the lattice expansion for Ni nanoparticles. Mater. Charact. 58(10), 1019–1024.

Wilkening L. L. and Marti K. (1976) Rare gases and fossil particle tracks in the Kenna ureilite. Geochim. Cosmochim. Acta 40(12), 1465–1473.

Yusupov R. G., Stanley C. J., Welch M. D., Spratt J., Cressey G., Rumsey M. S., Seltmann R. and Igamberdiev E. (2009) Mavlyanovite, Mn5Si3: a new mineral species from a lamproite diatreme, Chatkal Ridge, Uzbekistan. Mineral. Mag. 73, 43–50.

Zhang W. W., Xu H. H., Liang J. L., Xiong W. and Du Y. (2009) Phase equilibria of the Fe–Ni–Si system at 850 C. J. Alloys Compd. 481(1–2), 509–514.

Zhou G. F. and Bakker H. (1994) Atomic disorder and phase transformation in L12-structure Ni3Si by ball milling. Acta Metall. Mater. 42(9), 3009–3017.

CHAPTER 6

CONCLUSIONS AND FUTURE PERSPECTIVES

The study of carbon minerals in ureilites is of fundamental importance to understand geological processes on their parent body and add further information about the carbon cycle in Solar System. In this thesis work, the investigation of diamond and graphite by a multimethodological approach (SEM, XRD, MRS and TEM) in the studied samples allowed the characterization of these carbon phases, the determination of their crystallite size, and the estimation of the temperature recorded by the graphite. In particular, thanks to the results obtained on these ureilites with different shock degrees, it was possible to ascribe the origin of the formation process of diamond in ureilites and determine the processes through which these minerals grow (i.e. enhancing diamond growth by Fe-Ni catalysis).

The investigation of carbon phases in AhS 209b, AhS 72, AhS A135A, NWA 7983, Yamato 74123 and Kenna samples (Chapter 2, 3, 4 and 5) allowed me to:

- observe an intimate coexistence of nanodiamond, micro diamond and nano graphite always accompanied by Fe-Ni phases (or their compounds);
- demonstrate that the most likely process by which both micro diamonds and nanodiamonds in ureilites formed is a shock event characterized by a peak pressure possibly as low as 15 GPa, which is the shock level recorded by the silicates surrounding the carbon areas;
- estimate the temperature recorded by graphite in all different samples, which is between 1180 and 1419±120°C;
- demonstrate that graphite in our sample is nanometric, suggesting that the temperature recorded by graphite represents the shock-induced temperature excursion or corresponds to a subsequent post-shock temperature imprinted during the shock event.

This imprinting likely occurred during the strongest impact event it experienced during its history, which was probably the one disrupting the ureilite parent body;

- explain the coexistence of nano and micro diamond together with nano-graphite by the role of Fe-Ni metals (and eventually their compounds) as catalysts in diamond growth. Indeed, these compounds are crucial in favouring diamonds to grow directly from graphite during a shock event. It is well established that direct graphite to diamond transformation would require very high pressure and temperature conditions without any catalytic process. In addition, it is expected that for shock events of limited magnitude (15–20 GPa, as supported by textural features observed in the silicates), such direct transformation could only produce diamonds of nanometric size (Nestola et al. 2020 and references therein). Here it is demonstrated that combining a long shock pulse (a few seconds as expected for the disruption event of the UPB) with the presence of Fe-Ni phases, diamond growth from graphite can reach micrometer-size even for relatively low shock pressures (ca. 15–20 GPa).

The results from my PhD thesis did not indicate any evidence of diamond formation within large planetary bodies or by CVD in a solar nebula adding a “missing piece” in reconstructing the puzzle of the UPB and its asteroidal daughter bodies history.

However, to better understand the shock formation processes of these meteorites, further development in determining the level of shock features in ureilites is needed. In particular, in addition to the characterization of their carbon phases, to reconstruct the shock history of these meteorites, a correlation between carbon phases and silicates shock features in ureilites, that experienced different degrees of shock is needed using less ambiguous methods than optical microscopy. In particular, as reported in paragraph 1.2 of Chapter 1, a good candidate could be the XRD technique using the protocol developed by Vinet et al. (2011) on terrestrial olivine and used by Li et al. (2021) on ureilitic olivine. However, in their work, Li et al. (2021) did not study the carbon phases in ureilites, and therefore they did not compare the XRD results obtained on silicates with those observed on carbon phases of the same fragments. Instead, this comparison could provide more constraints on the shock level the meteorite recorded. In addition, Li et al. (2021) reported only a few measurements for each sample they studied without considering the shock impedance contrast between minerals (Ogilvie et al., 2011). Indeed, as reported in subchapter 1.2, the propagation of the shock wave in the parent body correlated to an impact event is different and, following Ogilvie et al. (2011), it is important to evaluate the shock level recorded by mineral taking into account the different contrast between the contiguous mineralogical phases involved in the event. For this reason, to observe any differences between crystals in ureilites of different shock degrees, a set of data on different crystals in different positions of the samples should be carried out. For example, diffraction data on olivine should be collected on crystals in contact with other mineralogical phases, like pyroxenes or close to a big carbon zone.

Instead, a development in the study of carbon phases in ureilites will be through the investigation of the disorder features at the nanoscale using X-ray diffraction and Transmission Electron Microscopy (TEM). TEM can provide key information about structural defects in graphite and diamond originating from shock deformation, such as dislocations, stacking faults and twinning. High-resolution images of defect microstructures could be obtained by weak beam dark field techniques. The carbon modifications could be identified from the SAED zone axes pattern and respective interplanar spacings calculated using a camera constant calibrated against synthetic and natural standards. Indeed, the carbon energy electron loss spectroscopy can identify different carbon species, and the energy-filtered images of the low loss region will allow imaging of the carbon distribution with sub-nm resolution. TEM data will also be used to confirm the presence of the stacking faults of diamond in our samples. Defect microstructures like dislocations and sub-grain boundaries will further be analyzed applying the g.b invisibility criterion. TEM will also be used to provide cross-validation against the results from micro X-Ray diffraction in terms of the crystallite size. In addition, the TEM study will be fundamental to investigate the reciprocal crystallographic orientations between diamond and graphite because it could provide hints on the genetic relationship between the two phases. The crystallite size does depend on the complexity of the sample, and peaks overlap with other phases, large size distribution, the coexistence of size peak broadening and microstrain.

A further very interesting development about the carbon phases study could be the investigation of carbon and nitrogen isotope signature by secondary ion mass spectroscopy (SIMS). Isotope data provide crucial information about the origin of carbon material and on the relationship between graphite and diamond. In addition, the examination of the distribution of C and N in meteorites could help trace the evolution of planet-forming processes, like aggregation, melting, differentiation, crystallization and brecciation (Grady and Wright 2003). However, literature data of carbon and nitrogen isotopes in ureilitic graphite and diamond mainly refer to bulk rocks and rarely on single phases (Grady and Wright 2003; Fisenko et al. 2004; Barrat et al. 2017). In particular, it will be fundamental to determine the carbon isotope signatures, the $\delta^{13}C$, in graphite and diamond by secondary ion mass spectroscopy (SIMS), their nitrogen content and, if the amount of N is not negligible (e.g., > 30-40 ppm), their $\delta^{15}N$ signatures. The great difficulty in performing such measurements mainly derives from the evidence that graphite and diamond within such meteorites are most intimately associated. Since we would like to determine the above isotope signatures on individual phases and not on the bulk, we should first perform the measure by SIMS on bulk sample and then on the material obtained from the removal of graphite from diamonds. In this way it will be possible to obtain the isotope signature of diamond (results obtained by the measure on purified sample) and on graphite (by subtracting the values of isotope signature obtained on purified sample from the bulk results).

APPENDIX I

Supplementary Information for

IMPACT SHOCK ORIGIN OF DIAMOND IN UREILITE METEORITE

Fabrizio Nestola*, Cyrena A. Goodrich, Marta Morana, Anna Barbaro, Ryan S. Jakubek, Oliver Christ, Frank E. Brenker, Maria Chiara Domeneghetti, Maria Chiara Dalconi, Matteo Alvaro, Anna Maria Fioretti, Konstantin Litasov, Marc D. Fries, Matteo Leoni, Nicola P. M. Casati, Peter Jenniskens, Muawia H. Shaddad

*Fabrizio Nestola
E-mail: fabrizio.nestola@unipd.it

Supplementary Information Text

Materials and Methods

Scanning Electron Microscopy (SEM) of specimens studied by Micro X-ray Diffraction

Imaging and characterization of non-carbon-coated sections of AhS 72, AhS 209b and NWA 7983 to be used for micro X-ray diffraction studies was done using a conventional petrographic microscope and the *JSM Jeol 6490* low vacuum SEM at CEASC at the University of Padova (Italy).

SEM and Electron Microprobe Analyses of Additional Sections for Petrography

Petrographic characterization of additional polished sections of the ureilites studied in this work was conducted at the Astromaterials Research and Exploration Science division at Johnson Space Center in Houston, Texas (USA). The JEOL 5910-LV SEM was used for backscattered electron imaging (BEI) of a non-carbon-coated section of NWA 7983 (Fig. S6).

The observations were made at 15 KeV accelerating potential in normal high vacuum mode, despite the lack of carbon coat, in order to allow higher beam currents (and hence greater BEI contrast). Under these conditions charging of silicates was observed, but carbon areas were sufficiently conductive to provide good images (Fig. S6b). The JEOL 8530-FE electron microprobe (EMP) was used for secondary electron imaging (SEI) and BEI observations, as well as quantitative analysis of phases, in carbon-coated sections of AhS 72, AhS 209b, and NWA 7983. Imaging was conducted at 15 KeV accelerating potential and a range of beam currents from ~10-30 nA). Quantitative analyses of silicates (olivine and pyroxene) were obtained at 15 KeV accelerating potential and 25 or 30 nA of beam current. Natural and synthetic silicates, oxides and metals were used as standards. Data reduction utilized the ZAF correction procedure.

Extraction of Samples for X-ray Diffraction

Small samples of carbon materials selected (by SEM) for X-ray diffraction were removed using a needle. The materials obtained through this procedure were quickly glued at the top of 100 μm diameter glass fibres. Fig. S7 shows reflected light images of the AhS 72 and AhS 209b samples mounted on the fibres. Fig. S11 shows the carbon-bearing aggregate of NWA 7983 ureilitic fragment.

Micro X-ray powder Diffraction (XRD)

Powder X-ray diffraction analyses of AhS samples were performed in Experimental Hutch 1 (EH1) of the Paul Scherrer Institute (PSI) (1), Switzerland. They utilized MS Powder diffractometer works in Debye-Scherrer geometry and is equipped with a unique solid-state silicon microstrip-detector, called MYTHEN (Microstrip sYstem for Time-resolved

ExperimeNts). The characteristic of MS – X04SA beamline at Paul Scherrer Institute are for our measurements are:

- Wavelength = 0.70861 Å;
- Energy = 17.497 keV;
- Focused spot size of 130 μm x 40 μm (1:1 focusing);

The MYTHEN II detector is a general-purpose detector, with maximum resolution of 3.7 mdeg in 2θ, and very high efficiency and rapidly acquisition time.

On polycrystalline samples of NWA 7983, we carried out XRD through an innovative method. To analyse this sample, with a size of a few microns aggregation, we used the Rigaku-Oxford Diffraction Supernova kappa-geometry goniometer with a X-ray Mo micro-source equipped with a Pilatus 200K Dectris detector in transmission mode, controlled by the Crysalis-Pro™ software at Department of Geosciences in Padova.

Diffraction line profile analysis using the High Score Plus Software package (Panalytical) was applied to estimate the crystallite size of the carbon phases. The integral breadths, which were obtained by the line profile analysis fitting, were then inserted into the Scherrer Eq. 1 to estimate the crystallite size of diamond.

$$\beta(2\theta) = \frac{K_\beta \times \lambda}{<D>_V \cos\theta_{hkl}} \qquad [1]$$

$$\frac{D_V}{K_\beta} = \frac{\lambda}{\cos\theta_{hkl}\ x\ \beta(2\theta)} \qquad [2]$$

The Scherrer Eq. 1, 2 gives a correlation between β peaks broadening and the dimension of diffracted domain, the crystallite size, D_V. K is a constant value between 0.5 and 1, and it describes the contribution of crystallites shape. K is a parameter that depends on the relative orientation of the scattering vector to the external shape of the crystallite.

Using only the two peaks of diamond at *d*-spacing 1.26 and 1.07 Å it is possible to obtain a reliable estimation of the crystallite size as such peaks do not show any overlap with peaks of other phases within the grains here analyzed.

Supplementary Table 1 reports the unit cell parameters for the diamond single crystal found in NWA 7983 and shows the results of the estimated crystallite size for polycrystalline diamond of AhS 209b (Fig. 2*A*), AhS 72 (Fig. S8) and NWA 7983 (Fig. 2*C*) samples. In NWA 7983 micro-diamond (Fig. 2*B*), nano-diamond, and graphite (Fig. 2*C*) coexist.

However, both of the AhS samples show a typical feature of diamond stacking faults (see in Fig. S9 the high magnification image showing the left shoulder of the 2.06 Å peak of diamond of the AhS 209b sample in Fig. 2*A*) and in order to take into account any defects in diamond and eventually graphite (which shows a significant peak asymmetry and broadening) not considered in the previous profile analysis, we performed a further profile analysis by using DIFFaX+ software (see Fig. S10).

The diffraction pattern is a linear combination of the patterns corresponding to the various species present in the specimen. By using the ICDD Sieve+ search match software linked to the ICDD PDF4+ database, it was possible to identify the simultaneous presence of diamond, graphite, iron and minor troilite. The univocal identification of other phases, present in small quantity, was not possible on the basis of a single diffraction pattern. Their exclusion from the analysis does not modify the information concerning the nanostructure of the diamond phase.

The peculiar shape of the peaks corresponding to the diamond phase are due to the presence of stacking defects and in particular to an intergrowth of diamond and lonsdaleite on the same crystals. The difference between these two Maximum Degree of Order (MDO) polytypes (2), is in the stacking of the dense planes. To model them, the diamond structure was described on a hexagonal lattice equivalent to the cubic one, whose base was built on the 111 plane of the original diamond cell. Faults along the stacking direction (<111> in the original lattice, corresponding to <001> in the remapped one) can lead to a local symmetry change from cubic to hexagonal. A similar phenomenon is observed in *fcc* or *hcp* metals prone to faulting (e.g. copper, gold, platinum, iron, nickel, cobalt). Two types of layers were defined: layer A with carbon atoms at $(\frac{1}{3},\frac{1}{6},\frac{1}{8})$ and at $(-\frac{1}{3},-\frac{1}{6},-\frac{1}{8})$, and layer B with atoms at $(-\frac{1}{3},-\frac{1}{6},\frac{1}{8})$ and $(\frac{1}{3},\frac{1}{6},-\frac{1}{8})$, respectively.

A statistical assembly of the two structural motifs was considered. The probabilities of a cubic sequence α_{AA} (AA layer stacking) and of an hexagonal one α_{AA} (B-B layer stacking) were employed as parameters. The simplest finite-state model that considers just 2-layer stacking probabilities and maps the corresponding Markov chain, can be described by a probability matrix α and a stacking matrix T:

$$\boldsymbol{\alpha} = \begin{pmatrix} \alpha_{AA} & 1-\alpha_{AA} \\ 1-\alpha_{BB} & \alpha_{BB} \end{pmatrix} \qquad \boldsymbol{T} = \begin{pmatrix} ({}^{2}/_{3},{}^{1}/_{3},1) & (0,0,1) \\ (0,0,1) & ({}^{1}/_{3},{}^{2}/_{3},1) \end{pmatrix}$$

The probability matrix was optimized using a modification of the DIFFaX+ software (3), combining the matrix method written in recursive form (4) for the description of the lattice structure and the Whole Powder Pattern Modelling (5) for the description of the size/shape effects. The optimized matrix was then employed in the TOPAS Rietveld software (6) for the final modelling of the whole pattern with multiple phases. The NIST SRM 640c Silicon standard was employed to calibrate the instrument (a_0 = 0.54311946 nm) and to obtain information about the intrinsic instrumental broadening. Albeit not a proper line profile standard, the 640c was used also to extract the instrumental resolution profile necessary for the final modelling of the data. The diffraction patterns of both the silicon and the meteorite sample were simultaneously modelled: the intrinsic profile data from the silicon were the same in both experiments.

The modelling of a system with stacking defects is intrinsically complex as the specimens are usually composed of a large quantity of grains each of them containing heterogeneous domains in terms of size, shape and stacking sequences. The phenomenon is visible in the 2D diffraction patterns that are rather spotty. As this is not an ideal powder case (uniform distribution of equal domains in all orientations), it is not possible here to model the whole diffraction pattern using a single model for the diamonds: the peaks have a peculiar shape with a sharp tip and a broad base, typical of systems showing a broad distribution of sizes. Considering that diffraction is a volume-sensitive technique and that the size of the domains is approximately inversely proportional to the peak breadth, a large quantity of small domains contributes to the broad peak base, whereas a progressively small quantity of domains contributes to the central narrow part of the peak. the observed effects can be due to the simultaneous presence of a large quantity of small domains together with a few large ones there is a broad distribution of sizes and the characteristics of the smaller domains can be rather different than those of the larger ones. A model was therefore sought here to reproduce most of the observed features with a minimal number of parameters. Four diamond families were employed: two families of nano diamonds (one with small and one with large percentage of hexagonal faults) and two families of large diamonds with a small percentage of hexagonal faults. The fault percentage is not very significant in the nanodiamonds as it is not possible, with the current system, to identify a probably stacking sequence. The large diamonds, on the contrary, show not just sharp maxima, but also peculiar features in the tail that evidence the presence of the local hexagonal symmetry. The smaller domains are on average 3-12 nm, whereas the larger ones are above 50 nm. Above ca. 100 nm, diffraction is no longer reliable for the determination of size and defects in materials.

Micro X-Ray Diffraction (XRD)

Single crystal diamond of NWA 7983 sample was analyzed by the Rigaku-Oxford Diffraction Supernova kappa-geometry goniometer at Department of Geosciences in Padova. An X-ray Mo micro-source equipped with a Pilatus 200K Dectris detector, controlled by the Crysalis-Pro™ software was used. We removed the single crystal analysed in our work from the carbon area shown in Fig. S12. NWA 7983 shows only diffraction spots, this point out that this sample is a single crystal diamond with a size as least as large as that of the fragment (~100 μm long).

Transmission electron Microscopy (TEM)

Transmission Electron Microscopy (TEM) was used to verify the estimated crystallite size obtained by XRD through line profile analysis. The crystallite size estimated by XRD does depend on the complexity of the sample, peak overlap with other phases, large size distribution, coexistence of size peak broadening and microstrain. For this reason, we used the TEM data to confirm the presence of the stacking faults of diamond in our samples.

The TEM laboratory is located at the Geoscience Institute of University of Frankfurt together with a preparation laboratory working with an Argon Ion Slicing (ArIS) for huge electron transparent thin section, and a focused ion beam for site specific preparation at the Department of Physics. The samples were covered with about 60 nm of gold to compensate the charges in the SEM and also for having a protective layer for the Focused Ion Beam (FIB) cutting preparation procedure. The FIB produced only a bit of amorphous layer in the first nanometers on the surface, but it does not modify the structure. However, the FIB could not cause deformation on diamond at all, but only in graphite (the power is not enough) and only in the first few nanometers depth. However, this procedure could implant Gallium inside the sample, causing a contamination on our samples.

For TEM analysis, a Philips CM 200 was used operating with a LaB6-cathode at 200 kV. Two FIB sections from the two coarse-grained carbon-aggregates of the Almahata Sitta ureilite were analyzed. The analysis was done using bright-field, dark-field and selected area electron diffraction (SAED) techniques. SAED patterns taken with a camera length of 1m were evaluated manually with an Al-powder as standard material. This led to a camera constant C of 23.64mmÅ. Further, the software Single Crystal together with CrystalMaker was used to index crystal reflexes and identify mineral phases.

Micro-Raman Spectroscopy

Raman imaging was performed using "Ratatoskr", a WITec alpha300R confocal Raman Microscope (XMB3000-3003) designed for the study of astromaterials and housed at the NASA Curation Office at Johnson Space Center (JSC). Raman spectra were collected using ~15 µw of 488 nm light generated by a WITec diode laser (XSL3100-1155). The Raman excitation beam was focused and the Raman scattered light was collected using a 50X objective. The 50X objective focused the incident light to a beam diameter of ~1.5 µm. The Rayleigh scattering was removed using a WITec Rayline long pass filter (XZF3100-0488). The Raman scattered light was dispersed using a UHTS600 spectrometer with a 300 g/mm grating (XMC3200-0600) and was detected using a thermoelectrically cooled (-60ºC), back-illuminated, CCD. The spectrometer resolution is ~2.8 cm^{-1}/pixel at the spectrum center and the wavenumber precision is ±0.15 cm^{-1} without the use of advanced calibration techniques (7). Raman images were collected by scanning the beam spot on the sample using a x-y-sample scanning stage (WITec XSP3000-0001). Raman spectra were collected with a spatial resolution of 5 μm. The beam was auto-focused on the sample using the WITec TrueSurface program to allow for the Raman image collection of a sample with rough topology.

Micro-Raman spectroscopy was used to image the diamond and graphite species in ureilites. The Raman spectrum of larger diamonds (~>45 nm) contains a large, narrow band at ~1332 cm^{-1} originating from its only Raman-active phonon (8,9). This allows for the easy identification of large diamond grains via Raman spectroscopy. For smaller nanodiamonds (~<45 nm) (9), phonon confinement results in a drastic decrease in intensity as well as an increased bandwidth and downshift of the ~1332 cm^{-1} diamond phonon (10). This decrease in intensity makes the observation of nanodiamonds difficult using Raman imaging with visible excitation wavelengths. Thus, our Raman images have low sensitivity to nanodiamonds but can easily observe larger diamonds. As a result, we expect that while our Raman images are able to image large diamond grains, nanodiamonds mostly go undetected due to the low signal of the nanodiamond Raman spectra within the Raman image. In addition, the broad and weak nanodiamond phonon band overlaps with the more intense graphite D band and large diamond 1332 cm^{-1} band further hindering its identification. Because of this, only a few Raman spectra were observed with a band characteristic of nanodiamonds. The presence of nanodiamonds in the ureilite samples was positively identified in this work using TEM and micro x-Ray diffraction. The lack of a ~1332 cm^{-1} diamond phonon peak in areas of the sample where diamonds are known to be present supports the observation of nanodiamonds by these techniques. For the Raman images shown in figures S6C and 1E, the intensity of red color indicates the relative intensity of the ~1332 cm^{-1} large diamond phonon band providing an image of large (~>45 nm) diamonds.

The Raman spectrum of graphite consists of two predominant first-order bands. The G band is found at ~1575 cm^{-1} and is a stretching mode of sp^2 hybridized carbons found in rings and chains (11). Thus, the G band is characteristic of sp^2 hybridized carbon regardless of the order of the graphite (12). In contrast, the D band is found at ~1350 cm^{-1} and is a ring breathing mode of sp^2 hybridized carbon (11). This vibration is forbidden for perfect, infinite-sheet graphite and is only observed for rings at the edges of graphite grains (12). Thus, the D band is more intense for graphite that is less ordered containing smaller grain sizes. Because the D band intensity varies with graphite order, we use the G band to identify graphite in our Raman images (Figures S6C and 1E), where the intensity of the blue color corresponds to the G band intensity.

Supplementary Information Figures

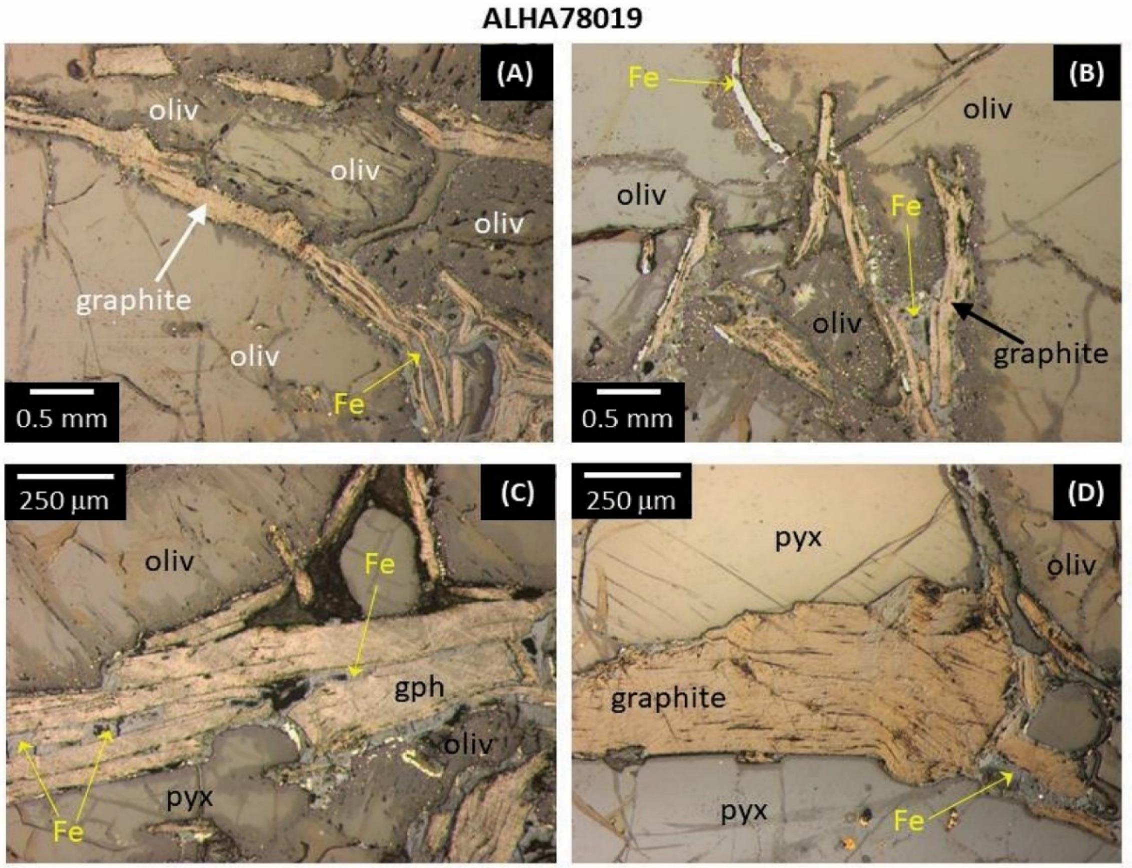

Fig. S1. Reflected light images of very low-shock ureilite ALHA78019, showing euhedral to subhedral (blade-shaped, tabular) graphite crystals with well-defined (0001) cleavage, located along silicate grain boundaries. Note that graphite is spatially associated with Fe,Ni metal (labelled Fe in images), some of which has been terrestrially altered to Fe-hydroxides (grey) in this sample. Abbreviations: oliv = olivine; pyx = pyroxene; gph = graphite. Berkley and Jones (13) and Treiman and Berkley (14) infer that such crystals were the primary (pre-shock) form of graphite in all ureilites.

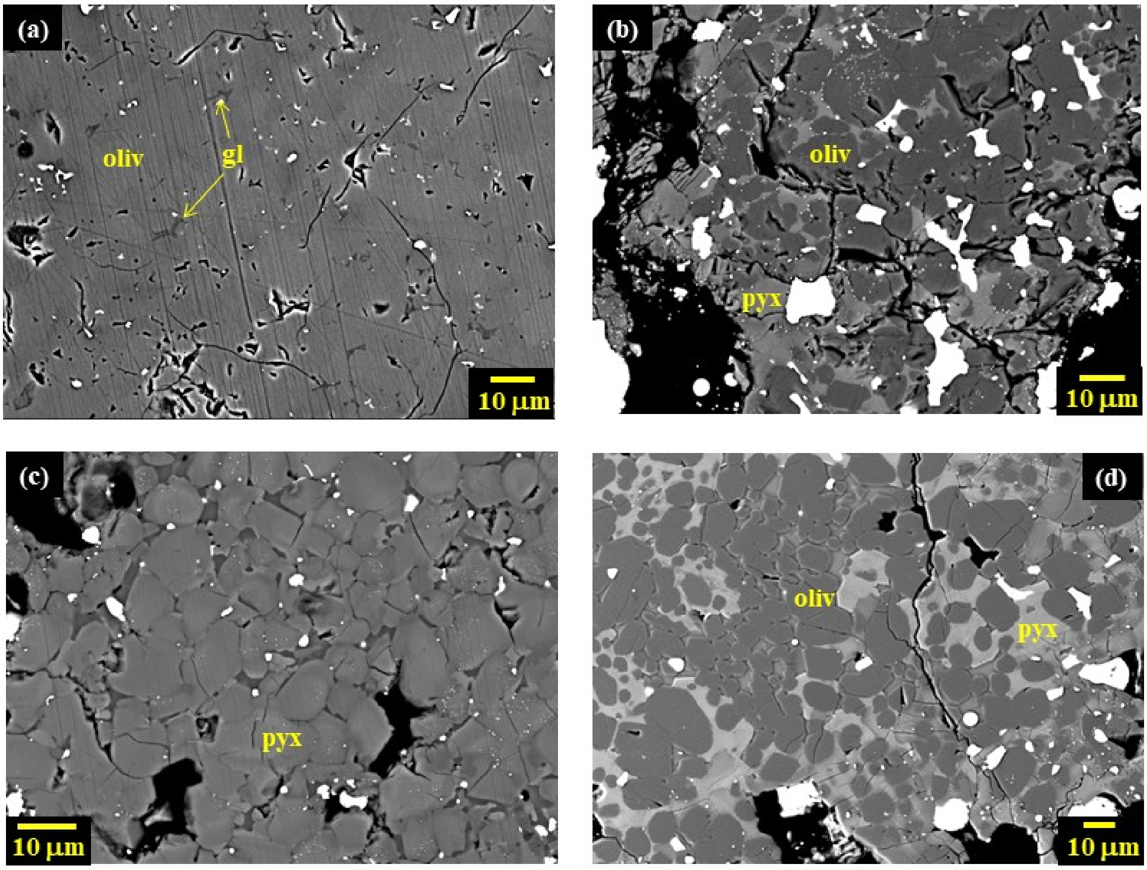

Fig. S2. (A) Back-scattered electron image (BEI) of AhS 209b, showing dominant texture of olivine areas (the parallel lines on the surface are scratches from polishing). Original olivine (oliv) crystals are completely mosaicized to ~5-20 µm-sized equigranular tiles, with minor interstitial Si-Al-enriched glass (gl). (B) BEI of less common, impact-smelted olivine area in AhS 209b, with ~5-20 µm-sized equigranular, rounded, grains of reduced olivine with interstitial pyroxenes (pyx). Metal and sulfide grains (bright) are common. (C) BEI of AhS 209b showing impact-smelted pyroxene, consisting of aggregates of ~5-10 µm-sized subhedral grains, with small amounts of interstitial Ca-enriched pyroxenes (px) and Si-Al-enriched glass. Pores and small grains of metal and sulfide (bright) are common. Pyroxenes are reduced relative to inferred primary compositions, and show further reduced outer rims. (D) BEI showing dominant lithology in AhS 72, similar to [B], of equigranular, rounded, highly reduced olivine with interstitial pyroxene.

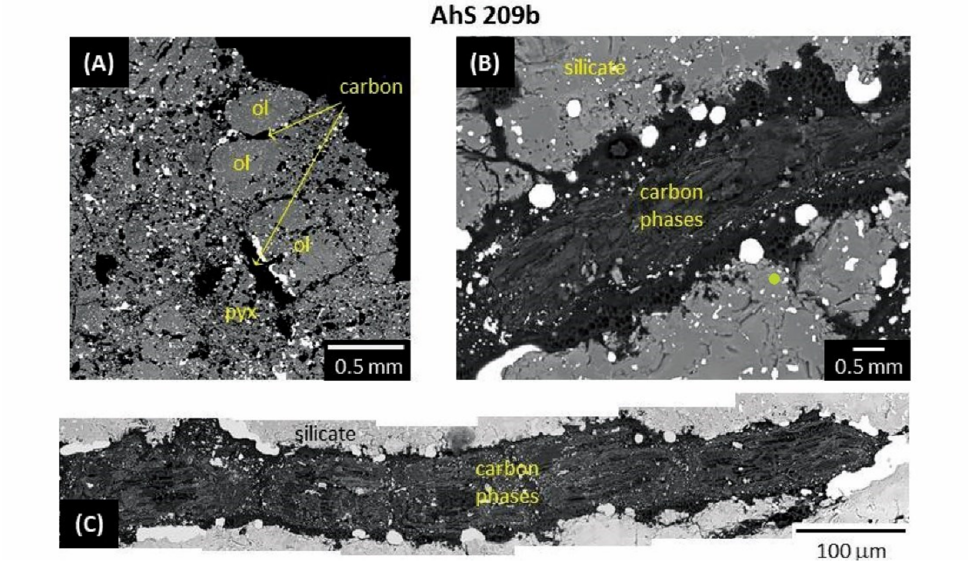

Fig. S3. Back-scattered electron images of AhS 209b. (A) Low-magnification image showing highly re-crystallized silicates, with ubiquitous pores and dispersed grains of metal and sulfide. In some areas, elongated masses of carbon phases are located along boundaries between aggregates of olivine and pyroxene that are inferred to represent primary, originally much larger, silicate crystals. (B) Elongated mass of carbon phases. (C) Collage of seven images showing part of ~1 mm-long elongated mass of carbon phases.

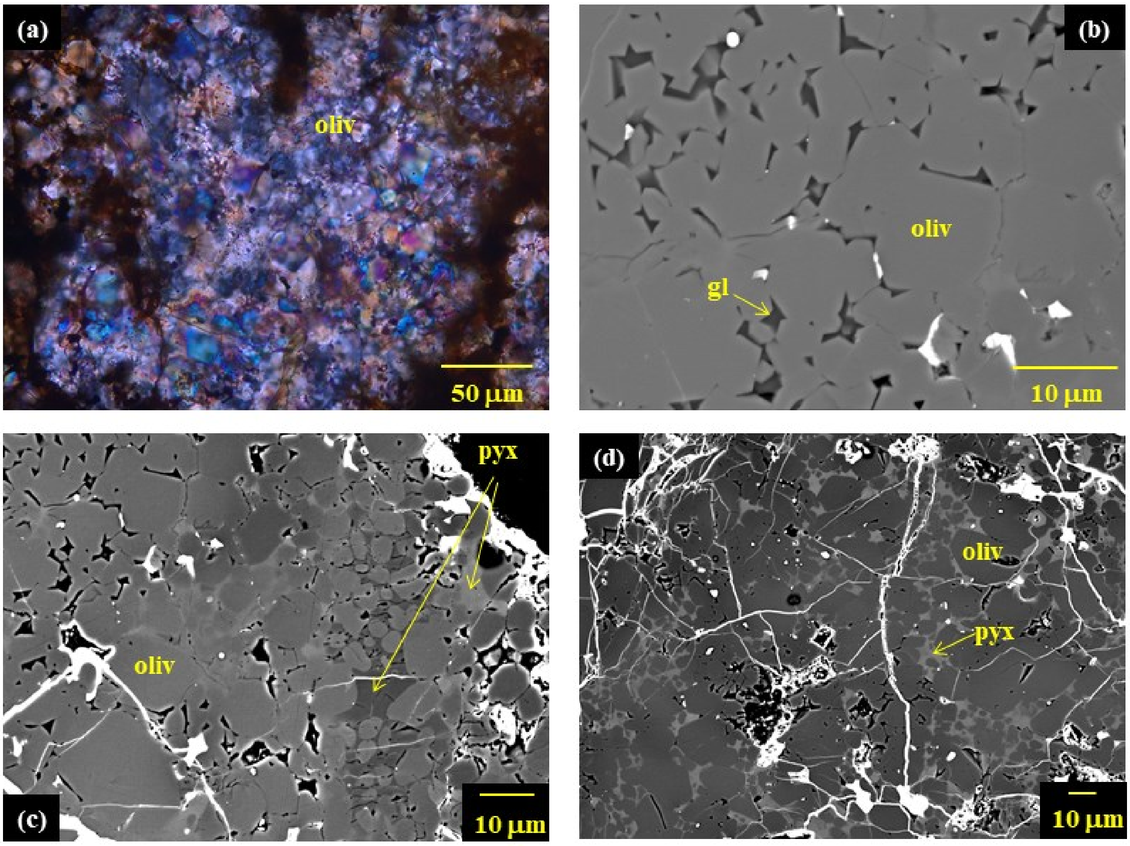

Fig. S4. (A) Transmitted cross-polarized light image of NWA 7983 showing dominant texture of completely mosaicized olivine. (B) BEI of mosaicized olivine in NWA 7983. Euhedral-subhedral tiles of olivine (oliv) with interstitial Si-Al-rich glass (gl). (C) BEI of NWA 7983 showing mosaicized olivine (upper left) grading into rounded, equigranular, grains of olivine with interstitial pyroxene (pyx) on the right. (D) BEI of NWA 7983 showing area of olivine similar to [C] but with more reduced compositions.

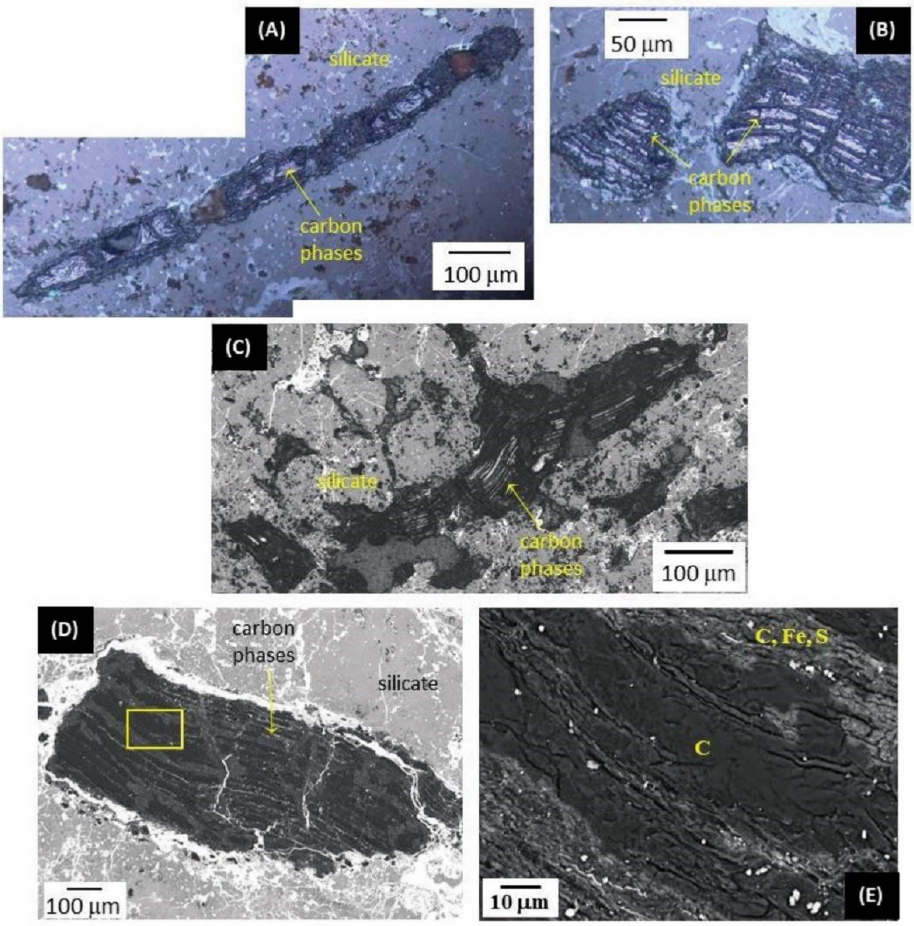

Fig. S5. Carbon masses in NWA 7983. (A,B,C) Reflected light images. Highly reflective, high-relief areas (stripes parallel to the external morphology of the whole carbon area) in carbon masses are inferred to be diamond, based on their optical properties. (D) BEI, showing dark and light strips, parallel to the external morphology of the whole carbon area. Dark areas tend to correlate with high relief, high-reflectance stripes in reflected light images. (E) Detail from area outlined by box in [D]. Dark areas show only C, while lighter areas show C, Fe, and S peaks in energy dispersive spectra (EDS).

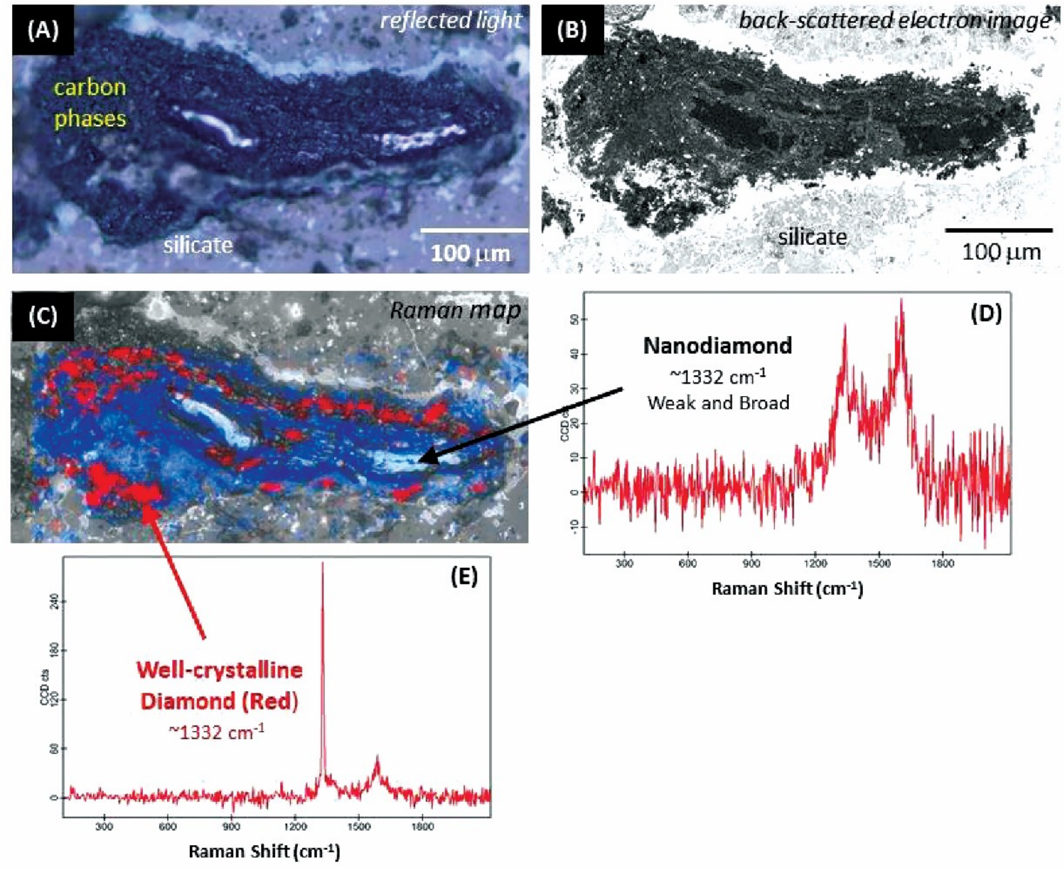

Fig. S6. Elongated carbon mass in NWA 7983. (A) Reflected light. Stripes of high reflection and high relief are inferred to be diamonds based on these optical properties and fluorescence under the electron beam. (B) Back-scattered electron image of non-carbon-coated sample in low vacuum mode (some charging in silicate areas). Darker areas correspond closely to the areas of high reflectance and high relief in [A]. Bright rim immediately surrounding the carbon mass represents original metal (now terrestrially altered to iron-oxide). (C) Raman image of diamond (red) and graphite (blue). The intensity of the diamond ~1332 cm^{-1} band is indicated by the brightness of the red coloring, and the intensity of the graphite G band (~1575 cm^{-1}) is indicated by the brightness of the blue coloring. Larger areas of high relief show few signs of diamond and have increased hardness compared to the low relief areas indicating the potential presence of small nanodiamonds (~<45 nm). (D) Raman spectrum of nanodiamond (~<45 nm) found in the Raman image of [A]. The weak, broad ~1332 cm^{-1} nanodiamond peak is found overlapping the broad graphite D band (~1350 cm^{-1}). (E) Raman spectrum of large diamond (~>45 nm) found in the Raman image of [A]. The intense, narrow ~1332 cm^{-1} band is the dominant feature in the spectrum.

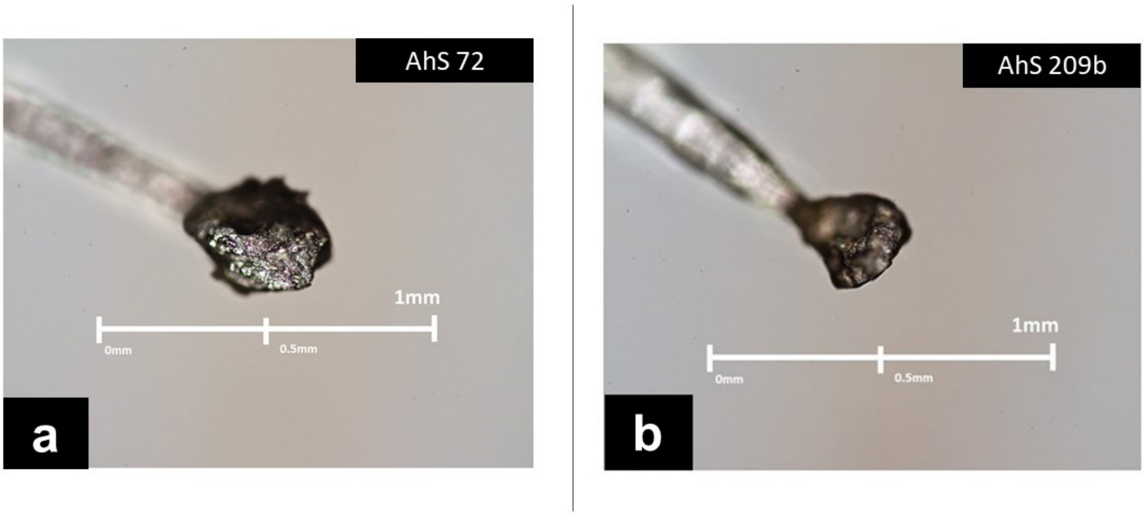

Fig. S7. Optical microscopy images (magnification 10x in reflection mode) by Nikon eclipse ME600 of (A) AhS 72 and (B) AhS 209b ureilitic samples glued at the top of 100 µm glass fibre. These samples were analyzed by Synchrotron radiation micro X-ray diffraction, carried out at the Paul Scherrer Institute, Villigen, Switzerland.

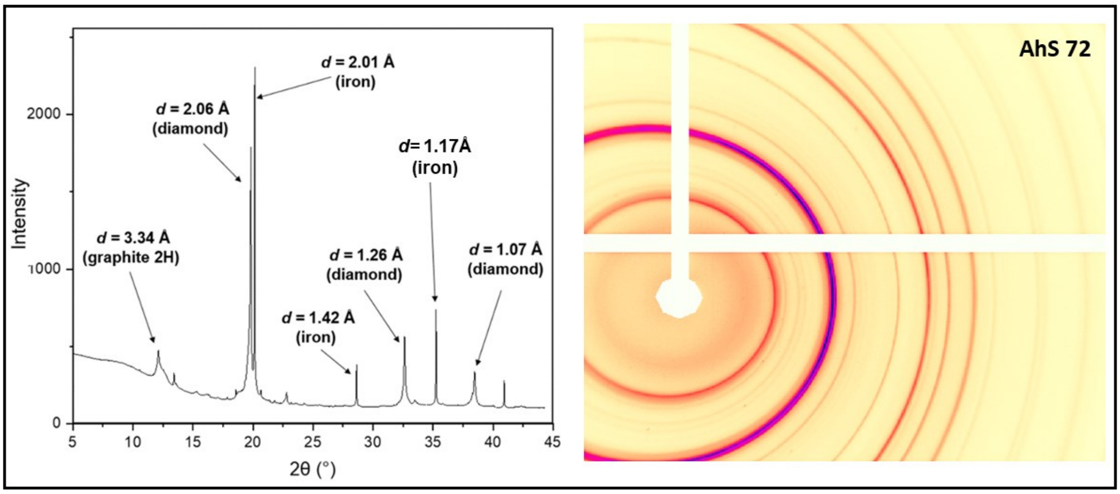

Fig. S8. (A) The diffractogram of AhS 72 and (B) the diffraction image of AhS 72 analyzed by Synchrotron radiation micro X-ray diffraction at the Paul Scherrer Institute, Villigen, Switzerland.

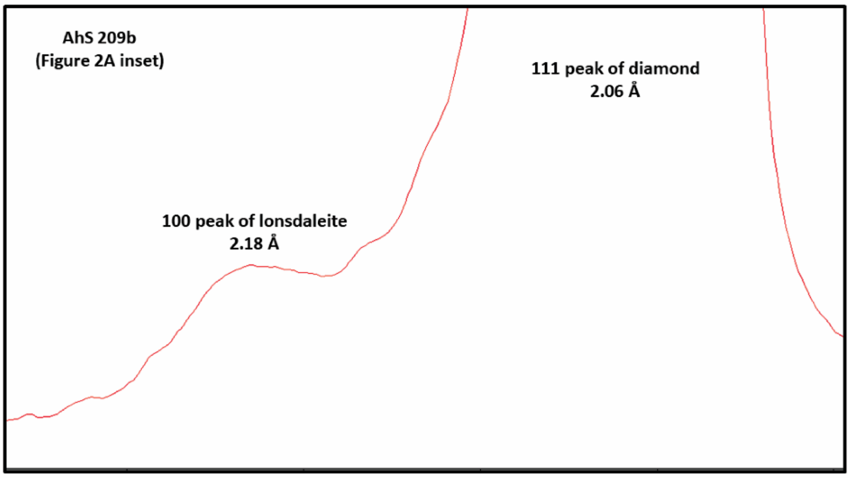

Fig. S9. Magnification of the left shoulder of the highest peak of diamond (2.06 Å) corresponding to stacking faults of diamond (2.18 Å) in the AhS 209b sample.

SI References

1. P. R. Willmott *et al.*, The Material Science beamline upgrade at the Swiss Light Source. *J. Synchrotron Radiat.* **20**, 667-682 (2013).

2. G. Ferraris, E. Makovicky, S. Merlino, "Application of modularity to structure description and modelling" in Crystallography of Modular Materials, G. Ferraris, E. Makovicky, S. Merlino, Eds. (Oxford University Press, 2008).

3. M. Leoni, A. F. Gualtieri, N. Roveri, Simultaneous refinement of structure and microstructure of layered materials, *J. Appl. Crystallogr*. **37**, 166-173 (2004).

4. M. M. J. Treacy, J. M. Newsamm M. W. Deem, A general recursion method for calculating diffracted intensities from crystals containing planar faults. *P. R. Soc.- Math. Phys. Sc.* **433**, 499-520 (1991).

5. P. Scardi, M. Leoni, Whole powder pattern modelling. *Acta Crystallogr. A* **58**, 190-200 (2002).

6. A. A. Coelho, J. S. O. Evans, I. R. Evans, A. Kern, S. Pearson, The TOPAS symbolic computation system. *Powder Diffr.* **26**, S22-S25 (2011).

7. R. S. Jakubek, M. D. Fries, Calibration of Raman wavenumber in large Raman images using a mercury-argon lamp. *J. Raman Spectrosc.* (2020).

8. S. A. Solin, A. K. Ramdas, Raman spectrum of diamond. *Phys. Rev. B* **1**, 1687 (1970).

9. V. I. Korepanov, H. Witek, H. Okajima, E. Ōsawa, H. Hamaguchi, Communication: Three-dimensional model for phonon confinement in small particles: Quantitative bandshape analysis of size-dependent Raman spectra of nanodiamonds. *J. Chem. Phys.* 140, 041107 (2014).

10. S. Osswald, V. N. Mochalin, M. Havel, G.Yushin, Y. Gogotsi, Phonon confinement effects in the Raman spectrum of nanodiamond. *Phys. Rev. B* **80**, 75419 (2009).

11. A. C. Ferrari, J. Robertson, Resonant Raman spectroscopy of disordered, amorphous, and diamondlike carbon. *Phys. Rev. B* **64**, 75414 (2001).

12. A. C. Ferrari, J. Robertson, Interpretation of Raman spectra of disordered and amorphous carbon. *Phys. Rev. B* **61**, 14095 (2000).

13. J. L. Berkley, J. H. Jones, Primary igneous carbon in ureilites: Petrological implications. *J. Geophys. Res.* **87**, A353-364 (1982).

14. A. H. Treiman, J. L. Berkley, Igneous petrology of the new ureilites Nova 001 and Nullarbor 010. *Meteoritics* 29, 843-848 (1994).

15. T. D. Varfolomeeva, Synthesis and investigation of polycrystalline diamond. *PhD Thesis, Institute for High pressure physics, USSR Academy of Sciences*, 154 p. (1971).

16. L. F. Vereschagin, E. N. Yakovlev, T. D. Varfolomeeva, A. Y. Preobrazhensky, V. N. Slesarev, V. A. Stepanov, L. E. Shterenberg, Method of producing polycrystalline diamonds, *United States Patent* No 4049783 (1977).

17. R. C. Burns, V. Cvetkovic, C. N. Dodge, D. J. F. Evans, M. L. T. Rooney, P. M. Spear, C. M. Welbourn, Growth-sector dependence of optical features in large synthetic diamonds. *Journal of Crystal Growth* **104**, 257-279 (1990).

18. M. Wakatsuki, W. Li, Y. Gohda, L. Y. Ding, Simulated growth process of single-crystal diamond at high pressure. *Diamond and Related Materials* **5**, 56-64 (1996).

APPENDIX II

OTHER ACTIVITIES

Fellowship and grants

2018-Present	Carbon minerals in Frontier Mountain ureilites of the Museo Nazionale dell'Antartide (COMMANDER) project, Programma Nazionale di Ricerche in Antartide (PNRA) 2018 grant PNRA18 00247–A to F. Nestola. Role: team member.
2019	Grant SIMP to attend the XV National Congress of Planetary Sciences 4th-8th February 2019, Florence (Italy).
2020	Grant SIMP to attend the XVI National Congress of Planetary Sciences 3rd-7th February 2020, Padova (Italy).
2020-Present	R.J. Angel, M. Morana, J. Gonzalez, M. Alvaro. Measuring palaeostress in the Earth's crust by in-situ diffraction of mineral inclusions", Long term project, (proposal ID: 20200057) at XPress, Elettra Sincrotrone, Basovizza, Italia. Role: team member.
2020-Present	Olivine-bearing ungrouped achondrites and their parents bodies (OL-BODIES) project, ASI-INAF 2018 grant 2018-16-HH.0 to C. Carli. Role: team member.
2021-Present	Europlanet 2024 RI: Water abundances and hydrogen isotopic ratios of pyroxenes in primitive achondrites 20-EPN2-011 at the Open University (UK) (10 days). Experimentalist.
2021-Present	The Barringer Family Fund for Meteorite Impact Research to support the research project titled: " Investigation of CaRbon Phases in Ureilitic meteorites with increasing SHock dEgRee comparison between ureilitic and terrestrial impact diamonds (CRUSHER)" ($1000) Principal Investigator.

In November 2021, I applied for the Peter Buck Fellowship Program at the National Museum of Natural History of the Smithsonian Institution with the project "Carbon compounds investigation in meteorites related to B-asteroids. Waiting for Bennu samples return (CONSISTENT)"

Supervision activities

- Co-supervisor bachelor thesis: Elia Cattaneo (B.Sc.): Graphite-based geothermometry on Almahata Sitta ureilites (University of Pavia), 2019-2020.
- Co-supervisor bachelor thesis: Leonardo Ravizza (B.Sc.): Geothermometric application on the graphite of Yamato 74123 ureilite (University of Pavia), 2019-2020.
- Co-supervisor bachelor thesis: Davide Sacchi (B.Sc.): Study of Al Huwaysah 010 ungrouped achondrite (University of Pavia), 2019-2020.
- Co-supervisor bachelor thesis: Arianna Tessarolo (B.Sc.): Un metodo alternativo per determinare il grado di shock delle meteoriti (University of Padova), 2020-2021.

Teaching activities

- Teaching assistant for Mineralogy: optics & crystallography (B.Sc degree in Earth Science, 12 CFU) Geological Sciences, University of Pavia (held by Prof. Domeneghetti), 2019 – 2020.
- Teaching assistant for Mineralogy: optics & crystallography (B.Sc degree in Earth Science, 12 CFU) Geological Sciences, University of Pavia (held by Prof. Domeneghetti), 2020 – 2021.
- Teaching assistant for Extra-terrestrial material course (M.Sc. degree in Earth Science, 6 CFU) Geological Sciences, University of Pavia (held by Prof. Alvaro), 2020 – 2021.
- Teaching assistant for Mineralogy (B.Sc degree in Earth Science, 12 CFU) Geological Sciences, University of Pavia (held by Prof. Domeneghetti), 2021 – 2022.
- Teaching assistant for Mineralogy: optics & crystallography (B.Sc degree in Earth Science, 12 CFU) Geological Sciences, University of Pavia (held by Prof. Domeneghetti), 2021 – 2022.
- Teaching assistant for Extra-terrestrial material course (M.Sc. degree in Earth Science, 6 CFU) Geological Sciences, University of Pavia (held by Prof. Alvaro), 2021 – 2022.

Dissemination activities

- Presentation “DIAMANTI IN CADUTA LIBERA”, Pillole di scienze, 23rd September 2021, European Researcher’s Night event in Pavia, 2021.

- Scientific curator of "Meteoriti. Viaggio dallo spazio profondo alla Terra" temporary exhibition at the Dept. of Geosciences of the University of Padova, Oct 2021 - Dec 2021.

Internships, courses, and workshops attended

- International Diamond School 2018, "Diamond: Geology, Gemmology and exploration", attended in Bressanone (Italy), from January 29th to February 2nd, 2018.
- X-ray based methods for the investigation of molecules and materials, with special focus on X-ray diffraction School 2018, "Introduction to structural crystallography and diffraction", attended the Department of Geoscience in Padova (Italy), from 4th to 8th June 2018.
- "Geology and exploration of planetary bodies" (10 CFU) course held by Prof. M. Massironi at Dept. of Geosciencesof University of Padova (Italy), Oct 2018-Jan 2019.
- "X-ray diffraction" (4CFU) course held by Dr. R. Angel at the Dept. of Earth and Environmental Sciences of University of Pavia (Italy), Oct 2018-Jan 2019.
- Course "Tecniche di microscopia elettronica a scansione (SEM-ESEM) e microanalisi (XRF-EDS) e Diffrattometria a raggi X da polveri (XRPD)" (4CFU) at Centro di Analisi e Servizi per la Certificazione (CEASC, University of Padova), Padova (Italy), 29th March-19th April 2019.
- Internship at the Department of Lithospheric Research of the University of Wien, during which I was able to expand and deepen my knowledge about meteorites. This experience allowed me to acquire the ability to classify meteorites using the optical microscopy, 1st -31st May 2019.
- Multidisciplinary geological field trip at Monginevro of the Dept. of Earth and Environmental Sciences of University of Pavia (Italy), 19th -21st July.
- Course "Physical Properties of minerals and rocks" (6CFU) held by Dr. R. Angel and Dr. M. Mazzucchelli at the Dept. of Earth and Environmental Sciences of University of Pavia (Italy), Oct 2020-Jan 2021.
- Corso operativo Microscopio elettronico SEM EM30AXPlus (2CFU) at Centro di Analisi e Servizi per la Certificazione (CEASC, University of Padova), Padova (Italy), 1st 31st Jan 2021.

Meetings, conferences, and seminars attended

1. Morana M., Murri M., Nestola F., Barbaro A., Fioretti A.M., Alvaro M., Domeneghetti M.C., Goodrich C., Shaddad M.H., Diamond formation in ureilites: a shock origin inferred from diamond in Almahata Sitta. Joint congress SIMP-SGI.SOGEI, 12th – 14th September 2018, Catania (Italy).
2. Morana M., Murri M., Nestola F., Barbaro A., Fioretti A.M., Alvaro M., Domeneghetti M.C., Goodrich C., Shaddad M.H. X-ray diffraction study of diamonds from the Almahata Sitta meteorite. 3rd Joint AIC-SILS conference 25th – 28th June 2018, Rome (Italy).
3. Barbaro A., Domeneghetti M. C., Meneghetti M., Litti L., Fioretti A. M., Goodrichd C., M. H. Shaddad, Alvaro M., Nestola F., Graphite based geothermometry of Almahata Sitta ureilites. XV National Congress of Planetary Sciences, 4th -8th February 2019, Florence, (Italy).
4. Barbaro A., Domeneghetti M.C., Meneghetti M., Litti L., Fioretti A.M., Goodrich C., Shaddad M. H., Alvaro M., Nestola F., Graphite-based geothermometry of Almahata Sitta ureilites, PhD Congress, 7th March 2019, Pavia (Italy).
5. Nestola F., Barbaro A., Morana M., Christ O., Brenker F.E., Domeneghetti M.C., Dalconi M.C., Alvaro M., Goodrich C., Fioretti A.M., Leoni M., Shaddad M.H., Origin of diamond in ureilites, Goldschmidt conference, 18th -24th August 2019, Barcelona (Spain).
6. Nestola F., Barbaro A., Morana M., Christ O., Brenker F.E., Domeneghetti M.C., Dalconi M.C., Alvaro M., Goodrich C., Fioretti A.M., Leoni M., Shaddad M.H., Diamond in ureilites: how did they form? Joint congress SIMP-SGI-SOGEI, 16th -19th September 2019, Parma (Italy).
7. Barbaro A.; Christ O.; Murri M.; Ferrière L.; Pittarello L.; Goodrich C. A., Domeneghetti M. C.; Fioretti A.M.; Alvaro M.; Brenker F.E.; Nestola F., Study of carbon phases in the Yamato 74123 and Kenna ureilites. XVI National Congress of Planetary Sciences, 3rd -7th February 2020, Padova, (Italy).
8. Carli C., Barbaro A., Pratesi G., Domeneghetti M.C., Langone A., Alvaro M., Casalini M., Murri M., Moggi Cecchi V., Roush T. L., OLivine-Bearing ungrOuped achonDrItES: OL-BODIES. XVI National Congress of Planetary Sciences, 3rd -7th February 2020, Padova, (Italy).

9. Nestola F., Goodrich C.A, Morana M., Barbaro A., Christ O., Brenker F.E, Domeneghetti M.C., Dalconi M.C, Alvaro M., Fioretti A. M., Leoni M., Casati N. P. M., Jenniskens P.J., Shaddad M.H., Origin of diamond and graphite in ureilites: a timely topic in planetary geology. XVI National Congress of Planetary Sciences, 3rd -7th February 2020, Padova, (Italy).

10. Barbaro A., Alvaro M., Pratesi G., Morelli M., Moggi Cecchi V., Faggi D., Murri M., Domeneghetti M. C., LUNATIC: the crowdfunding project to implement with lunar samples a collection of meteorite thin sections. XVI National Congress of Planetary Sciences, 3rd -7th February 2020, Padova, (Italy).

11. Barbaro A., M. Domeneghetti C., Meneghetti M., Litti L., Fioretti A. M., Goodrich C., Christ O., Brenker F. E., Shaddad M. H., Alvaro M., Nestola F., SHOCK TEMPERATURE RECORDED BY GRAPHITE IN UREILITES FROM ALMAHATA SITTA (#1480). 51st Lunar and Planetary Science Conference 2020 – 17th-21st March 2020, Houston (TX, USA)

12. Barbaro A., Nestola F., Pittarello L., Ferrière L., Murri M., Christ O., Alvaro M., Domeneghetti M. C., Graphite based geothermometry of Yamato 74123 ureilitic meteorite. NIPR Symposium on Polar Science, 1st – 3rd Dec 2020.

13. Barbaro A., Nestola F., Pittarello L., Ferrière L., Murri M., Christ O., Alvaro M., Domeneghetti M. C. Impact Shock Origin of Carbon Phases in Yamato 74123 Ureilite (#1123). 52nd Lunar and Planetary Science Conference 2021 – 15th-19th March 2021, Houston (TX, USA) virtual Conference.

14. Barbaro A., Domeneghetti M. C., Litasov K. D., Ferrière L., Pittarello L., Christ O., Lorenzon S., Alvaro M., Nestola F. Carletonmooreite (Ni3Si) in shocked diamond-bearing Kenna ureilite (2609 id. 6066). 84th Annual meeting of the Meteoritical Society 2021 – 15th – 21st August 2021, Chicago (Illinois).

15. Christ O., Barbaro A., Brenker F.E., Domeneghetti M.C., Nestola F. Shock Temperature records in graphite from the Northwest Africa 6871 Ureilite (2609 id. 6052). 84th Annual meeting of the Meteoritical Society 2021 – 15th – 21st August 2021, Chicago (Illinois).

16. Carli C., Barbaro A., Murri M., Domeneghetti M., Langone A., Bruschini E., Alvaro M., Stefani S., Cuppone T., Casalini M., Moggi Cecchi V., Migliorini A., Roush T., Pratesi G. Characterization of

Al Huwaysah 010 ungrouped achondrite (#0285). 3rd European Mineralogical Conference 2020 – 29th August – 2nd September 2021, Cracow (Poland) virtual Conference.

17. Carli C., Bruschini E., Barbaro A., Cuppone T., Murri M., Domeneghetti M.C., Pratesi G. VNIR spectral properties of olivine bearing Ungrouped Achondrites (23-14). 90th Congress of Italian Geological Society - 13th-16th September 2021, Trieste (Italy).

18. Casalini M., Cuppone T., Avanzinelli R., Carli C., Barbaro A., Langone A., Domeneghetti M.C., Pratesi G. Preliminary results on mineralogical and geochemical analysis on ungrouped achondrites (23-10). 90th Congress of Italian Geological Society - 13th-16th September 2021, Trieste (Italy).